

TOWARD RELIABLE AND ROBUST WIRELESS PERSONAL  
AREA NETWORKS

A Dissertation  
Presented to  
the Faculty of the Department of Electrical and Computer  
Engineering  
University of Houston

In Partial Fulfillment  
of the Requirements for the Degree  
Doctor of Philosophy  
in Electrical Engineering

by  
Guanbo Zheng  
August 2013

© Copyright by Guanbo Zheng 2013  
All Rights Reserved

# TOWARD RELIABLE AND ROBUST WIRELESS PERSONAL AREA NETWORKS

---

Guanbo Zheng

Approved:

---

Chair of the Committee  
Dr. Zhu Han, Associate Professor  
Dept. of Electrical and Computer Engineering  
University of Houston

---

Co-Chair of the Committee  
Dr. Rong Zheng, Research Associate Professor  
Dept. of Computer Science  
University of Houston

Committee Members:

---

Dr. Yuhua Chen, Associate Professor  
Dept. of Electrical and Computer Engineering  
University of Houston

---

Dr. Jiming Bao, Assistant Professor  
Dept. of Electrical and Computer Engineering  
University of Houston

---

Dr. Bo Sun, Associate Professor  
Dept. of Computer Science, Lamar University

---

Dr. Cunqing Hua, Associate Professor  
School of Information Security Engineering  
Shanghai Jiao Tong University, China

---

Dr. Suresh K. Khator, Associate Dean,  
Cullen College of Engineering

---

Dr. Badrinath Roysam, Professor and Chairman,  
Electrical and Computer Engineering

## Acknowledgements

I am very grateful for every aspect that everyone has helped me with in the last four years, which has made my PhD study an unforgettable experience.

First of all, I would like to express my sincere gratitude to my advisor, Professor Rong Zheng, for her esteemed guidance and constant encouragement in the course of my graduate studies. Without her continuous support, this dissertation would not have been possible. Her constructive advice and keen insights has significantly improved both my research and professional development, which will be an invaluable assets for my future career.

Furthermore, I would like to thank Professor Zhu Han, Professor Yuhua Chen, Professor Jiming Bao, Professor Cunqing Hua and Professor Bo Sun for being on my committee and providing helpful comments. Specifically, I have been privileged to collaborate with Professor Zhu Han, Professor Cunqing Hua and Professor Qixin Wang. I am very grateful to them for their insightful comments and contribution on my dissertation.

I would like to express big thanks to all the WiSeR members including: Soji Omiwade, Huy Ngyuen, Pallavi Arora, Thanh Le, Kuntal Ray, Khuong Vu, Sai Shiva Kailaswar, Tina Mathews and Nam Ngyuen, as well as my collaborators including Yufei Wang and Zheng Zeng for the helpful discussions and great cooperation in my research.

I am grateful to all my dear friends for enriching my PhD life in Houston, including Zhou Yuan, Ziyang Li, Zijing Zhao, Rui Hu, Dong Han, Siyu Li, Ran Liu, Yilun Mao, Jie Chen and Cui Wang. They have directly or indirectly helped make my life much easier and more fun in the USA.

I also would like to thank Jackie L. Baum and Anh N. Nash in the CS depart-

ment and Mytrang Baccam in the EE department for their great help when I was in need of any administrative processing.

Finally and most importantly, I would like to give my greatest gratitude to my beloved family: my parents, Meihua Zheng and Xianfeng Yin, my wife, Miao Sui and my elder brother, Pinguan Zheng, who have been standing by my side and providing unconditional and continuous support all these years. Without their encouragement, I would never have achieved this accomplishment!

TOWARD RELIABLE AND ROBUST WIRELESS PERSONAL  
AREA NETWORKS

An Abstract  
of a  
Dissertation  
Presented to  
the Faculty of the Department of Electrical and Computer  
Engineering  
University of Houston

In Partial Fulfillment  
of the Requirements for the Degree  
Doctor of Philosophy  
in Electrical Engineering

by  
Guanbo Zheng  
August 2013

# Abstract

Wireless personal area networks (WPANs) have been widely deployed for providing low power, low cost wireless connectivity that facilitates seamless operation among wireless devices centered around an individual person. However, pervasive deployment of WPANs has introduced several challenging problems on coexistence and resource provisioning.

First of all, most commercial-of-the-shelf (COTS) WPAN devices typically provide limited information of the current condition of wireless channels, which would lead to misinformed decisions and under-utilization of available resources. In this dissertation, we revisit the issue of link quality prediction in IEEE 802.15.4 low rate WPANs, and decipher *RSSI*, *LQI* readings available in Zigbee radios with TI CC2420 chipset. In order to predict the instantaneous link quality, we develop an inference model under different channel environments that uses instantaneous *LQI* readings as input.

Secondly, neighbor discovery and contention relationship inference are two corner stones of operating and managing ad-hoc WPANs. In this dissertation, we investigate the problem of joint neighbor discovery and contention relationship inference while most existing work focuses on one of the two problems. An active inference algorithm is proposed, called the ternary inference algorithm that utilizes decentralized randomized schedules to infer the neighboring and contention relationships through mixed signal at the receiver nodes. We analyze the sources of errors in the proposed scheme, and evaluate the impact of loose synchronization, network size, and other parameter settings.

Lastly, newly developed high rate WPAN applications pose more stringent requirements on quality-of-service (QoS), which makes it more vulnerable to network dynamics and uncertainty in wireless channel environment. We investigate the relay

placement and route selection solution to combat the uncertain link failure in the IEEE 802.15.3c mmWave WPANs. Specifically, two robust problems are formulated, robust minimum relay placement (RMRP) and robust maximum utility relay placement (RMURP), with the objective to minimize the number of relays deployed and maximize the network utility, respectively. Efficient algorithms are developed to solve both problems and have been shown to incur less service disruption in the presence of moving subjects that may block the LOS paths in the environment.

# Table of Contents

Acknowledgements	iv
Abstract	vii
Table of Contents	ix
List of Figures	xiii
List of Tables	xvii
List of Algorithms	xviii
1 Introduction and Background	1
1.1 Overview . . . . .	1
1.2 Related Work . . . . .	4
1.3 Main Contributions . . . . .	5
1.4 Organizations of This Thesis . . . . .	7
2 Reliable Link Quality Prediction in WPANs	8
2.1 Introduction . . . . .	8
2.1.1 Contributions . . . . .	9
2.2 Preliminaries . . . . .	10
2.2.1 IEEE 802.15.4 Zigbee . . . . .	10
2.2.2 Hardware and Software Toolkits . . . . .	11
2.3 Measurement Study of <i>RSSI</i> and <i>LQI</i> . . . . .	14

2.3.1	Deciphering <i>RSSI</i> . . . . .	14
2.3.2	Deciphering <i>LQI</i> . . . . .	16
2.4	Analytical Model of <i>CORR</i> . . . . .	17
2.4.1	Derivation of Chip Correlation . . . . .	18
2.4.2	Simulation Validation . . . . .	20
2.5	Proposed Link Quality Prediction Model Using <i>LQI</i> . . . . .	22
2.5.1	Derivation of Link Quality . . . . .	22
2.5.2	Simulation Validation . . . . .	24
2.6	Experiment Results . . . . .	25
2.6.1	Cabled Connection Environment . . . . .	26
2.6.2	Outdoor Environment . . . . .	27
2.7	Summary . . . . .	27
3	Joint Neighbor Discovery and Contention Relationship Inference in ad-hoc WPANs . . . . .	29
3.1	Introduction . . . . .	29
3.1.1	Contributions . . . . .	30
3.2	Related Work . . . . .	30
3.3	Network Model and Problem Statement . . . . .	32
3.3.1	Network Model . . . . .	32
3.3.2	Problem Statement . . . . .	34
3.4	Ternary Inference Model and Algorithm . . . . .	35
3.4.1	Modeling The Observations . . . . .	35

3.4.2	Inference Algorithm . . . . .	37
3.4.3	Analysis of Errors . . . . .	40
3.5	Performance Evaluation . . . . .	43
3.5.1	Inference Completion Rate . . . . .	44
3.5.2	Inference Error Rate . . . . .	45
3.5.3	Impact of Loose-Synchronization . . . . .	46
3.6	Conclusion . . . . .	47
4	Robust Relay Placement and Routing Selection in WPANs . . . . .	49
4.1	Introduction . . . . .	49
4.1.1	Contributions . . . . .	50
4.2	Related Work . . . . .	52
4.3	Geometric Model for Link Connectivity . . . . .	53
4.4	Why Robustness is Needed . . . . .	55
4.5	Robust Relay Placement and Route Selection in an Interference-free 60GHz WPANs . . . . .	57
4.5.1	Problem Statement . . . . .	57
4.5.2	Robust Minimum Relay Placement . . . . .	59
4.5.3	Robust Maximum Utility Relay Placement . . . . .	64
4.5.4	Simulation Results . . . . .	72
4.6	Robust Relay Placement and Route Selection in 60GHz WPANs with Directional Antenna . . . . .	80
4.6.1	Problem Statement . . . . .	80

4.6.2	Link-Link Spatial Contention . . . . .	81
4.6.3	Robust Minimum Relay Placement . . . . .	82
4.6.4	Robust Maximum Utility Relay Placement . . . . .	90
4.6.5	Simulation Results . . . . .	94
4.6.6	Summary . . . . .	99
5	Conclusions and Future Work	102
5.1	Summary of Contributions . . . . .	102
5.2	Future Work . . . . .	103
	Bibliography	106

## List of Figures

1.1	WPAN topologies . . . . .	2
2.1	IEEE 802.15.4 frame structure . . . . .	11
2.2	Tmote-Sky wireless sensor . . . . .	12
2.3	Software-defined radio architecture using USRP . . . . .	13
2.4	USRP2 hardware platform by Ettus Research . . . . .	13
2.5	Signal <i>RSSI</i> and noise floor readings VS. Gaussian noise generated by USRP2 in the cabled connection environment on channel 26. Two different attenuators are used, 6dB and 12dB. . . . .	16
2.6	<i>LQI</i> readings Vs. the measured <i>SNR</i> for different TmoteSky Zigbee nodes in the cabled connection environment on channel 26. . . . .	17
2.7	Basic communication model. . . . .	18
2.8	The estimated <i>SNRs</i> from <i>CORR</i> averaged over 1000 packets in the simulation of perfect decoding. . . . .	21
2.9	<i>SER</i> performance with respect to <i>SNR</i> for AWGN, Rician with $K=6$ and Rayleigh fading environment respectively. Both simulated and theoretical curves are plotted. . . . .	25
2.10	Comparison of the predicted <i>SER</i> from <i>LQI</i> readings and the measured <i>SER</i> with respect to the received <i>SNR</i> in the cabled connection environment. . . . .	26
2.11	Comparison of the predicted <i>SER</i> from <i>LQI</i> readings and the measured <i>SER</i> with respect to the received <i>SNR</i> in the outdoor channel environment. . . . .	27

3.1	A random on-off signaling . . . . .	32
3.2	Network node degree with respect to the number of nodes in the network with different sensitivity SNR $\Gamma_1$ . . . . .	43
3.3	Performance of observation error rate with respect to the number of nodes in the ternary model with $L = 200$ , $\Gamma_1 = 3dB$ , $\Gamma_2 = -7dB$ . . .	43
3.4	Performance of completion rate with respect to the number of tests in the ternary model with $\Gamma_1 = 3dB$ , $\Gamma_2 = -7dB$ and 95% confidence: (a) neighbor discovery with $TOL = 1$ , an aloha-like algorithm is used for comparison; (b) t-tolerance neighbor discovery with $N = 30$ ; (c) contention relationship inference with $TOL = 1$ . . . . .	44
3.5	Performance of inference error rate with respect to the number of tests in the ternary model with $TOL = 1$ , $\Gamma_1=3dB$ , $\Gamma_2=-7dB$ , and 95% confidence. . . . .	45
3.6	Performance of inference error rate with respect to the number of tests in the ternary model with $N = 30$ , $\Gamma_1=3dB$ , $\Gamma_2=-7dB$ , and 95% confidence. . . . .	46
3.7	Performance of inference error rate with respect to the number of tests in the ternary model with $TOL=1$ , $N = 30$ , and 95% confidence . . .	46
3.8	Impact of loose-synchronization on the observation and inference error rates in the ternary inference model with $L = 200$ , $N = 30$ , $\Gamma_1 = 3dB$ , $\Gamma_2 = -7dB$ and 95% confidence. The $x\%$ decision error is introduced to randomly invert the decisions. . . . .	47
4.1	The overlapped visibility region between DEV1 and DEV2 is the shadow area bounded by the line segments of each DEV's visibility polygon and their transmission radii. . . . .	54

4.2	A 10m × 10m room with a fixed mmWave TX/RX and a dedicated relay, $M$ human subjects moving randomly inside. . . . .	56
4.3	Link blockage with and without relays due to moving human subjects. . . . .	56
4.4	The relationship between mmWave links ( $U$ ) and relays ( $S$ ). . . . .	57
4.5	An illustration of RMRP in an example network with $N=4$ , $d_0=4$ , $M=10$ and $\Gamma_k/ L_k =1$ . In (a), the solid blue lines denote indirect paths, the solid red lines denote direct paths; In (b) the solid red lines are primary paths, the dash red lines are secondary paths. . . . .	74
4.6	Performance of RMRP in an mmWave home network deployed in a 10m×10m room. . . . .	75
4.7	An illustration of RMURP in an example network with $N=4$ , $d_0=4$ , $M=10$ and $\Gamma_k/ L_k =1$ . The solid red lines are primary paths, the dash red lines are secondary paths. . . . .	77
4.8	Performance of RMURP on utility in an mmWave home network deployed in a 10m×10m room, Bisection Search algorithm with 1.0 tolerance and GBD algorithm. . . . .	78
4.9	Performance of RMURP on link blockage in an mmWave home network deployed in a 10m×10m room, Bisection Search algorithm with 1.0 tolerance and GBD algorithm. . . . .	79
4.10	Three types of physical links. . . . .	85
4.11	Performance of RMRP in an mmWave home network deployed in a 10m×10m room. . . . .	96
4.12	Mobility performance of RMRP in an mmWave home network deployed in a 10m×10m room. . . . .	97

4.13 Performance of RMURP using Bisection Search algorithm with 0.01 $TOL$ , in an mmWave home network deployed in a 10m×10m room. . . . .	99
4.14 Performance of RMURP using Bisection Search algorithm with 0.01 $TOL$ , in an mmWave home network deployed in a 10m×10m room. . . . .	100
4.15 Mobility performance of RMURP using Bisection Search algorithm with 0.01 $TOL$ , in an mmWave home network deployed in a 10m×10m room. . . . .	101

## List of Tables

1.1	Comparison between IEEE 802.15 WPAN standards [1]	2
2.1	Correlation matrix of quasi-orthogonal modulation	19
3.1	Notations	34
3.2	The ternary operators AND $\wedge$ and OR $\vee$	35
3.3	The observation on link $m \rightarrow n$ due to transmitters $m, k$	36
3.4	Simulation setup	42
4.1	Key notations	59
4.2	Simulation setup	74

## List of Algorithms

1	Ternary Neighbor Discovery . . . . .	38
2	t-tolerance Neighbor Discovery Algorithm . . . . .	39
3	Contention Relationship Inference . . . . .	41
4	Bisection Search for RMURP in an Interference-free Model . . . . .	68
5	Generalized Benders' Decomposition . . . . .	73
6	Bisection Search for RMURP in a Directional Antenna Model . . . . .	94

# Chapter 1

## Introduction and Background

### 1.1 Overview

A wireless personal area network (WPAN) is a wireless network that interconnects wireless devices centered around an individual person. While wireless local area networks (WLAN) (also called Wi-Fi) have been focusing on relatively long range applications up to 100 meters, typical WPANs mainly target short-range applications, which permits the communication within about 10 meters only. The objective of WPANs is to get rid of cable connections and provide a low power, low cost wireless connectivity that facilitates seamless operation among home or business wireless devices and systems [1].

Various standards have been developed for WPANs to support different purposes of applications with different Quality-of-Service (QoS) requirements. For instance, IEEE 802.15.1 standard [2], known as Bluetooth [3], is proposed as a cable replacement technology in wireless personal devices like cellphones, computers, PDAs and etc. IEEE 802.15.3 standard [4] is developed for high rate WPAN (HR-WPAN) applications, which have very stringent QoS requirements. IEEE 802.15.4 standard [5], known as Zigbee [6], is proposed for low rate WPAN (LR-WPAN) applications with relaxed QoS need. The comparison between IEEE 802.15 WPAN standards is discussed in Table 1.1.

Generally, there are two types of topologies used in WPANs, star topology and peer-to-peer topology. In star topology, the communication is only established between devices and a central controller, namely PAN coordinator. In contrast, in peer-to-peer topology, any device can communicate with any others as long as they

are in the close range of each other. This ad-hoc and self-organizing nature allows more complex network formulation to be implemented. Mesh and cluster tree are two examples of the peer-to-peer topology, as shown in Figure 1.1.

Table 1.1: Comparison between IEEE 802.15 WPAN standards [1]

IEEE Standard	Topic	Spectrum	Data rate	Range	Suitable Applications	QoS Need
802.15.1	Bluetooth	2.4GHz ISM	1 Mbps	10 meters	Cellphones, Computers, PDAs and etc	QoS suitable for voice applications
802.15.2	Coexistence of Bluetooth and 802.11b	N/A	N/A	N/A	N/A	N/A
802.15.3	High-rate WPAN	2.4/60GHz ISM, 3.1-10.6GHz UWB	>110 Mbps	10 meters	Low power, low cost solutions for portable consumer of digital imaging and multimedia applications	Very high QoS
802.15.4	Low-rate WPAN	868/915MHz/2.4GHz ISM	<250 kbps	10 meters nominal, 1-100 meters based on setting	Industrial, agricultural, vehicular, residential, medical applications, sensors, actuators with very low power consumptions and low cost	Relaxed needs for data rate and QoS

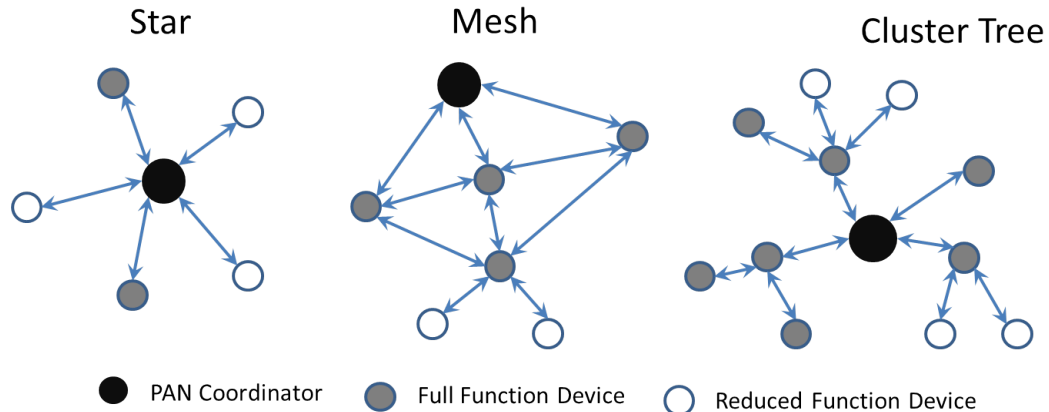


Figure 1.1: WPAN topologies

In recent years, pervasive deployment of WPANs has introduced several challenging problems on coexistence and resource provisioning. First of all, most commercial-of-the-shelf (COTS) WPAN devices typically provide limited information of the current condition of wireless channels. The lack of detailed PHY knowledge for cross-

layer resource management and provisioning usually leads to misinformed decisions and under-utilization of available resources. Secondly, neighbor discovery and contention relationship inference are two corner stones of operating and managing ad-hoc WPANs. Without the knowledge of neighbor and link contention relationships, multiple coexisting devices would interfere with each other, resulting in severe quality-of-service (QoS) degradation. The problem becomes more complex considering the dynamic network scenarios due to the movement of WPANs nodes as well as the variation of wireless channel environment. Lastly, newly developed high rate WPAN applications pose more stringent requirements on quality-of-service (QoS), which makes it more vulnerable to network dynamics and uncertainty in wireless channel environment. For example, multimedia applications in 60GHz mmWave WPANs may suffer from the service disruption, which can occur due to change of channel conditions or LOS link blockage by moving objects in the space. How to perform robust resource provisioning to account for the uncertain link failure is still an open problem.

The main objective of our work is to study and analyze the coexistence and resource provisioning issues toward reliable and robust WPANs. We explore different kinds of WPANs and research the new analytical methodologies and robust solutions. In essence, our work aims to answer a number of questions including:

- By using commodity WPAN devices, do we have accurate knowledge regarding the current channel condition? Do we truly know the quality of wireless link? If not, then how do we predict the accurate instantaneous link quality such as bit/symbol/packet error rate (BER/SER/PER)?
- Given an ad-hoc WPAN with a set of randomly deployed wireless nodes, how do we discover the neighbors for each node accurately using as few measurements as possible? Meanwhile, how do we infer the link contention relationships between any two links?

- Given a WPAN with stringent QoS requirements for link connectivity, how do we model and evaluate effect of the network dynamics and uncertainty? How do we perform robust resource provisioning to account for the uncertain link failure?

## 1.2 Related Work

Increasingly deployed WPANs have introduced the important issue of coexistence which would affect the QoS performance significantly. How to achieve better coexistence with the QoS guarantee in WPANs has attracted a lot of interest from both the academic and the industrial community.

Several experimental work has been conducted to measure the performance degradation of WPANs due to coexistence. Golmie et al. analyzed the performance of a Zigbee-based WPAN for medical applications when multiple WPAN devices coexist in a patient's hospital room [7]. The authors confirmed that the packet error loss of WPANs increases significantly as the number of concurrent transmitters increases. When coexisting a Zigbee-based WPAN with IEEE 802.11 WLAN, Yoon et al. demonstrated in the experiments that the co-channel interference would affect the performance of WPAN significantly, while causing negligible affect on WiFi [8]. This is because Zigbee with smaller bandwidth is considered as the partial band jammer noise to WLAN. The same observation is supported by other researchers [9–11]. Similar results can be observed when coexisting Bluetooth with WLAN [12].

To avoid the mutual interference, frequency planning is generally used to enable the coexistence of WPANs. This may be feasible for static networks, however can not be applied for the dynamic scenarios in which WPANs may be moving. Significant prior literature have proposed the approaches in different layers for coexistence in WPANs. Shah et al. proposed an interference detection and mitigation solution

to leverage the collaboration between interfering WPANs [13]. The drawback of this solution is, it requires the collaboration between the coordinators of multiple WPANs. In addition, it does not work for the scenario when coexisting with other types of wireless devices like WiFi. Ghanem et al. applied the concept of multiuser detection (MUD) to build a robust interference cancelation scheme in CDMA-based WPANs [14]. Khan et al. investigated the interference rejection with the help of multiple antenna technology for two WPANs operating in the near vicinity of each other in the on-body channel environment [15]. However, those two approaches pose high computation complexity in battery-supported WPAN devices. Golmie et al. demonstrated careful tuning on the MAC parameters like packet segmentation and backoff parameters would improve the overall performance of WPANs [7]. In [16], Filo et al. proposed to use cognitive pilot channel (CPC) to enable the radio system coexistence in heterogeneous network for UWB-based WPANs, assuming the perfect prior knowledge of existing systems in the proximity. None of those prior works may be directly applicable to the scenarios when multiple WPANs coexist in the near vicinity of each other without the central coordination.

### 1.3 Main Contributions

In this dissertation, we research the new analytical methodologies and propose solutions to design reliable and robust WPANs analytically and experimentally. Our contribution in this dissertation is three-fold.

**Link Quality Prediction:** We revisit the issue of link quality prediction in IEEE 802.15.4 low rate WPANs and decipher the received signal strength indicator (*RSSI*) and link quality index (*LQI*) readings available in commodity Zigbee radios with TI CC2420 chipset. We demonstrate through measurement study for the first time that *LQI* truly reflects the signal-to-noise ratio (SNR) at the receiver. Furthermore, in

order to predict the instantaneous link quality (e.g. symbol error rate ( $SE_R$ )), we develop an prediction model under different channel environments that uses instantaneous  $LQI$  readings as input. The proposed model is validated through extensive simulation and experiment study. We believe it will lead to more informed resource management decisions in WPANs.

**Joint Neighboring and Contention Relationships Inference:** We investigate the problem of joint neighbor discovery and contention relationships inference in ad-hoc WPANs with multiple broadcast domains. An active inference algorithm is proposed, called the ternary inference algorithm, that utilizes decentralized randomized schedules to infer the neighboring and contention relationships through mixed signal at the receiver nodes. Simulation studies show that the proposed algorithm outperforms an Aloha-like algorithm in neighbor discovery time, and can achieve high accuracy in determining the relationships.

**Joint Relay Placement and Routing Selection:** We explore a relay placement and route selection solution in IEEE 802.15.3c mmWave based WPANs for better resource provisioning. To combat the uncertainty in link failure, two robust problems are formulated, robust minimum relay placement (RMRP) and robust maximum utility relay placement (RMURP), with the objective to minimize the number of relays deployed and maximize the network utility, respectively. We first consider an interference-free model, then extend the work by incorporating a classic directional antenna model and characterizing the link contention. By applying D-norm uncertainty model in robust optimization theory, RMRP and RMURP can be reformulated into mixed integer linear programming (MILP) and mixed integer nonlinear programming (MINLP). Efficient algorithms are developed to solve both problems and have been shown to incur less service disruption in presence of moving subjects that may block the LOS

paths in the environment.

## 1.4 Organizations of This Thesis

This dissertation is organized as follows: In Chapter 2, we study link quality prediction in IEEE 802.15.4 Zigbee based WPANs, where an inference model is proposed to predict the instantaneous link quality parameters using LQI readings. In Chapter 3, we present efficient solutions to joint neighbor discovery and contention graph inference in ad-hoc WPANs. In Chapter 4, we explore the relay placement and routing selection problem in IEEE 802.15.3c mmWave based WPANs and propose two robust formulations. We first present an interference-free model, and then extend to a more complex interference model with directional antenna. Finally, we summarize our contributions and discuss potential research directions for future work.

## Chapter 2

# Reliable Link Quality Prediction in WPANs

### 2.1 Introduction

One major challenge that wireless network designers and operators are facing is the real-time estimation of PHY and MAC characteristics. Unfortunately, commercial-of-the-shelf (COTS) devices typically only provide limited information regarding the current condition of wireless channels. The lack of detailed PHY knowledge for cross-layer resource management and provisioning usually leads to misinformed decisions and under-utilization of available resources.

For example, IEEE 802.15.4 Zigbee radios with TI CC2420 chipset only provide received signal strength indicator (*RSSI*), link quality indicator (*LQI*), which are stored in frame check sequence (FCS) of MAC frames. However, there has been the under-determined ambiguity regarding those readings collected at Zigbee radios.

- Is *RSSI* a good index for channel condition?
- Does *LQI* really characterize the link quality?
- Is there a direct way to obtain the instantaneous link quality such as bit error rate (BER) or packet error rate (PER)?

For instance, most wireless interfaces cannot distinguish received signal strength from interference and instead provide a single received signal strength indicator (*RSSI*) number<sup>1</sup>. Based on the assumption that *RSSI* reflects received signal strength and there is a correlation between received signal strength and signal-to-noise ratio (*SNR*), many studies suggest to use *RSSI* information for rate adaptation

---

<sup>1</sup>Roughly speaking, separation of the two requires subtraction of useful signal from the total received signal strength after decoding.

or route selection for packet forwarding [17–19]. However, recent works have proved that it is not an accurate index [20–22].

To address the deficiency of *RSSI* in predicating link quality, authors in [23–25] suggest the use of link quality indication (*LQI*), which is an output required by the IEEE 802.15.4 protocol to indicate the quality of a received packet. In the CC2420 datasheet [26], a correlation value (*CORR*) is supplied by the chip that “provides an average correlation value for each incoming packet, based on the 8 first symbols following the SFD” (start of frame delimiter). Furthermore, “software must convert the correlation value to the range 0-255”, “by calculating  $LQI = (CORR - a) \cdot b$ ”, “where  $a$  and  $b$  are found empirically based on PER measurements as a function of correlation value” (presumed by each manufacturer separately). However, the fundamental question remains, how to use *LQI* to predict the real instantaneous link quality? On the practical side, how to determine  $a$  and  $b$ ?

### 2.1.1 Contributions

The main goal of our research is to revisit the issue of link quality prediction in IEEE 802.15.4 low rate wireless personal area networks (LR-WPAN) and try to understand the available readings available at commodity Zigbee radios.

We make several contributions to this topic:

- We decipher the *LQI* measurements in 802.15.4 Zigbee radios, and demonstrate that *LQI* truly reflects the signal-to-noise ratio (*SNR*) at receiver. To the best of our knowledge, our work is the first that provides experimental evidence to link the two qualities.
- We also provide an analytical form for the chip correlation (*CORR*) defined in TI CC2420 data sheet, and establish the relationship between *LQI* and *CORR* through both simulation and measurement studies.

- In order to predict the instantaneous link quality (e.g., *SER*, *PER*) for commodity Zigbee radios, we develop an inference model under different channel environments that uses instantaneous *LQI* readings as input. The proposed model is validated using extensive simulation and experimental study. We believe it will lead to more informed resource management decisions in WPANs.

## 2.2 Preliminaries

### 2.2.1 IEEE 802.15.4 Zigbee

The IEEE 802.15.4 is a standard for low-rate wireless personal area networks (LR-WPANs), which provides a simple wireless connectivity, relaxed throughput, low power, short distance and low cost wireless solution [5]. 802.15.4 radio has a bandwidth of 5 MHz, but most of the energy is within a 2 MHz band. It operates in the 2.4 GHz ISM bands, and uses 16-ary quasi-orthogonal modulation. A 32-chip direct sequence spread spectrum (DSSS) code is used to spread the signal and achieve both processing coding and processing gain. Bits come from the physical protocol data unit (PPDU), which handles the physical framing, at a data rate of 250 kbit/s. The bits get converted to data symbols of 4 bits, and each symbol is spread according a given spreading sequence. Before transmission, the stream of chips (at rate 2 Mchip/s) are modulated on the carrier using offset quadrature phase shift keying (OQPSK) with half-sine pulse shaping. A non-coherent receiver is typically used to demodulate the OQPSK signal, which is then passed into a clock recovery block and output symbols for slicing. After chip to symbol de-spreading, the MAC Protocol Data Unit (MPDU) is recovered. The frame structure of IEEE 802.15.4 is presented in Figure 2.1.

Zigbee Alliance is an industrial organization with a mission to define reliable, cost-effective, low-power wireless networked, monitoring and control products based

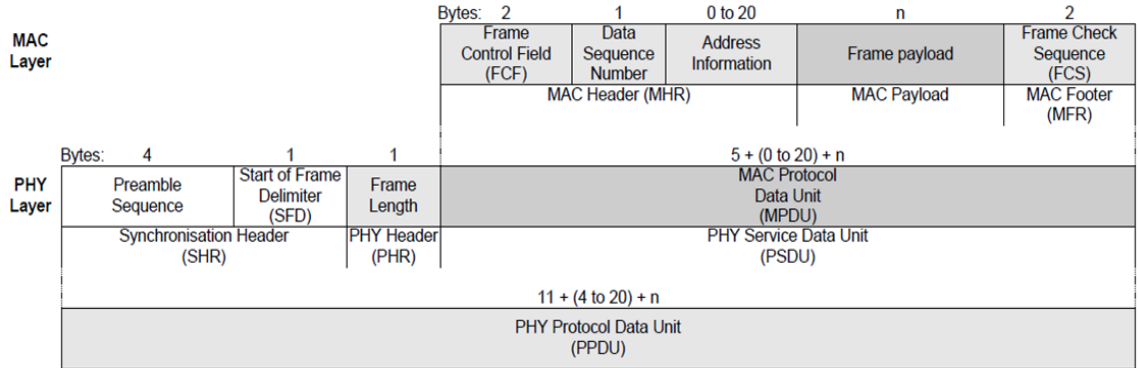


Figure 2.1: IEEE 802.15.4 frame structure

on an open global standard. It takes full advantage of a power physical radio specified by IEEE 802.15.4 and continues to work closely with IEEE to ensure an integrated and complete solution for the market. The Alliance provides the inter-operability, certification testing and branding for IEEE 802.15.4 compliant Zigbee radios from different manufacturers.

## 2.2.2 Hardware and Software Toolkits

In this section, we introduce the hardware and software toolkits used for measurement study.

### 2.2.2.1 Tmote-Sky Sensor Module

Developed by the University of California-Berkeley, Tmote-Sky (also named as Telos-B) from Moteiv Corporation is an ultra low power IEEE 802.15.4 compliant wireless sensor module. It has been widely used in sensor networks, monitoring applications and other prototype applications.

Tmote-Sky sensors boast several key features. First, it is the first available IEEE 802.15.4 wireless transceiver supporting 250kbps on 2.4 GHz using Texas Instrument Chipcon CC2420 [26]. With ultra low current consumption, it provides an integrated

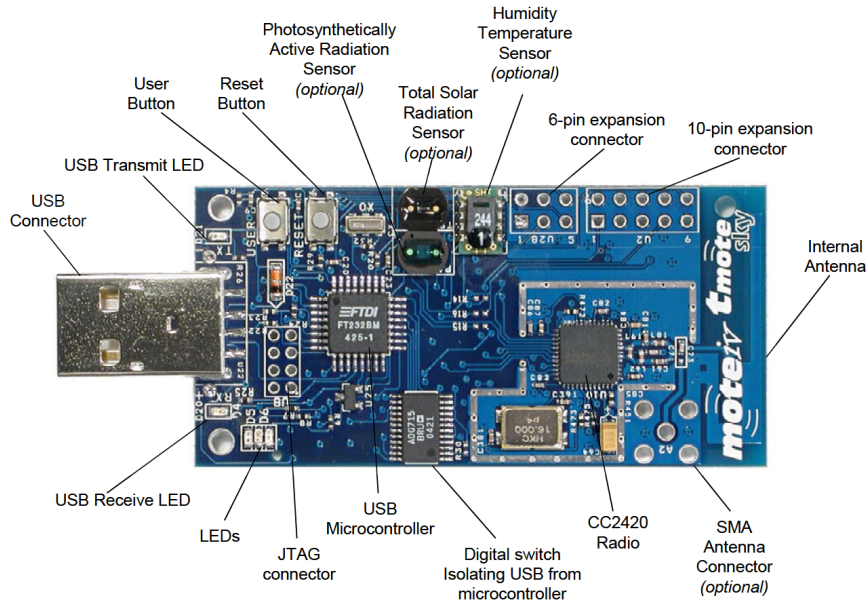


Figure 2.2: Tmote-Sky wireless sensor

on-board antenna which can reach up to 50m range indoors and 125m range outdoors and enables fast wakeup from sleep (less than  $6\mu s$ ). For easy development, Tmote-Sky uses the USB protocol to connect with a host machine for programming, debugging and data collection. The Tmote-Sky nodes can also connect with additional devices such as digital peripherals and GPS receivers, through two expansion (6-pin and 10-pin) connectors as shown in Figure 2.2.

#### 2.2.2.2 USRP & GNU-Radio

The Universal Software Radio Peripheral (USRP) is designed and sold by Ettus Research to provide the solution of computer-hosted software defined radios. As a comparatively inexpensive hardware platform for software defined radios, the USRP product family has been commonly used by a lot of research labs and universities.

The architecture of software-defined radio using USRP is presented in the Figure 2.3. USRPs connect to a host computer through a high-speed USB or Gigabit Ethernet link that is used by the host-based software to control the USRP hardware and transmit/receive data. Each USRP has a mother-board and a daughter-board.

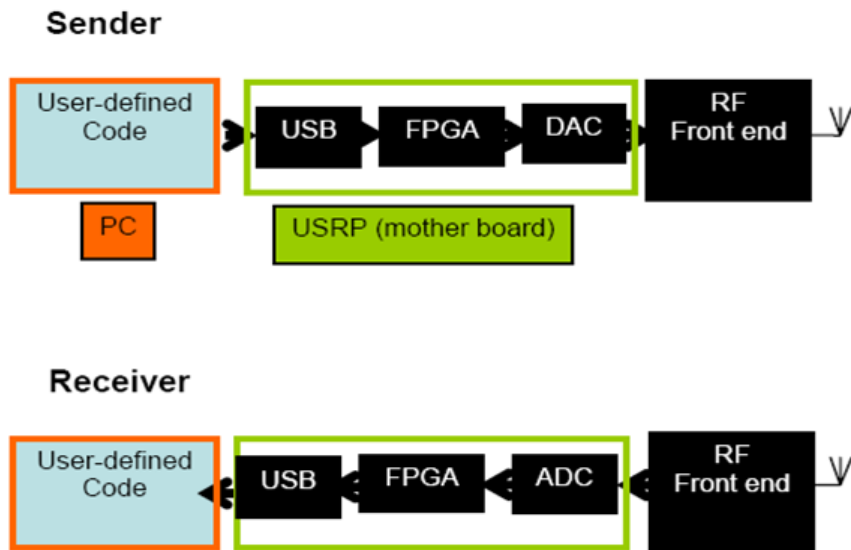


Figure 2.3: Software-defined radio architecture using USRP



Figure 2.4: USRP2 hardware platform by Ettus Research

The mother-board provides the basic components for baseband processing of signals, including FPGA, analog-to-digital converters, digital-to-analog converters, clock generation and synchronization and etc. The daughter-board is a modular RF front-end used for analog operations such up/down conversion, filtering and other signal processing. The advantage of modularity is to permit the USRPs to serve different applications that operate between DC and 6 GHz.

GNU-Radio is an well-known open source software development kit that provides signal processing blocks to implement software-defined radios in host-computers.

By designing performance-critical signal processing path in C++ using processor float-point extensions and writing the applications in Python, the developer is able to implement a real-time, high-throughput radio systems in a simple-to-use, application-development environment. The newest GNU-Radio version can support different distributions of Linux as well as Windows.

The USRP platform with GNU-Radio toolkit has been widely used in many research efforts on wireless radio design. In one of our previous works, we employed GNU-Radio to obtain the RF features of Zigbee motes for device identification [27]. We also applied GNU-Radio in MAC design of WiFi, in which we proposed WiCop, an open-source SDR solution that can help to engineer WiFi temporal white spaces for the transmissions of safety-critical wireless personal area networks in medical applications [11].

In this work, we select USRP2 in the Figure 2.4 and the daughter-board XCVR2450 to generate the controlled Gaussian noise signals at 2.4GHz ISM band. We installed GNU-Radio 3.2.2 in Ubuntu 9.10. The installation note can be found at [28].

## 2.3 Measurement Study of *RSSI* and *LQI*

In this section, we examine the ambiguity regarding the *RSSI* and *LQI* readings collected at Zigbee radios through measurement study. Our objective is to decipher the readings of *RSSI* and *LQI* and perform the reverse engineering.

### 2.3.1 Deciphering *RSSI*

To find out the relationship of *RSSI* with the receive signal strength and interference level, we have setup the measurements using Tmote-Sky sensors with TI CC2420 chipset [26] and Universal Software Radio Peripheral (USRP2) [28] boards supported by GNU Radio software suite. In the measurements, one fixed node acts

as a transmitter and the other node operates as a receiver, connecting through SMA coaxial cables (the so-called cabled connection) to approximate an additive white Gaussian noise (AWGN) channel. In addition to the fixed transmit signal, a controlled varying Gaussian noise generated from USRP2 is also injected to the receiver via a SMA coaxial cable. At each noise level, 1000 packets with the packet length of 40 bytes are transmitted and two types of *RSSI* readings are recorded, signal *RSSI* and noise floor <sup>2</sup>:

- signal *RSSI* corresponds to the received signal strength reported by Zigbee receiver during packet transmission;
- noise floor reports the power of ambient noise recorded between packets.

Zigbee Channel 26 (2.479GHz - 2.481GHz) is used in the experiments to avoid unintended interference from the campus WiFi network. Packet errors are detected using the cyclic redundancy check (*CRC*), while symbol error rate (*SER*) is determined by comparing the known bit pattern in the transmitted packets with the received packets. The Agilent spectrum analyzer N9020A is also utilized in the measurements for cross validation.

Figure 2.5 shows the signal *RSSI* and noise floor with respect to the noise levels controlled by USRP2 in the cabled connection environment. Attenuators are used to attenuate transmit signal for a wider range of readings. From the figure, a few observations can be made. First, as the controlled noise level increases, both *RSSI* and noise floor indeed increases. This is consistent with the observations made by other researchers [20–22]. Second, *RSSI* is always bigger than noise floor, which is consisted with the fact that *RSSI* is roughly the sum of the actual received signal strength and the noise floor. However, we found both *RSSI* and noise floor are not always linear with the actual noise floor due to quantization errors and other factors,

---

<sup>2</sup>In this work, we do not distinguish the noise from interference.

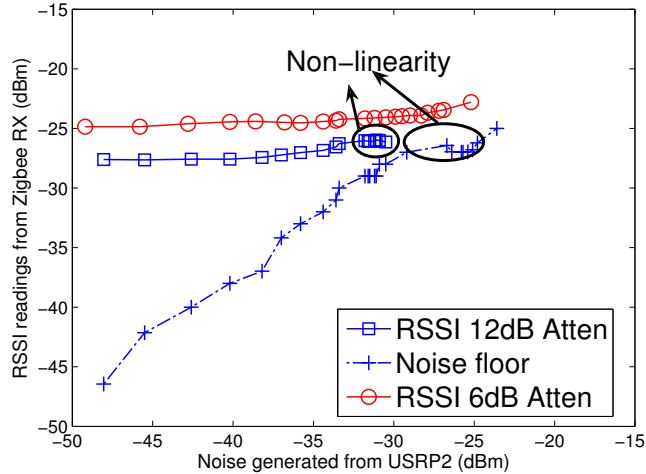


Figure 2.5: Signal  $RSSI$  and noise floor readings VS. Gaussian noise generated by USRP2 in the cabled connection environment on channel 26. Two different attenuators are used, 6dB and 12dB.

as indicated by the black ellipses. Non-linearity was first reported in [29]. In our experiment, we observed that there are two non-linearity regions as wide as 6dB in  $RSSI$  and noise floor readings reported by Zigbee devices, locating around -26dBm and -58dBm. Clearly, due to the non-linearity, the difference between  $RSSI$  and noise floor readings is not a reliable measure to approximate  $SNR$ .

### 2.3.2 Deciphering $LQI$

Next, we continue the experiments to verify if  $LQI$  is a good index of link quality using the same setup. In addition to controlling the noise generated by USRP2, we further control the received signal strength by using commercial microwave-rated attenuators to obtain a wider  $SNR$  range. In this experiment, the  $SNR$  is determined from the signal strength and noise floor measured directly from a spectrum analyzer across a 2MHz bandwidth.

Figure 2.6 shows the relationship between the measured  $LQI$  and the measured  $SNR$  for three TmoteSky Zigbee nodes on channel 26. The curves of all three nodes are approximately linear and are close to one another. The small gap between the

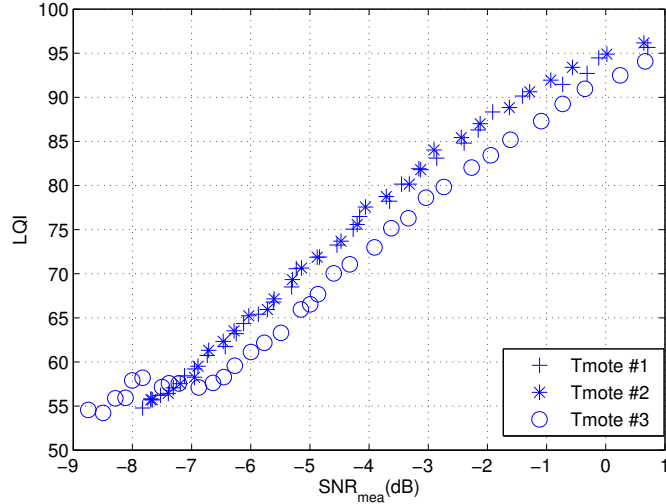


Figure 2.6:  $LQI$  readings Vs. the measured  $SNR$  for different TmoteSky Zigbee nodes in the cabled connection environment on channel 26.

curve of Tmote #3 and the others is likely due to manufacturing artifacts. Thus, we can model  $LQI$  measurement(dBm) and  $SNR$ (dB) as

$$LQI = p_1 \times SNR + p_2, \quad (2.1)$$

where  $p = [p_1 \ p_2]$  are the factors obtained using linear regression. From the experiments, we have  $p_1 = 5.3145$ ,  $p_2 = 97.0477$ .

From the measurement results, we observe that the  $LQI$  readings in Zigbee chipset reflect a very good approximation of the instantaneous  $SNR$  values at the receiver. This is seemingly inconsistent with the specification, which states that the  $LQI$  is calculated from the  $CORR$  values from the first 8 symbols. Next, we provide an analytical study to support our claim that these two are in fact in line with one another.

## 2.4 Analytical Model of $CORR$

For analysis, we focus on the baseband process of decoding symbols after the demodulator and model the modulator/demodulator as part of the channel.

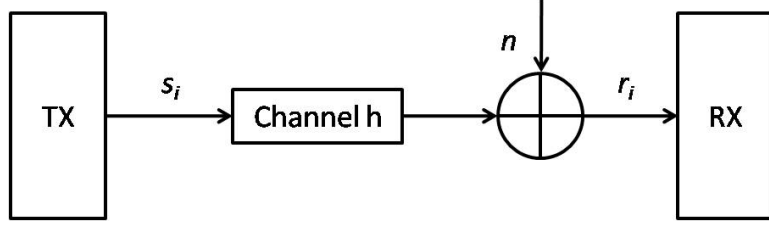


Figure 2.7: Basic communication model.

As demonstrated in Figure 2.7, the received signal at RX is described as

$$\vec{r}_i = h\vec{s}_i + \vec{n}, \quad (2.2)$$

where  $h$  is the channel response,  $\vec{n}$  is the additive white Gaussian noise vector,  $n_k \sim \mathcal{N}(0, \sigma_n^2), k = 1, 2, \dots, N$ . Note that  $\vec{s}_i$ ,  $\vec{n}$  and  $\vec{r}_i$  are  $N \times 1$  vectors, and  $N$  is the number of chips, i.e.,  $N = 32$ .

Thus, the received signal power and noise power per symbol can be computed as

$$P_s = \langle h\vec{s}_i, h\vec{s}_i \rangle = C_{ii}h^2, \quad P_n = N * 2\sigma_n^2 = 64\sigma_n^2, \quad (2.3)$$

and the received  $SNR$  is calculated as

$$\rho = \frac{P_s}{P_n} = \frac{C_{ii}h^2}{64\sigma_n^2} = \frac{h^2}{2\sigma_n^2}. \quad (2.4)$$

#### 2.4.1 Derivation of Chip Correlation

Based on the TI CC2420 data sheet [26], we define the chip correlation( $CORR$ ) as follows,

$$CORR = \frac{1}{8} \sum_i \max_j \langle \vec{r}_i, \vec{s}_j \rangle. \quad (2.5)$$

In other words,  $CORR$  is the inner product between the received signal with the symbol (possibly erroneous) that has the maximum correlation, averaged over first 8 symbols following the start of frame delimiter (SFD) [26].

If we define

$$v_{ij} = \langle \vec{r}_i, \vec{s}_j \rangle = hC_{ij} + n^T s_j, \quad (2.6)$$

$$Z_i = \max_j(v_{ij}).$$

Then  $v_{ij}$  is a Gaussian random variable with mean and variance:

$$E(v_{ij}) = E(hC_{ij} + n^T s_j) = hC_{ij}, \quad (2.7)$$

$$Var(v_{ij}) = Var(hC_{ij} + n^T s_j) = \sigma_n^2 C_{jj}.$$

For a fixed  $i$ ,  $\vec{v}_i = [v_{i1}, v_{i2}, \dots, v_{iN}]$  is a multi-dimensional Gaussian random vector, with a joint probability density function (*PDF*) as

$$f_{\vec{v}_i}(v_{i1}, v_{i2}, \dots, v_{iN}) = \frac{1}{(2\pi)^{N/2} \det(\Sigma)^{1/2}} e^{-\frac{1}{2}(\vec{v}_i - \vec{\mu})^T \Sigma^{-1} (\vec{v}_i - \vec{\mu})}. \quad (2.8)$$

The covariance matrix  $\Sigma$  has non-zero off-diagonal elements. More specifically,  $\Sigma_{kk} = Var(v_k) = \sigma_n^2 C_{kk}$ , and  $\Sigma_{kl} = \sigma_n^2 C_{kl}$ .

Table 2.1: Correlation matrix of quasi-orthogonal modulation

$S_i$	1	2	3	4	5	6	7	8	9	10	11	12	13	14	15	16
1	32	0	-4	-8	-8	-8	-4	0	0	8	4	-8	-8	-8	4	8
2	0	32	0	-4	-8	-8	-8	-4	8	0	8	4	-8	-8	-8	4
3	-4	0	32	0	-4	-8	-8	-8	4	8	0	8	4	-8	-8	-8
4	-8	-4	0	32	0	-4	-8	-8	-8	4	8	0	8	4	-8	-8
5	-8	-8	-4	0	32	0	-4	-8	-8	-8	4	8	0	8	4	-8
6	-8	-8	-8	-4	0	32	0	-4	-8	-8	-8	4	8	0	8	4
7	-4	-8	-8	-8	-4	0	32	0	4	-8	-8	-8	4	8	0	8
8	0	-4	-8	-8	-8	-4	0	32	8	4	-8	-8	-8	4	8	0
9	0	8	4	-8	-8	-8	4	8	32	0	-4	-8	-8	-8	-4	0
10	8	0	8	4	-8	-8	-8	4	0	32	0	-4	-8	-8	-8	-4
11	4	8	0	8	4	-8	-8	-8	-4	0	32	0	-4	-8	-8	-8
12	-8	4	8	0	8	4	-8	-8	-8	-4	0	32	0	-4	-8	-8
13	-8	-8	4	8	0	8	4	-8	-8	-4	0	32	0	32	0	-4
14	-8	-8	-8	4	8	0	8	4	-8	-8	-8	-4	0	32	0	-4
15	4	-8	-8	-8	4	8	0	8	-4	-8	-8	-8	-4	0	32	0
16	8	4	-8	-8	-8	4	8	0	0	-4	-8	-8	-8	-4	0	32

Determination of the distribution of  $Z_i = \max_j(v_{ij})$  is non-trivial since  $Z_i$  may not be the symbol sent. However, in a relatively good channel condition, the perfect decoding can be assumed, in which  $Z_i$  always returns the max correlation of the symbol actually sent. Therefore, the mean and variance of  $CORR$  can be approximated as

$$\begin{aligned}\mu_{CORR} &\approx \frac{1}{8} \sum_i E[\langle hs_i + n, s_i \rangle] = hC_{ii}, \\ \sigma_{CORR}^2 &\approx \frac{1}{8} Var[\langle hs_i + n, s_i \rangle] = \frac{1}{8} C_{ii} \sigma_n^2 = 4\sigma_n^2.\end{aligned}\tag{2.9}$$

Combining with (2.4), we can obtain the estimated  $SNR$  in terms of  $\mu_{CORR}$  and  $\sigma_{CORR}$  as

$$SNR_{est} = \frac{2\mu_{CORR}^2}{C_{ii}^2 \sigma_{CORR}^2}.\tag{2.10}$$

## 2.4.2 Simulation Validation

Simulations are setup based on the IEEE 802.15.4 standard [5], with focus on the encoding and decoding procedure. The wireless channel is assumed to be flat and the noise floor is approximately -111dBm<sup>3</sup>. We vary the channel gain  $h$  or the transmitted signal power to represent different locations. For each location, 1000 packets are sent from TX to RX independently, each has 40 symbols. Symbol-by-symbol decoding is conducted by finding the one with the maximum correlation with the received symbol.

Figure 2.8 shows the estimated  $SNR$  from formula (2.10) averaged over 1000 packets and the true  $SNR$ . As shown in the figure, the perfect decoding obtains good accuracy in approximating  $SNR$  when  $SNR$  is larger than -8dB, which is the typical operating regime of Zigbee receivers. The difference between the estimated and true

---

<sup>3</sup>For Zigbee radios in 2.4GHz with 2MHz bandwidth,  $NF(dBm) = -174 + 10\log_{10}(BW)$  is used as a lower bound of the noise floor level.

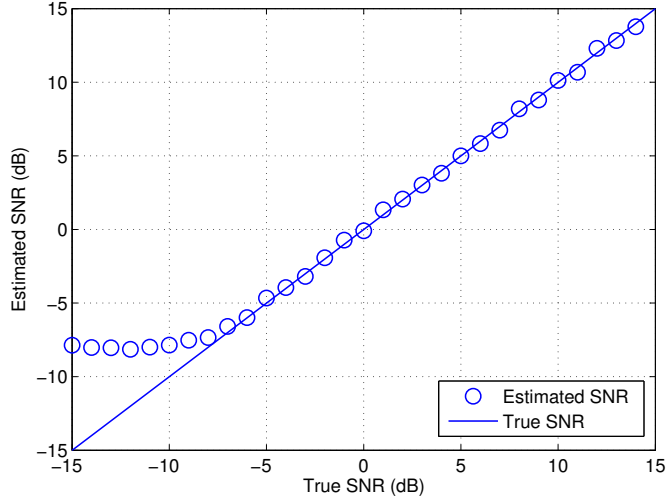


Figure 2.8: The estimated  $SNRs$  from  $CORR$  averaged over 1000 packets in the simulation of perfect decoding.

$SNR$  becomes larger in the low  $SNR$  regime. This is mainly because the assumption of perfect decoding no longer holds.

To this end, we have established an approximation for the relationship between  $SNR_{est}$  and  $\mu_{CORR}$  as well as  $\sigma_{CORR}$  for the IEEE 802.15.4 Zigbee radios. From formula (2.10), we see that  $SNR$  is linear with respect to the ratio of the square of the mean and variance of the  $CORR$ . Recall that the measurement study shows that  $SNR$  is roughly linear to  $LQI$ , as described as (2.1). This implies that  $LQI$  can be determined by the mean and variance of  $CORR$  values for  $SNR > -8dB$ . Thus, we can describe the relation between  $LQI$  measurement and  $CORR$  as

$$LQI = (V - a) * b, \quad (2.11)$$

where  $V$ ,  $a$  and  $b$  can be computed respectively as:

$$V = 10 \log_{10} \left( \frac{\mu_{CORR}^2}{\sigma_{CORR}^2} \right), \quad (2.12)$$

$$a = -10 \log_{10} \left( \frac{2}{C_{ii}^2} \right) - \frac{p_2}{p_1}, \quad b = p_1.$$

Note that,  $a$  and  $b$  are the calibration parameters tracked from the empirical experiments.

## 2.5 Proposed Link Quality Prediction Model Using *LQI*

The *SER* measure typically defines as the index for link quality. However, to measure *SER* generally requires a large number of packets. In this section, we explore a link quality prediction model to determine the instantaneous link quality from *LQI*.

### 2.5.1 Derivation of Link Quality

At the receiver, a symbol error occurs when the symbol decoded is not the same as the transmitted one. Thus, let  $\langle x, y \rangle$  be the inner product of vector  $x$  and  $y$ , *SER* can be derived as,

$$P_{e|(i,j)} = Prob\{\langle \vec{r}_i, \vec{s}_i \rangle < \langle \vec{r}_i, \vec{s}_j \rangle \mid TX \text{ sends } i, RX \text{ decides } j\}, \quad (2.13)$$

where  $r_i$  is the received signal when  $i$  symbol is sent,  $s_i$  and  $s_j$  are binary chip sequences for the  $i$ th and  $j$ th symbol ( $i \neq j$ ), respectively. Applying (2.2), we have

$$\begin{aligned} P_{e|(i,j)} &= Prob\{\langle h\vec{s}_i + \vec{n}, \vec{s}_i \rangle < \langle h\vec{s}_i + \vec{n}, \vec{s}_j \rangle \mid (i, j)\} \\ &= Prob\{hC_{ii} + \langle \vec{n}, \vec{s}_i \rangle < hC_{ij} + \langle \vec{n}, \vec{s}_j \rangle \mid (i, j)\} \\ &= Prob\{(\vec{s}_j - \vec{s}_i)^T \vec{n} > h(C_{ii} - C_{ij}) \mid (i, j)\}, \end{aligned} \quad (2.14)$$

where  $C_{ij} \triangleq \langle \vec{s}_i, \vec{s}_j \rangle$ .

Since  $\vec{n}$  is a vector of independent Gaussian random variables,  $n_x = (\vec{s}_j - \vec{s}_i)^T \vec{n}$  is also Gaussian distributed with expectation and variance as:

$$\begin{aligned} E(n_x) &= E[(\vec{s}_j - \vec{s}_i)^T \vec{n}] = 0, \\ Var(n_x) &= E(n_x^2) - E(n_x)^2 = E[(\vec{s}_j - \vec{s}_i)^T \vec{n} \vec{n}^T (\vec{s}_j - \vec{s}_i)] \\ &= \sigma_n^2 E[\vec{s}_j^T \vec{s}_j - \vec{s}_j^T \vec{s}_i - \vec{s}_i^T \vec{s}_j + \vec{s}_i^T \vec{s}_i] \\ &= 2\sigma_n^2 (C_{ii} - C_{ij}). \end{aligned} \quad (2.15)$$

Clearly,  $C_{ii} > C_{ij}$ . Given a specific  $i$  and  $j$ , the *SER* can be further written as the tail probability,

$$P_{e|(i,j)} = Q \left[ \sqrt{\frac{h^2(C_{ii} - C_{ij})}{2\sigma_n^2}} \right]. \quad (2.16)$$

Assuming that the symbol error is dominated by the nearest neighbors (In Zigbee system, i.e., the neighbors with cross-correlation equal to  $\pm 8$  in the correlation matrix (Table 2.1)), we can approximate for each transmitted symbol  $i$  the conditional error probability as

$$\begin{aligned} P_{e|i} &= \sum_j P_{e|(i,j)} P(j) \approx 128 * \frac{1}{16} * Q \left( \sqrt{\frac{h^2(C_{ii} - C_{ij})}{2\sigma_n^2}} \right) \\ &= 8Q \left( \sqrt{\frac{3C_{ii}h^2}{8\sigma_n^2}} \right). \end{aligned} \quad (2.17)$$

Therefore, under the assumption that all symbols are transmitted with equal probability, the *SER* is given by

$$P_{SER} = \sum_i P_{e|i} P(i) = 8Q \left( \sqrt{\frac{3C_{ii}h^2}{8\sigma_n^2}} \right), \quad (2.18)$$

where  $C_{ii} = 32, \forall i$ , is the autocorrelation of the  $i$ th symbol.

After applying (2.4), we can rewrite (2.18) as

$$P_{SER} = 8Q \left( \sqrt{24\rho} \right). \quad (2.19)$$

Note that, (2.19) is the general formula of the symbol error rate in the IEEE 802.15.4, where  $h$  depends on different channel models, e.g., for *AWGN* channel,  $h=1$ .

The Rayleigh fading channel with no line-of-sight (LOS) can be modeled as a complex Gaussian random variable  $h \sim \mathcal{CN}(0, \sigma^2)$  [30], where the *PDF* of amplitude is given by

$$f(r) = \frac{r}{\sigma^2} \exp \left( \frac{-r^2}{2\sigma^2} \right), r \geq 0, \quad (2.20)$$

and the square of the amplitude is exponentially distributed [30]. Thus, for standard Rayleigh fading where  $\sigma = 1$ , the corresponding  $SEER$  can be computed as

$$P_{SEER} = E_{\|h\|} \left[ 8Q(\sqrt{24\rho}) \right] = 4 \left( 1 - \frac{1}{\sqrt{\sigma_n^2/6 + 1}} \right). \quad (2.21)$$

Similarly, for Rician channel, the  $SEER$  is given by

$$P_{SEER} = \frac{1}{M} \sum_{i=2}^M (-1)^i \binom{M}{i} \frac{(1+K)/\rho}{(1+K)/\rho + 1 - 1/i} \cdot \exp \left( -\frac{K(1 - 1/i)}{(1+K)/\rho + 1 - 1/i} \right), \quad (2.22)$$

where  $M$  denotes the codebook of 32 symbols,  $K$  is the ratio of the signal power in LOS path over the scattered power in non-LOS paths [31].

In summary, given the knowledge of channel environment, we can predict the  $SEER$  based on the  $SNR$  level at the receiver by selecting the proper formula (2.19) (2.21) or (2.22). The  $BER$  and  $PER$  can be computed from  $SEER$  as well. Since from (2.1), we can rewrite as

$$\rho(dB) = (LQI - p_2)/p_1. \quad (2.23)$$

Then, we can build up the one-by-one mapping between the link quality  $SEER$  and  $LQI$  readings as:

$$P_{SEER} = \mathcal{F}(LQI), \quad (2.24)$$

where  $\mathcal{F}$  denotes the mapping function. Finally, as described in our analytical model,  $SEER$  can be determined only based on the  $LQI$  readings available on Zigbee radios.

## 2.5.2 Simulation Validation

The simulation setup is similar to the previous section. For each  $SNR$ , 10000 packets are sent from TX to RX. We compare the  $SEER$  performance of the Zigbee

radio under different fading channel models, including AWGN, Rician fading with  $K=6$ dB and the Rayleigh fading channel.

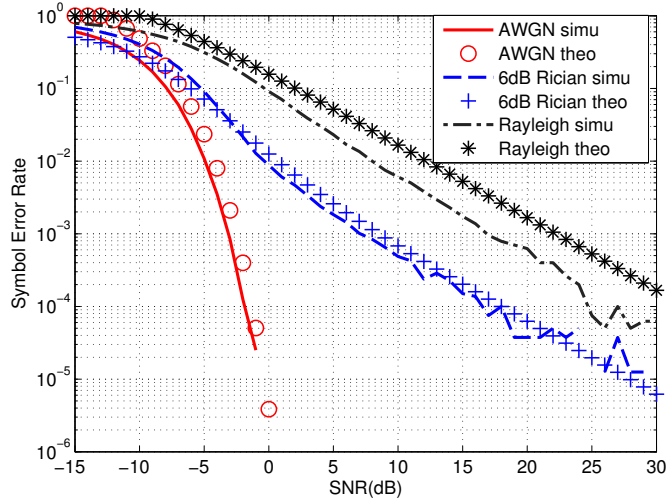


Figure 2.9: *SER* performance with respect to *SNR* for AWGN, Rician with  $K=6$  and Rayleigh fading environment respectively. Both simulated and theoretical curves are plotted.

As shown in Figure 2.9, when the channel condition degrades (from AWGN to Rayleigh), the *SER* degrades as expected. Furthermore, theoretical and simulation results agree very well. Specifically, for a fixed *SER*, the prediction error in the Rayleigh channel is around 4dB. Another important observation is, when the received *SNR* is smaller than -8dB, the *SER* performance degrades to less than 10% for all channel models, which is out of Zigbee operational range for almost all the applications. This further validates our analytical model using *CORR* to estimate the received *SNR* under the assumption of perfect decoding.

## 2.6 Experiment Results

In this section, we conduct the field experiments to validate the analytical model under two different settings, namely, the cabled connection environment to emulate the AWGN channel and an outdoor environment with LOS as the Rician channel. Zigbee channel 26 is used to avoid the unnecessary external interferences.

In the AWGN channel, we vary the noise levels generated by USRP2 to emulate different  $SNR$  conditions. In the outdoor setting, we vary the transmitter’s locations while keeping the receiver node fixed, to emulate different fading and shadowing environments. For each transmitter location, 1000 packets are transmitted from TX to RX. Along with each packet, the  $LQI$ , signal  $RSSI$  and noise floor readings are recorded. Then, the instantaneous  $SNR$  are computed as signal  $RSSI(\text{dBm})$  minus noise floor( $\text{dBm}$ ). The measured  $SER$  are determined by comparing the known bit pattern in the transmitted packets with the received packets. Our purpose is to compare the predicted  $SER$  inferred in our model based on the instantaneous  $LQI$  readings with the measured  $SER$  from experiment.

### 2.6.1 Cabled Connection Environment

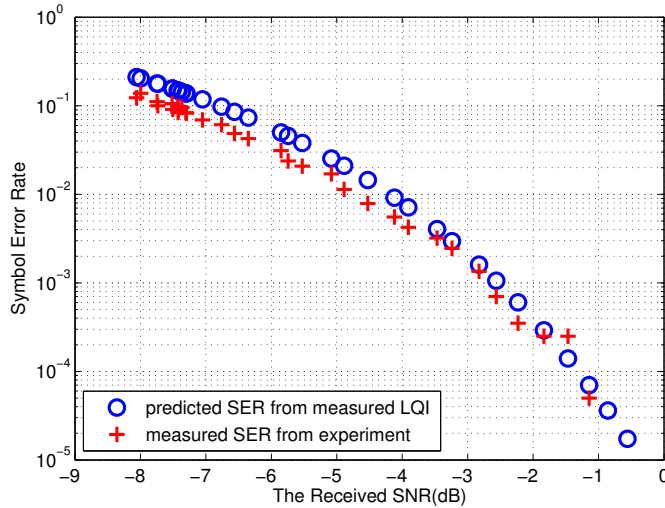


Figure 2.10: Comparison of the predicted  $SER$  from  $LQI$  readings and the measured  $SER$  with respect to the received  $SNR$  in the cabled connection environment.

Figure 2.10 shows the  $SER$  performance corresponding to the received  $SNR$  in a cabled connection environment. The blue circles denote the predicted  $SER$  values, which is computed from  $LQI$  based on our analytical model in section 2.5. The red pluses represent the measured  $SER$  which is used to evaluate our inference model.

As shown in the figure, the predicted  $SE_R$  matches very well with the measured one. When  $SNR$  increases, the gap decreases as expected.

### 2.6.2 Outdoor Environment

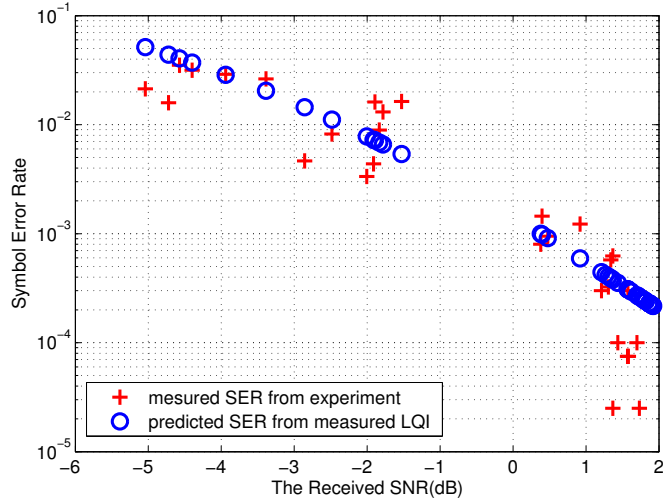


Figure 2.11: Comparison of the predicted  $SE_R$  from  $LQI$  readings and the measured  $SE_R$  with respect to the received  $SNR$  in the outdoor channel environment.

Figure 2.11 shows the result for the outdoor setting. We select the formula of Rician channel with the parameters  $M=4$  and  $K=12\text{dB}$  in our analytical model<sup>4</sup>. Although the measured  $SE_R$  fluctuates due to fading, the predicted  $SE_R$  is close to the measured value in general. However, in the high  $SNR$  region, the predicted  $SE_R$  errors on the higher side. This is mainly because when nodes are very close, the Rician channel model with  $M = 4$  and  $K = 12\text{dB}$  may not be suitable any more.

## 2.7 Summary

The link quality prediction is important for better system provisioning and resource management. In this chapter, we have utilized both analytical modeling with simulations as well as measurement study to decipher  $LQI$  readings from Zigbee

<sup>4</sup>Determination of the Rician channel parameters from measurements will be considered in our future work.

radios. The key finding is that  $LQI$  is in fact linear with respect to the instantaneous  $SNR$  over the operational range of Zigbee radios. As a result,  $LQI$  can be used as an input to the proposed analytical model to predict instantaneous link quality  $SER/PER$  given the knowledge of channel models. We believe our study will lead to more informed resource management decisions in WPANs.

## Chapter 3

# Joint Neighbor Discovery and Contention Relationship Inference in ad-hoc WPANs

### 3.1 Introduction

Neighbor discovery and contention relationship inference are two corner stones of operating and managing wireless networks such as WPANs. Neighbor discovery identifies communicating peers in proximity, while contention relationship (or conflict graph) characterizes whether multiple transceiver pairs can transmit concurrently without severely degrading the respective packet delivery. For static networks, the two procedures are typically carried out in the bootstrapping phase. In semi-stationary networks, periodical discovery is needed. In both cases, fast and accurate neighbor discovery and contention relationship inference are instrumental in many resource management decisions such as channel and spectrum allocation, power control, routing and scheduling.

In this dissertation, we investigate joint neighbor discovery and contention relationship inference, while most existing work focuses on one of the two problems. We propose an active algorithm, called the ternary inference algorithm, that utilizes decentralized randomized schedules to infer the neighboring and contention relationships through the mixed signal at the receiver nodes. In contrast to [32, 33], we represent neighboring relationship as ternaries  $\{1, 0, \delta\}$  based on the strength of the received signal. A procedure akin to group testing is devised to infer the neighbor and contention relationship. A t-tolerance variant is further introduced to improve the robustness to observation and inference errors. We analyze the sources of errors in the proposed scheme, and evaluate the impact of loose synchronization, network size, and other parameter settings. The simulation results demonstrate the superior

performance of the proposed algorithm in terms of completion rate and accuracy.

### 3.1.1 Contributions

The main objective of our work is to develop efficient solutions to neighbor discovery and contention relationship inference by using active measurements in ad-hoc WPANs. We have made several contributions toward this objective:

- We present the ternary inference algorithm that utilize group testing to infer the neighbor and contention relationship.
- We further introduce a t-tolerance improved algorithm to improve the robustness to observation and inference errors.
- We analyze the sources of errors in the proposed scheme, and compare it to an aloha-like scheme. We also evaluate the impact of loose synchronization, network size, and other parameter settings.

## 3.2 Related Work

Given the importance of the two problems in wireless networks, unsurprisingly, there exists vast literature addressing them. Existing approaches can be classified utilizing multiple criterion, namely, passive vs. active, deterministic vs. randomized, and whether information from multiple transmissions is incorporated.

Passive approaches rely on opportunistic listening to learn about a node’s neighbors, or relative timing between transmitting frames to infer contention relationship [34–36]. While passive approaches do not introduce additional signaling or messages in the network, due to their opportunistic nature, the inference process tends to be lengthy. Among approaches that utilize active transmissions or probes, one central question is when and which sets of nodes will be transmitting and receiving.

Active approaches using a deterministic schedule [37–39] typically require a central coordinator and nodes take turns in transmission. In contrast, in randomized approaches [40–43], nodes follow decentralized randomized schedules.

Another distinction among existing work is the treatment of multiple concurrent transmissions. Randomized neighbor discovery protocols [40, 41, 44, 45] that assume single packet reception at the the receiver, aim to devise a good schedule that trades off collision probabilities and total discovery time – essentially a channel access problem. Multiple packet reception in neighbor discovery has been considered in [42, 43] where at most  $K$  concurrent transmissions can be decoded. A fundamentally different approach that departs from single packet reception assumption in neighbor discovery is proposed by Luo and Guo, which uses binary group testing [32, 33, 46]. In [32, 33, 46], neighboring relations are associated with binary variables. Binary observations at receivers are then modeled as OR mixtures as the result of the transmission schedule and the neighbor relations. Our ternary inference approach is inspired by [32, 33], in which we represent neighboring relationship as ternaries  $\{1; 0; \delta\}$  based on the strength of the received signal.

There are also many existing work on conflict graph inference using a per-link signal measurement based approach [34, 39, 47], and an artificial radio propagation model based approach [48–50]. For example, [39] captured the pairwise signal measurements among links to determine the link contention one by one, which is impractical for unsupervised networks like ad hoc WPANs. [50] built a conflict graph using measurement-calibrated propagation models, the accuracy of which was evaluated through real-world measurements. However, all of the existing approaches assume the target locations are known beforehand.

In this dissertation, we investigate joint neighbor discovery and contention relationship inference. We propose an active algorithm, called the ternary inference

algorithm, that utilizes decentralized randomized schedules to infer the neighboring and contention relationships through the mixed signal at the receiver nodes.

### 3.3 Network Model and Problem Statement

#### 3.3.1 Network Model

We consider a multihop wireless personal area network consisting of  $N$  nodes. During the phase of neighbor discovery and contention relationship inference, time is divided into equal-length slots. The slot boundary is assumed to be synchronized. We will discuss the impact of misaligned slot boundary in Section 3.5. Each node follows a randomized on-off schedule alternating between transmitting and receiving modes, as shown in Fig. 3.1. The randomized schedule is calculated using a pseudo random generator seeded by the node's ID (assumed to be unique) and a parameter  $q$  common to all nodes.

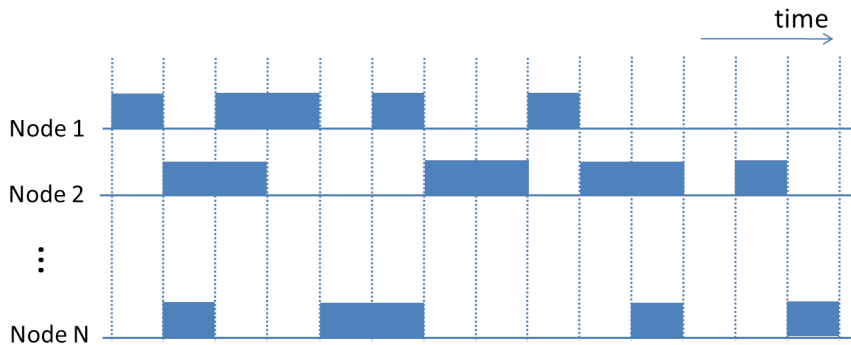


Figure 3.1: A random on-off signaling

Let the length of the discovery phase to be  $L$ . The activity of a node  $n$  at time  $t$  is denoted by  $s_n(t)$ ,  $n \in \{1, \dots, N\}$ ,  $t \in \{1, \dots, L\}$ , where

$$s_n(t) = \begin{cases} 1, & \text{transmitting mode} \\ 0, & \text{receiving mode} \end{cases}, \quad (3.1)$$

and the node's activity follows the i.i.d Bernoulli distribution with  $P(s_n(t) = 1) = 1 - P(s_n(t) = 0) = q, \forall n, t$ .

The set of transmitting nodes at time  $t$ , denoted as  $T(t)$ , can be written as:  $T(t) = \{n : s_n(t) = 1, n \in \{1, \dots, N\}\}$ ; Similarly, the set of the receiving nodes at time  $t$  is written as  $R(t) = \{n : s_n(t) = 0, n \in \{1, \dots, N\}\}$ . At time  $t$ , the collection of  $s_n(t), \forall n$  is called a test, denoted by  $s(t)$ .

The observation of a receiver node  $n$  at time  $t$  is denoted by as  $y_n(t)$ . It can be of two forms:

- Ternary model:  $y_n(t)$  takes values in  $\{0, 1, \delta\}$  as defined as follows,

$$y_n(t) = \begin{cases} 1, & \text{signal decodable} \\ \delta, & \text{signal observed but undecodable} . \\ 0, & \text{no signal observed} \end{cases} \quad (3.2)$$

- Linear model:  $y_n(t)$  is the total received signal power at node  $n$ .

Additionally, depending on whether the received signal is decodable,  $z_n(t)$  gives the set of IDs decoded.

The neighbor relationship between any two nodes  $n$  and  $m, n, m \in \{1, \dots, N\}$ , denoted by  $x(n, m)$ , is given by,

$$x(n, m) = \begin{cases} 1, & m \text{ is a neighbor of } n \\ \delta, & n \text{ can sense the carrier from } m . \\ 0, & m \text{ is not a neighbor of } n \end{cases} \quad (3.3)$$

Note that  $x(n, m)$  is not necessary the same as  $x(m, n)$ , namely, we can account for asymmetric relationships. The determination of  $x(n, m)$  depends on the received signal quality at node  $n$  from  $m$ , in terms of the signal-to-noise (SNR) ratio. We employ two thresholds  $\Gamma_1$  and  $\Gamma_2$  corresponding to the decoding threshold and interference threshold, respectively. When the SNR is above  $\Gamma_1$ , the transmitted signal can be

successfully decoded, while the transmitted signal can be detected but not decoded if the SNR is between  $\Gamma_1$  and  $\Gamma_2$ .

The link contention relationship is denoted by  $c(n, m; k)$ ,  $n, m, k \in \{1, \dots, N\}$ , namely, transmitter  $k$  interfere with link  $m \rightarrow n$ ,

$$c(n, m; k) = \begin{cases} 1, & m \rightarrow n \text{ is interfered by } k \\ 0, & m \rightarrow n \text{ is not interfered by } k \end{cases} \quad (3.4)$$

In other words,  $c(n, m; k) = 1$  if the packet transmission from node  $m$  cannot be successfully decoded if node  $k$  transmits concurrently. The key notations used in this chapter are summarized in Table. 3.1.

Table 3.1: Notations

$L$	the number of tests
$N$	the number of nodes in the network
$t$	the $t$ -th time slot, where $t \in \{1, \dots, L\}$
$n, m, k$	the $n/m/k$ -th node, where $n, m, k \in \{1, \dots, N\}$
$s_n(t)$	the activity of node $n$ at time $t$
$\mathcal{S}$	$\{s_n(t)   n \in \mathcal{N}, t = 1, 2, \dots, L\}$
$y_n(t)$	the observation at node $n$ at time $t$
$\mathcal{Y}$	$\{y_n(t)   n \in \mathcal{N}, t = 1, 2, \dots, L\}$
$z_n(t)$	the IDs decoded at node $n$ at time $t$
$\mathcal{Z}$	$\{z_n(t)   n \in \mathcal{N}, t = 1, 2, \dots, L\}$
$x(n, m)$	the neighbor relationship if $m$ is a neighbor of $n$
$\mathcal{X}$	$\{x(n, m)   n, m \in \mathcal{N}\}$
$c(n, m; k)$	the link contention relationship if $m \rightarrow n$ is contended by transmitter $k$
$O(n, m; k)$	the outcome of $m \rightarrow n$ interfered by transmitter $k$
$\Gamma_1$	decoding threshold
$\Gamma_2$	carrier sensing threshold

### 3.3.2 Problem Statement

The objective of neighbor discovery and contention relation inference is to determine  $x(m, n)$  and  $c(n, m; k)$ , given  $S_n(t)$  and  $y_n(t)$ ,  $t = 1, 2, \dots, L$ ,  $n = 1, 2, \dots, N$  using as few number of tests  $L$  as possible. Note that  $L$  is not fixed a priori. Additional tests will be conducted if the percentage of inferred values or the confidence is below a certain threshold.

### 3.4 Ternary Inference Model and Algorithm

In this section, we first introduce the observation model and then present the ternary inference approach.

#### 3.4.1 Modeling The Observations

We define the ternary operators  $\wedge$  and  $\vee$  that are analogous to logical AND and OR for binary variables, as show in Table 3.2.

Table 3.2: The ternary operators AND  $\wedge$  and OR  $\vee$

(a) Ternary $\wedge$	(b) Ternary $\vee$																																
<table border="1" style="border-collapse: collapse; margin: auto;"> <tr> <td style="padding: 2px 5px;"></td> <td style="padding: 2px 5px;">1</td> <td style="padding: 2px 5px;">0</td> <td style="padding: 2px 5px;"><math>\delta</math></td> </tr> <tr> <td style="padding: 2px 5px;">1</td> <td style="padding: 2px 5px;">1</td> <td style="padding: 2px 5px;">0</td> <td style="padding: 2px 5px;"><math>\delta</math></td> </tr> <tr> <td style="padding: 2px 5px;">0</td> <td style="padding: 2px 5px;">0</td> <td style="padding: 2px 5px;">0</td> <td style="padding: 2px 5px;">0</td> </tr> <tr> <td style="padding: 2px 5px;"><math>\delta</math></td> <td style="padding: 2px 5px;"><math>\delta</math></td> <td style="padding: 2px 5px;">0</td> <td style="padding: 2px 5px;"><math>\delta</math></td> </tr> </table>		1	0	$\delta$	1	1	0	$\delta$	0	0	0	0	$\delta$	$\delta$	0	$\delta$	<table border="1" style="border-collapse: collapse; margin: auto;"> <tr> <td style="padding: 2px 5px;"></td> <td style="padding: 2px 5px;">1</td> <td style="padding: 2px 5px;">0</td> <td style="padding: 2px 5px;"><math>\delta</math></td> </tr> <tr> <td style="padding: 2px 5px;">1</td> <td style="padding: 2px 5px;">1</td> <td style="padding: 2px 5px;">1</td> <td style="padding: 2px 5px;">1</td> </tr> <tr> <td style="padding: 2px 5px;">0</td> <td style="padding: 2px 5px;">1</td> <td style="padding: 2px 5px;">0</td> <td style="padding: 2px 5px;"><math>\delta</math></td> </tr> <tr> <td style="padding: 2px 5px;"><math>\delta</math></td> <td style="padding: 2px 5px;">1</td> <td style="padding: 2px 5px;"><math>\delta</math></td> <td style="padding: 2px 5px;"><math>\delta</math></td> </tr> </table>		1	0	$\delta$	1	1	1	1	0	1	0	$\delta$	$\delta$	1	$\delta$	$\delta$
	1	0	$\delta$																														
1	1	0	$\delta$																														
0	0	0	0																														
$\delta$	$\delta$	0	$\delta$																														
	1	0	$\delta$																														
1	1	1	1																														
0	1	0	$\delta$																														
$\delta$	1	$\delta$	$\delta$																														

Since the observations  $y_n(t)$  is the mixture of signal from all transmitters in  $T(t)$ , we need to first derive the observation as the result of two concurrent transmitters. Let  $O(n, m; k)$  be the observation on node  $n$  with respect to  $m$  when both  $m$  and  $k$  are transmitting. It is easy to show that  $O(n, m; k)$  satisfies Table 3.3. For example, when  $x(n, m) = 1$ ,  $c(n, m; k) = 1$ ,  $O(n, m; k) = \delta$  as the transmission from  $m$  cannot be decoded by  $n$  due to the interference from  $k$  in Case 1 and 3. On the other hand,  $x(n, m) = 1$ ,  $x(n, k) = 1$ ,  $c(n, m; k) = 0$ ,  $O(n, m; k) = 1$  implies successive cancelation is possible to decode the transmission from  $m$  (as indicated in the ID field).

With  $O(n, m; k), \forall m, k \in T(t)$ , we can now compute  $y_n(t)$  as,

$$y_n(t) = \bigvee_{m \in T(t)} \left( \bigwedge_{k \in T(t), k \neq m} O(n, m; k) \right). \quad (3.5)$$

Table 3.3: The observation on link  $m \rightarrow n$  due to transmitters  $m, k$

Cases	$x(n, m)$	$x(n, k)$	$c(n, m; k)$	$O(n, m; k)$	ID(n,m;k)
1	1	1	1	$\delta$	$\emptyset$
2	1	1	0	1	$\{m\}$
3	1	$\delta$	1	$\delta$	$\emptyset$
4	1	$\delta$	0	1	$\{m\}$
5	1	0	0	1	$\{m\}$
6	$\delta$	1	1	$\delta$	$\emptyset$
7	$\delta$	1	0	$\delta$	$\emptyset$
8	$\delta$	$\delta$	1	$\delta$	$\emptyset$
9	$\delta$	$\delta$	0	$\delta$	$\emptyset$
10	$\delta$	0	0	$\delta$	$\emptyset$
11	0	1	1	0	$\emptyset$
12	0	1	0	0	$\emptyset$
12	0	$\delta$	1	0	$\emptyset$
14	0	$\delta$	0	0	$\emptyset$
15	0	0	0	0	$\emptyset$

The inner  $\bigwedge$  operations give the observation with respect to transmitter  $m$  on  $n$  from all other nodes in  $T(t)$  as potential interferers. The outer  $\bigvee$  is due to the fact that by definition a successful (carrier-sensed but non-decodable) transmission from any transmitter will result in decodable (carrier-sensed but non-decodable) packet at the receiver. The set of decoded IDs at node  $n$  is given by,

$$z_n(t) = \bigcup_{m \in T(t)} \left( \bigcap_{k \in T(t), k \neq m} ID(n, m; k) \right). \quad (3.6)$$

Consider the example of  $T(t) = \{m, k\}$ . Clearly, we have

$$y_n(t) = O(n, m; k) \vee O(n, k; m), \quad (3.7)$$

and

$$z_n(t) = ID(n, m; k) \cup ID(n, k; m). \quad (3.8)$$

### 3.4.2 Inference Algorithm

Given the collection of tests  $\mathcal{S}$  and the observations  $\mathcal{Y}$ ,  $\mathcal{Z}$ , the proposed inference algorithm proceeds in two steps: First, it performs neighbor discovery to obtain  $\mathcal{X}$  using  $\mathcal{Y}$ ,  $\mathcal{Z}$  and  $\mathcal{S}$ . Next, it resolves the contention relationship  $\mathcal{C}$  from  $\mathcal{X}$ ,  $\mathcal{Y}$ ,  $\mathcal{Z}$  and  $\mathcal{S}$ .

#### 3.4.2.1 Neighbor Discovery

The neighbor discovery algorithm is presented in Algorithm 1. For every test  $t = \{1, \dots, L\}$ , we evaluate the observation  $y(t)$  on all the receiver nodes in  $R(t)$ . If the observation at a receiver  $n$  is zero, all the concurrent transmitter nodes are flagged non-neighbor to  $n$ . In the case of multiple concurrent active transmitters, the observation may be a mixture, which may be resolved if we know the neighbor relationship of a subset of transmitter nodes in the mixture. Algorithm 1 iterates through all tests and every pair of nodes until either no further improvement can be made or all entries in  $\mathcal{X}$  have been resolved.

*t*-tolerance Neighbor Discovery To increase the robustness of neighbor discovery in presence of measurement errors, we introduce a *t*-tolerance algorithm in Algorithm 2. The basic idea is that each inferred relationship needs to be independently verified by *t* tests. The tolerance factor *t* tradeoffs reliability and the total number of tests to complete neighbor discovery.

#### 3.4.2.2 Contention Relationship Inference

We observe that if  $x(n, m) \in \{\delta, 0\}$ , the knowledge of  $c(n, m, k)$  has little utility since we cannot decode the data from  $m$  to  $n$  even in absence of any other transmitters. Thus, we limit the inference to links that can support successful direct communication.

---

Algorithm 1: Ternary Neighbor Discovery

---

Input : Node Activity  $\mathcal{S}$ , Observation  $\mathcal{Y}$

Output: Neighbor Relationship  $\mathcal{X}$

begin

    Set  $flag = 1$ ;

    while  $flag = 1$  do

        for  $t = 1$  to  $L$  do

            Find  $T(t)$  and  $R(t)$  from  $\mathcal{S}(t)$

            if  $y_n(t) = 0, n \in R(t)$  then

                |  $x(n, m) \leftarrow 0, \forall m \in T(t)$ ;

            end

            if  $y_n(t) = \delta$  and  $|T(t)| = 1, n \in R(t)$  then

                |  $x(n, m) \leftarrow \delta, \forall m \in T(t)$ ;

            end

            if  $y_n(t) = 1$ , TX ID  $m$  decoded,  $n \in R(t)$  then

                |  $x(n, m) \leftarrow 1$ ;

            end

            if  $y_n(t) > 0$  and  $|T(t)| \geq 2, n \in R(t)$  then

                | if exist  $x(n, m) < y_n(t), m \in T(t)$  then

                    | remove  $m$  from  $T(t)$ ;

                    | if  $|T(t)| = 1$  then

                        |  $flag \leftarrow 1$ , Continue;

                    | else

                        |  $flag \leftarrow 0$ , Continue;

                    | end

                | end

            end

        end

    end

end

---

---

**Algorithm 2: t-tolerance Neighbor Discovery Algorithm**

---

Input : Node Activity  $\mathcal{S}$ , Observation  $\mathcal{Y}$ , Tolerance Factor  $t$ Output: Neighbor Relationship  $\mathcal{X}$ 

begin

Set  $flag = 1$ ;while  $flag = 1$  doinitialization:  $u_m \leftarrow t, v_m \leftarrow t, w_m \leftarrow t, m \in \{1, \dots, N\}$ ;for  $i = 1$  to  $L$  doFind  $T(i)$  and  $R(i)$  based on  $\mathcal{S}()$ if  $y_n(i) = 0, n \in R(i)$  then|  $u_m \leftarrow u_m - 1, \forall m \in T(i)$ ;| if  $u_m \leq 0$  then| |  $x(n, m) \leftarrow 0, \forall m \in T(i)$ ;

| end

end

if  $y_n(i) = \delta$  and  $|T(i)| = 1, n \in R(i)$  then|  $v_m \leftarrow v_m - 1, \forall m \in T(i)$ ;| if  $v_m \leq 0$  then| |  $x(n, m) \leftarrow \delta, \forall m \in T(i)$ ;

| end

end

if  $y_n(i) = 1$ , TX ID  $m$  decoded,  $n \in R(i)$  then|  $w_m \leftarrow w_m - 1, \forall m \in T(i)$ ;| if  $w_m \leq 0$  then| |  $x(n, m) \leftarrow 1$ ;

| end

end

end

for  $i = 1$  to  $L$  do| if  $y_n(i) > 0$  and  $|T(i)| \geq 2, n \in R(i)$  then| | if exist  $x(n, m) < y_n(i), m \in T(i)$  then| | | remove  $m$  from  $T(i)$ ;| | | if exist  $|T(i)| = 1$  then| | | |  $flag \leftarrow 1$ , Continue;

| | | else

| | | |  $flag \leftarrow 0$ , Continue;

| | | end

| | end

| end

end

end

end

---

From Table 3.3, it is easy to see that when  $x(n, m) = 1$  (the shaded rows), if  $O(n, m; k)$  is known, then  $c(n, m; k)$  can be uniquely determined. In fact,  $c(n, m; k) = 0$  if  $O(n, m; k) = \delta$ , and  $c(n, m; k) = 1$  if  $O(n, m; k) = 1$ . Therefore, it suffices to infer  $O(n, m; k)$  for  $n, m, k \in \mathcal{N}$  from  $y_n(t), z_n(t), \forall n \in T(t), t = 1, 2, \dots, L$ .

From (3.5) and (3.6), we note that if  $m \in z_n(t)$ ,  $\bigwedge_{k \in T(t), k \neq m} O(m, n; k) = 1$ , which implies that  $O(m, n; k) = 1, \forall k \in T(t), k \neq m$ . In other words, a decodable message yields the contention relationship of many links. On the other hand, if  $m \notin z_n(t)$ ,  $\bigwedge_{k \in T(t), k \neq m} O(m, n; k) = 0$ . The mixture can only be solved when we have sufficient number of known  $O(m, n; k)$ 's.

In Algorithm 3, when there are only two concurrent transmitter nodes in a test, the contention relationship can be computed directly as evident from (3.7) and (3.8). In the case of multiple concurrent transmitters,  $O(n, m; k)$  will be inferred recursively. Finally, from  $O(n, m; k)$  and Table 3.3 we can determine  $c(n, m; k)$ .

### 3.4.3 Analysis of Errors

The ternary interference model makes assumptions regarding the superposition of the signals at a receiver. In particular, multiple strong signals always add up to an even stronger signal; while the aggregates of multiple weak signals remain to be weak. In practice, these assumptions may not hold. Consider a quantized linear superposition model satisfying

$$\tilde{y}_n(t) = \begin{cases} 1, & \sum_{m \in T(t)} h_{mn} \tilde{x}_m(t) \geq \Gamma_1 \\ \delta, & \Gamma_1 > \sum_{m \in T(t)} h_{mn} \tilde{x}_m(t) \geq \Gamma_2, \\ 0, & \sum_{m \in T(t)} h_{mn} \tilde{x}_m(t) < \Gamma_2 \end{cases}, \quad (3.9)$$

where  $\tilde{y}_n(t), \tilde{x}_m(t), h_{mn}$  are the aggregated received signal at  $n$ , the transmitted signal from node  $m$ , and the channel gain from  $m$  to  $n$  (including antenna gains), respectively.

---

**Algorithm 3: Contention Relationship Inference**

---

Input : Node Activity  $\mathcal{S}$ , Observations  $\mathcal{Y}$  and  $\mathcal{Z}$ , Neighbor Relationship  $\mathcal{X}$

Output: Contention relationship  $\mathcal{C}$

begin

    Set  $flag = 1$ ;

    while  $flag = 1$  do

        for  $t = 1$  to  $L$  do

            Find  $T(t)$  and  $R(t)$  from  $\mathcal{S}(t)$

            if  $y_n(t) = 0, n \in R(t)$  then

                |  $c(n, m; k) \leftarrow 0, c(n, k; m) \leftarrow 0, \forall m, k \in T(t)$ ;

            end

            if  $y_n(t) = 1, n \in R(t)$  then

                |  $c(n, m; k) \leftarrow 0, \forall m \in z_n(t), k \neq m \in T(t)$ ;

            end

            if  $y_n(t) == \delta, n \in R(t)$  then

                if  $|T(t)| = 2$  then

                    | Find  $c(n, m; k)$  and  $c(n, k; m)$  using  $x(n, m), x(n, k)$  and  $y_n(t), \forall m, k \in T(t)$ , using (3.7), (3.8) and Table 3.3;

                else

                    | Find  $O(n, m, k)$  and  $O(n, k, m)$  using available  $x(n, m), x(n, k), c(n, m; k), c(n, k; m), \forall m, k \in T(t)$ , using Table 3.3;

                    if  $O(n, m, k) == 0$  then

                        | remove  $m$  from  $T(t)$ ;

                    else if  $O(n, k, m) == 0$  then

                        | remove  $k$  from  $T(t)$ ;

                    end

                    if exist  $|T(t)| = 2$  then

                        |  $flag \leftarrow 1$ , Continue;

                    else

                        |  $flag \leftarrow 0$ , Continue;

                    end

                end

            end

        end

    end

end

---

Two types of observation errors in the ternary model are possible: If the linear superposition model gives the observation 0 (or  $\delta$ ), while our ternary model observed  $\delta$  (or 1), it is called a false positive error. This may occur when multiple strong signals cancels out. On the other hand, if the linear superposition model decides  $\delta$  (or 1) but our ternary model decides 0 (or  $\delta$ ), it is called a false negative error. This may occur when multiple weak signals aggregate. The two sources of errors would lead to misidentification of the neighboring and contention relationships in our ternary approach.

To see the impact of parameter  $\Gamma_1$  and  $\Gamma_2$  on two sources of errors, we conduct simulations by putting  $N$  nodes with the parameters in Table 3.4.

Table 3.4: Simulation setup

PHY parameters	Values
Path Loss	3
Center Freq	2.4 GHz
Transmit power	1mW
Noise floor	-102dBm
Fading channel	AWGN
Active probability $q$	0.2
Node density	$0.001/m^2$

The parameters are chosen in consistent with the IEEE 802.15.4 transceivers [5]. In the experiments, scheduled transmitters send a '1' bit modulated using BPSK and carrier frequency 2.4GHz. The received signal is subjected to propagation delay between the transmitters and receivers. The node degree in the network is shown in Figure 3.2.

Figure 3.3 shows the observation errors of the ternary model with respect to the number of nodes with  $\Gamma_1 = 3dB$ ,  $\Gamma_2 = -7dB$ . A total of  $L = 200$  random tests are conducted. The observation errors are computed as the percentage of discrepancy in the observations in our ternary model compared to the linear superposition model. From Figure 3.3, we observe that the false positive and negative errors are comparable

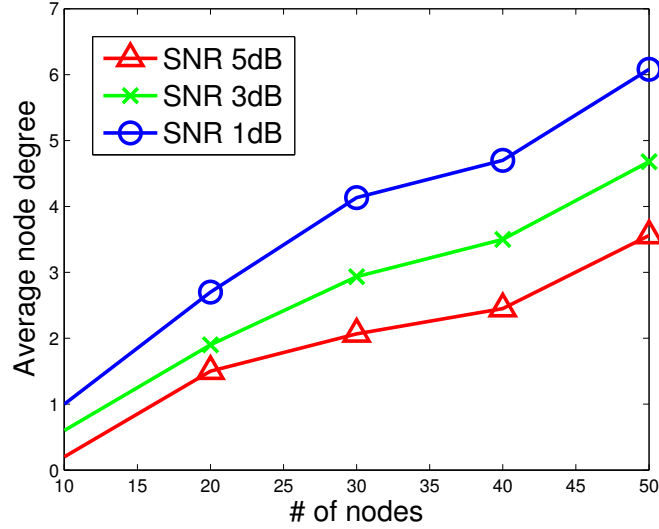


Figure 3.2: Network node degree with respect to the number of nodes in the network with different sensitivity SNR  $\Gamma_1$ .

both increasing with more number of nodes in the network. Increasing the thresholds  $\Gamma_1$  and  $\Gamma_2$  decreases the false positive errors, and increases the false negative errors as expected.

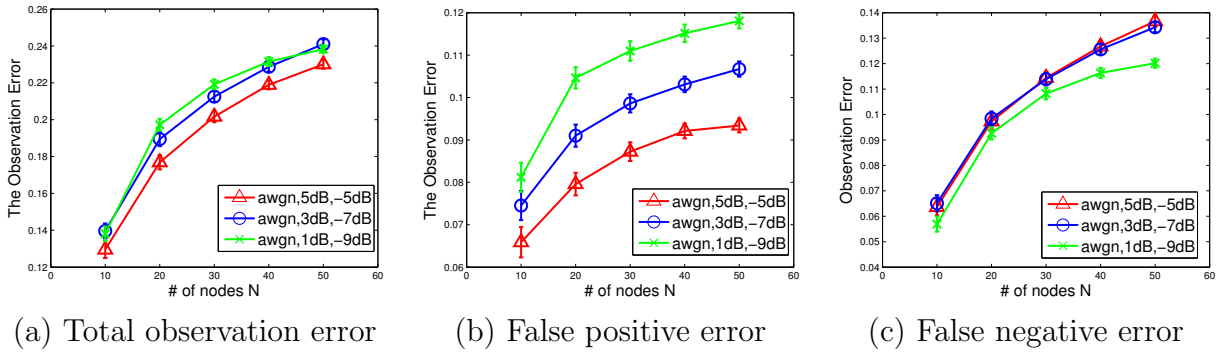


Figure 3.3: Performance of observation error rate with respect to the number of nodes in the ternary model with  $L = 200$ ,  $\Gamma_1 = 3dB$ ,  $\Gamma_2 = -7dB$ .

### 3.5 Performance Evaluation

In this section, we evaluate the performance of the ternary inference approach using simulations. We use the same setup as in Section 3.4.3.

### 3.5.1 Inference Completion Rate

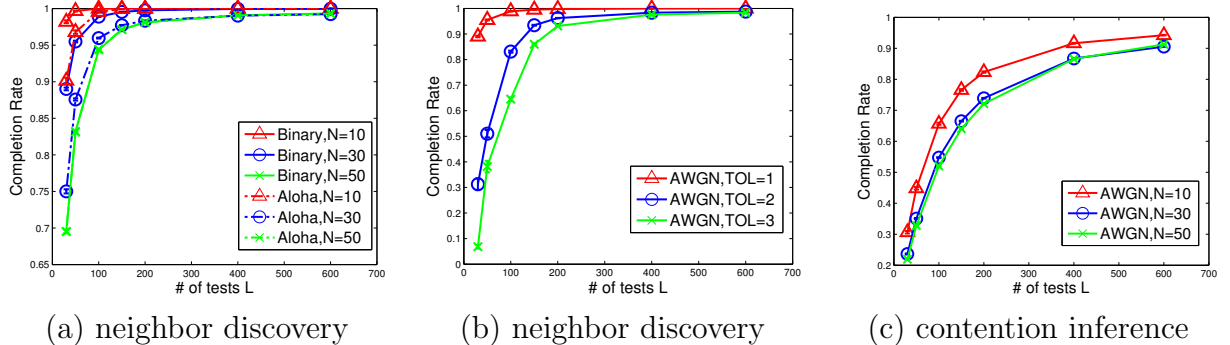


Figure 3.4: Performance of completion rate with respect to the number of tests in the ternary model with  $\Gamma_1 = 3dB$ ,  $\Gamma_2 = -7dB$  and 95% confidence: (a) neighbor discovery with  $TOL = 1$ , an aloha-like algorithm is used for comparison; (b) t-tolerance neighbor discovery with  $N = 30$ ; (c) contention relationship inference with  $TOL = 1$ .

Fig. 3.4 shows the performance of completion rate of neighbor discovery and contention inference with respect to the number of tests in the ternary model, respectively. In Fig. 3.4(a), we compare the completion rate of neighbor discovery in the ternary model and an aloha-like model. A few observations can be made. As the number of tests increases, the completion rate increases as expected. Increasing the number of nodes in the network decreases the completion rate accordingly. Compared to an aloha-like model, our proposed ternary model can achieve higher completion rate. This is because our model explores the mixture over the time to achieve more completion.

Fig. 3.4(b) shows the completion rates of neighbor discovery using the t-tolerance improved algorithm in our ternary inference approach with  $N = 30$ . We can observe that, increasing the tolerance improves the reliability of decision, but decreases the completion rate as expected.

Fig. 3.4(c) shows the completion rates of contention relationship inference with respect to the number of tests. As the number of tests increases, the completion rate increases as expected. However, compared to Fig. 3.4(a), the the link contention

inference process is much slower. This is because the contention relationship inference depends on the results of neighbor discovery.

### 3.5.2 Inference Error Rate

Fig. 3.5 and Fig. 3.6 show the performance of inference error rates using the proposed ternary inference approach with respect to the number of tests  $L$  by varying the number of nodes  $N$  and the tolerance factor  $TOL$ , respectively. The SNR pair  $\Gamma_1=3\text{dB}$ ,  $\Gamma_2=-7\text{dB}$  are selected for this experiment.

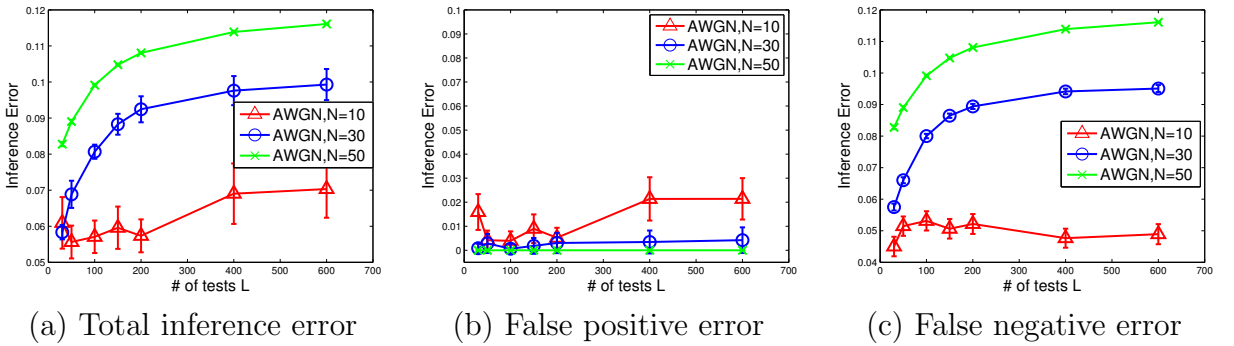


Figure 3.5: Performance of inference error rate with respect to the number of tests in the ternary model with  $TOL = 1$ ,  $\Gamma_1=3\text{dB}$ ,  $\Gamma_2=-7\text{dB}$ , and 95% confidence.

Fig. 3.5(a)(b)(c) demonstrate the total inference error, the false positive error and the false negative error by varying the number of nodes in the network with  $TOL = 1$ , respectively. As the number of tests increases, all inference error rates increase. Increasing the number of nodes in the network decreases the false positive errors, but increases the false negative errors. This is because, concurrent transmitting weak signals would more likely aggregate to be strong at the receiver as the number of nodes increases. Another observation is, false negative errors dominate the inference errors in our proposed ternary model.

In Fig. 3.6(a)(b)(c), we present the inference error rate by varying the tolerance factor  $TOL$  using the t-tolerance neighbor discovery algorithm. Increasing the tolerance improves the inference errors significantly as expected.

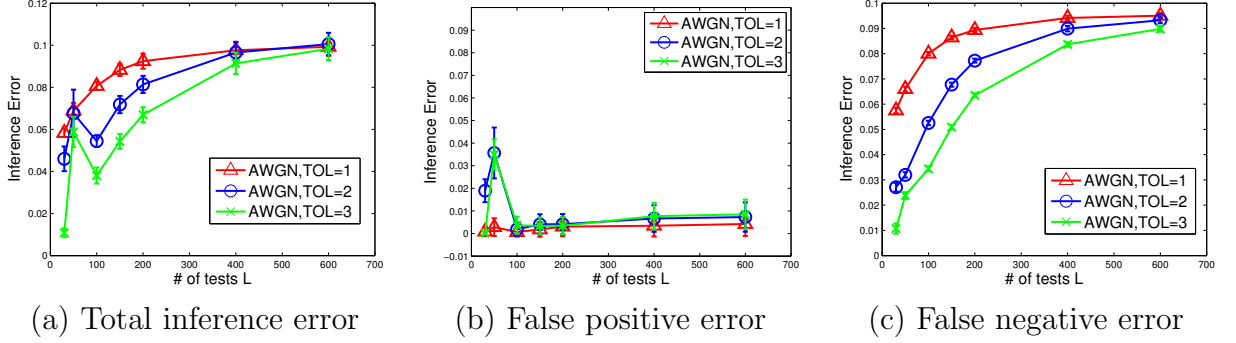


Figure 3.6: Performance of inference error rate with respect to the number of tests in the ternary model with  $N = 30$ ,  $\Gamma_1=3\text{dB}$ ,  $\Gamma_2=-7\text{dB}$ , and 95% confidence.

Lastly, we evaluate the performance of inference error rate by varying the SNR threshold pairs in Fig. 3.7. Generally, increasing the SNR threshold pair increases the total inference errors significantly.

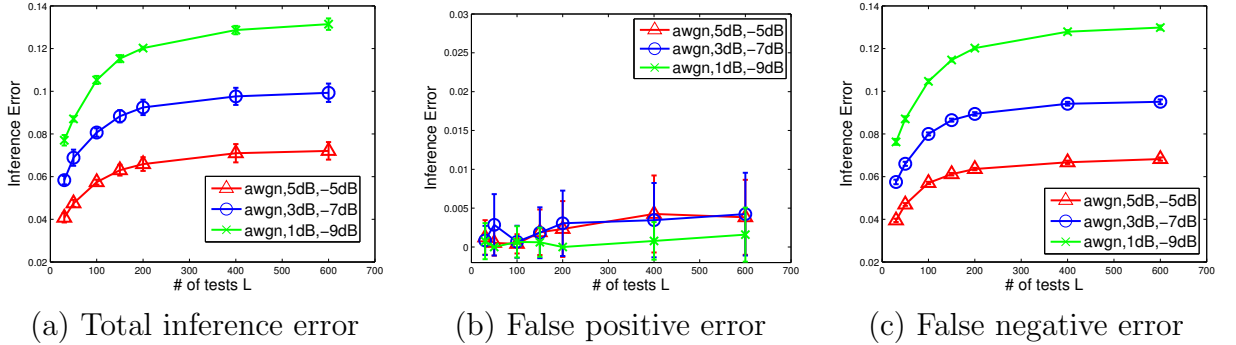
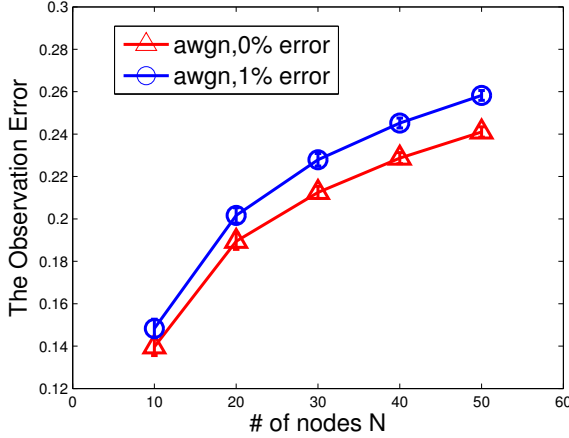


Figure 3.7: Performance of inference error rate with respect to the number of tests in the ternary model with  $TOL=1$ ,  $N = 30$ , and 95% confidence

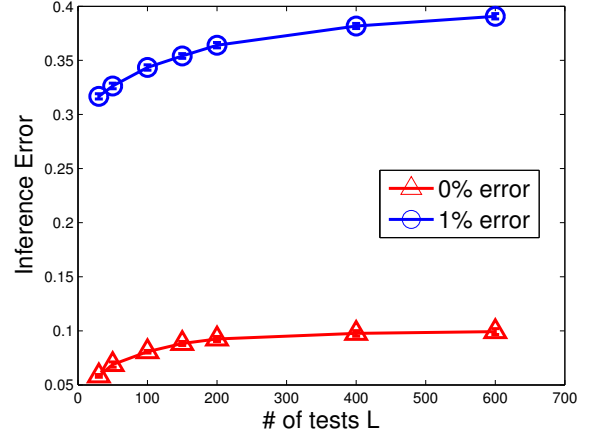
### 3.5.3 Impact of Loose-Synchronization

In this section, we evaluate the impact of misaligned time slot boundary in the proposed ternary model, in which  $x\%$  decision error is introduced to randomly invert the decisions on observation and inference. We refer the decision error to the scenario when unsynchronized TX signals are accumulated at RX, which introduce the additional error on decision compared to perfect synchronous transmission.

Figure 3.8(a) shows the observation error rate of the ternary model with re-



(a) Total observation error rate



(b) Total inference error rate

Figure 3.8: Impact of loose-synchronization on the observation and inference error rates in the ternary inference model with  $L = 200$ ,  $N = 30$ ,  $\Gamma_1 = 3dB$ ,  $\Gamma_2 = -7dB$  and 95% confidence. The  $x\%$  decision error is introduced to randomly invert the decisions.

spect to the number of nodes in the network. As expected, increasing decision errors increases the observation errors.

Fig. 3.8(b) shows the inference error rate with respect to the number of tests by varying the decision error. Increasing the decision error increases the inference errors significantly. This indicates our ternary model is sensitive to the accuracy of decision.

### 3.6 Conclusion

In this dissertation, we considered the problem of joint neighbor discovery and contention graph inference in wireless networks, which are fundamental building blocks in resource management. Compared to an Aloha-like neighbor discovery scheme, the novelty of the proposed ternary algorithm lies in the exploitation of mixed signal at the receiver nodes. The simulation results demonstrate the superior performance of the proposed algorithm in terms of completion rate and accuracy.

There are a number of issues that need to be resolved as part of our future

work. First, we will devise an analytical model for the completion rate and inference errors. Second, adaptive randomized schedules will be explored that vary the active probability  $q$ .

## Chapter 4

# Robust Relay Placement and Routing Selection in WPANs

### 4.1 Introduction

The millimeter wave (mmWave) band has attracted considerable commercial interests due to the advance in low-cost mmWave radio frequency integrated circuit design. The mmWave band provides 7GHz unlicensed spectrum resource at the center frequency of 60GHz<sup>1</sup>, which would enable many high data rate applications like high definition streaming multimedia, high-speed kiosk data transfer and point-to-point terminal communication in data center [51–55], etc. There have been significant standardization efforts in this area, such as IEEE 802.11ad [56], IEEE 802.15.3c [57, 58], as well as *WiGig* [59] and *WirelessHD* [60].

In contrast to many existing RF technologies such as 2.4GHz WiFi radios, mmWave radios have several unique physical characteristics [52, 53]. First, the propagation and attenuation loss are much more severe in the 60GHz band. It is shown that the free space path loss in 60GHz is more than 20dB larger than that in 5GHz. The oxygen absorption loss is as high as 5 ~ 30dB/km. Furthermore, the penetration loss is also much higher through typical building materials [51]. As a result, line-of-sight (LOS) path is the predominant path for signal transmission, while signals along the second-order and higher-order reflection paths are highly attenuated and often negligible. Second, to combat such significant signal degradation, directional antenna technology is essential in mmWave devices. By using directional antenna on both the transmitter and the receiver sides, mmWave radios can obtain significant gain in the received signal strength, while incurring negligible interference to/from other radios [61–64]. In this chapter, we consider an mmWave wireless personal area

---

<sup>1</sup>57 - 64GHz in North America, and 59 - 66GHz in Europe and Japan

network (WPAN) equipped with directional antenna on all devices.

In addition to high bandwidth demands, multimedia applications in 60GHz WPANs have stringent requirements on service disruption (defined as the duration of time that the network connectivity is not available), which can occur due to change of channel conditions or LOS link blockage by moving objects in the space. This motivates us to consider the use of relays for two purposes:

- relays can be used to relay traffic from transmitters to receivers that do not have direct connectivity
- relays can provide a secondary (2-hop) path in case of blockage on the primary (direct) path.

Generally, there are two types of relays proposed for mmWave in the literature, namely, active relay [65–67] and passive relay [68–70]. A passive relay (also known as relay) reflects the mmWave radiation from the transmitter to the receiver. It can be as simple as a flat metal plate that does not require any power source. However, passive relays introduce losses due to reflection, as well as the additional path loss as the result of longer propagation path. In contrast, an active relay is an active mmWave transceiver with beamforming capabilities. It can amplify and forward the mmWave signal from the transmitter to any intended direction, at the cost of higher complexity. In this chapter, we consider active relays for the ease of control of reflection directions and signal boost.

#### 4.1.1 Contributions

In this chapter, we investigated two relay placement problems in 60GHz mmWave WPANs to achieve better resource provisioning. Robust minimum relay placement (RMRP) that attempts to find the minimum number of relays and their best place-

ments from a set of candidate locations with bandwidth and robustness constraints, and robust maximum utility relay placement (RMURP) that aims to maximize network utility given a fixed number of relays. Two vertex-disjoint (except for the endpoints) paths (one called the primary path, and the other the secondary path) are provisioned between each pair of transmitter and receiver. Consequently, seamless switching to the secondary path is facilitated in event of channel degradation or blockage on the primary path avoiding service disruption.

Several key contributions have been made:

- We characterize the geometric constraints of link connectivity.
- In an interference-free model, we characterize the worst-case TDMA scheduling constraints for every relay in 60GHz mmWave WPANs, while in directional antenna model, we further explore the scheduling constraints for every physical link.
- We propose the robust formulations for two relay placement problems (RMRP and RMURP) in mmWave WPANs to combat the uncertainty in link failure. The D-norm uncertainty model in robust optimization theory is applied in the formulation.
- We derive the detail proof that both RMRP and RMURP are NP-hard.
- We design two efficient algorithms to solve RMURP, the heuristic solution that has a near-optimal performance and the optimal solution.
- We present a random-walk based mobility model to validate the proposal models and algorithms.

## 4.2 Related Work

Significant prior literature have been produced on different aspects of 60GHz radios, from CMOS circuit design to network protocol development. In this section, we summarize prior work on MAC design in mmWave WPANs.

A spatial time-division multiple access (STDMA) scheme was proposed for a realistic multi-Gbps mmWave WPAN in [71]. With the help of a heuristic scheduling algorithm, it is able to achieve significant throughput enhancement as much as 100% compared to conventional TDMA schedules. In [72], Cai et al. presented an efficient resource management framework based on the unique physical characteristics in a MC-DS-CDMA based mmWave networks. The authors also conducted extensive analysis of spatial multiplexing capacity in mmWave WPANs with directional antennae in [73, 74]. In [62], Madhow et al. conducted a probabilistic analysis of the interference in an mmWave network, as the result of uncoordinated transmission. It is concluded that an mmWave link can be abstracted as a “pseudo-wired link” with negligible interference when the beam width is 20 degree. Similar observations are made in [61, 75]. Therefore, the primary interference at the transmitter or receiver devices is the predominant source of contention. In [76, 77], to address the deafness problem induced by directionality, Gong et al. proposed a new directional CSMA/CA protocol for IEEE 802.15.3c 60GHz WPANs. With virtual carrier sensing, the central coordinator can distribute the network allocation vector (NAV) information, to avoid collisions among the devices occupying the same channel. The author also extended the work to a multi-user scenario in [78]. A distributed scheduling protocol is proposed by coordinating mmWave mesh nodes in [63], and can achieve high resource utilization with time division multiplexing (TDM). However, none of the above work model or address relay placement problems in mmWave WPANs with directional antenna.

There are also some existing work on repeater selection and relay operation scheduling in mmWave WPANs. Repeater selection was investigated in [66], with the objective to maximize data rate for each transmitter and receiver pair by determining the best link allocation. In [79,80], Lan et al. explored time slot scheduling for relay operations in the scenario of directional antenna on mmWave devices and formulated the throughput maximization problem as an integer programming problem. However, both schemes do not consider robustness in presence of uncertain link blockage.

Our work is also related to multihop routing in wireless networks with directional antenna [81–83] with two key differences. First, relays in our work are dedicated devices that do not generate or receive application layer packets. Second, we allow at most 2-hop paths between any mmWave transmitter-receiver pairs, considering the fact that mmWave WPANs are deployed in a small indoor environment with stringent QoS requirement.

To the best of our knowledge, we are the first to explore robust relay placement in 60GHz WPANs. The publications regarding this work are presented in [84–86]. In this work, we begin with an Interference-free model. Then, we consider a more realistic interference model, in which a classic directional antenna radiation pattern [64,79,80] is adopted to explore the spatial contention for every pair of mmWave physical links. We also impose the bandwidth constraints for both mmWave devices and relays in time division duplex fashion.

### 4.3 Geometric Model for Link Connectivity

In this section, we introduce a geometric model to determine the link connectivity in 60GHz mmWave WPANs. First, we define the notation of the visibility region of a point as follows:

Definition 4.1. Given a  $2D$  plane of interest, any two points  $(a, b)$  are visible to each

other if the line segment between them does not intersect with any obstacles and the length of the segment is less than  $t$ . The visibility region  $V(a)$  of a point  $a$  in the plane is the bounded polygon consisting of all points visible from  $a$ .

By this definition, visibility is a symmetric relation. Furthermore, two visible points must have overlapping visibility regions. The connectivity of any mmWave logical link (shorten as mmWave link for simplicity) can be modeled by the overlapped visibility regions. Consider two devices  $a$  and  $b$ , the connectivity of link  $(a, b)$  is thus indicated by

$$\lambda(a, b) = \begin{cases} 1, & \text{iff } V(a) \cap V(b) \neq \emptyset \\ 0, & \text{otherwise} \end{cases}. \quad (4.1)$$

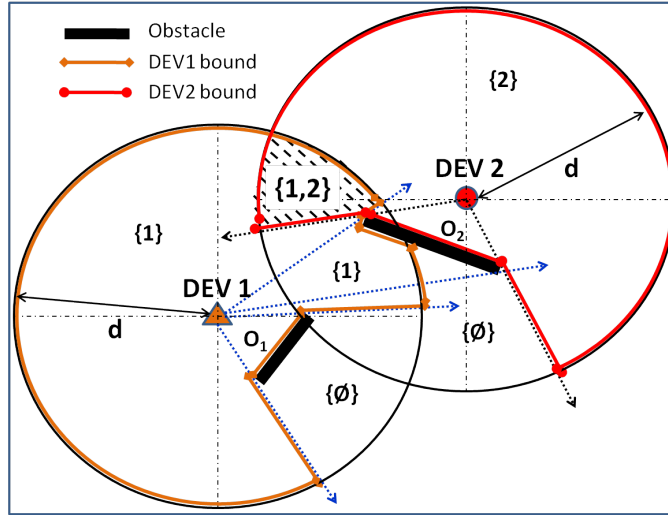


Figure 4.1: The overlapped visibility region between DEV1 and DEV2 is the shadow area bounded by the line segments of each DEV's visibility polygon and their transmission radii.

If  $\lambda(a, b) = 1$ , link  $(a, b)$  is feasible (directly or via an intermediary relay in the overlapping region), otherwise, it is infeasible. For the rest of the chapter, we only consider feasible mmWave links. In particular, let  $S_0$  denote the set of all links in the network, then the set of feasible mmWave links is given by:

$$\Omega = \{i \mid \lambda(s_i, d_i) = 1, \forall i \in S_0\}, \quad (4.2)$$

where  $s_i, d_i$  are the transmitter and receiver of the  $i$ -th logical link respectively.

Fig. 4.1 gives the simple model to demonstrate the visibility region of two mmWave devices, DEV1 and DEV2. The visibility region of DEV1 is a bounded polygon composed by the line segments in dark yellow and its transmission radius. As shown in the shadow area, there is an overlapped visibility region between DEV1 and DEV2, which is the candidate region for placing relays. Note that, overlapped visibility region describes the link connectivity for both LOS and NLOS link.

#### 4.4 Why Robustness is Needed

Relays serve two purposes: i) providing the primary communication path for NLOS logical links; and ii) providing secondary (backup) communication path for LOS or NLOS logical links. Provisioning of secondary paths reduces service disruption when the primary path is obstructed.

To see the impact of secondary paths, we conduct a simple simulation study. Consider a home-network environment in Fig. 4.2, where there is a LOS logical link  $l$  and a dedicated relay at a fixed location. In the robust setting, one relay is used to provide a secondary communication path for  $l$ . Inside the room, there are  $M$  moving human subjects modeled as a circle with a radius of 0.3 meters. We adopt the random walk model [87, 88], where in each step, a person moves 0.3 meters with the direction randomly chosen from the set  $\{-90^\circ, -45^\circ, 0^\circ, 45^\circ, 90^\circ\}$ . Without relays, the communication between TX and RX is disrupted when a person blocks the direct LOS path. With relays, an outage occurs only when both the primary (LOS) path and the secondary path (via the relay) are blocked.

Fig. 4.3 shows the percentage of link blockage time and the mean blockage duration with a 90% confidence interval by varying the number of moving human subjects, respectively. When the number of moving subjects increases, the percentage of link

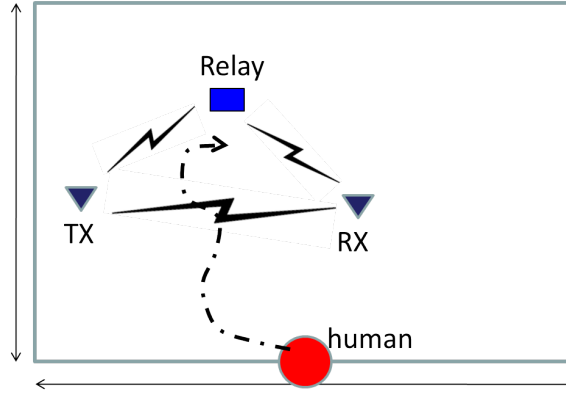
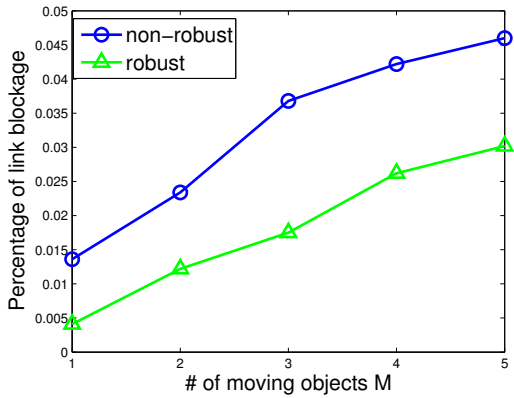
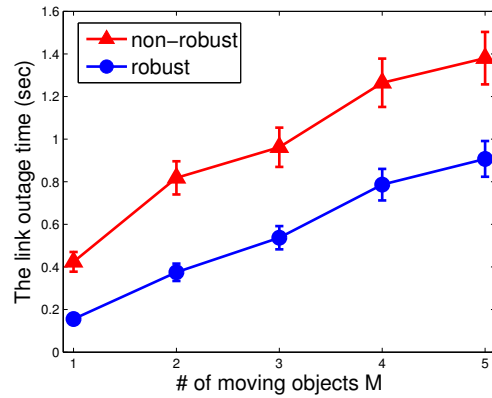


Figure 4.2: A  $10\text{m} \times 10\text{m}$  room with a fixed mmWave TX/RX and a dedicated relay,  $M$  human subjects moving randomly inside.



(a) Percentage of link blockage



(b) Mean blockage duration with 90% confidence interval

Figure 4.3: Link blockage with and without relays due to moving human subjects.

blockage and blockage duration increase with and without the secondary path. However, the use of backup path reduces both the blocking probability and the duration of each outage. This translates to better quality of service (QoS) at the application layer.

## 4.5 Robust Relay Placement and Route Selection in an Interference-free 60GHz WPANs

### 4.5.1 Problem Statement

Consider a mmWave network consisting a set of  $L$  mmWave links, each link  $i \in L$  is associated with a transmitting device  $s_i$  and receiving device  $d_i$ , and a flow rate  $r_i$ . Relays are devices that can repeat or relay transmission between transmitters and receivers, which can be placed at a set of  $K$  candidate locations. There exist a set of  $M$  obstacles with known locations.

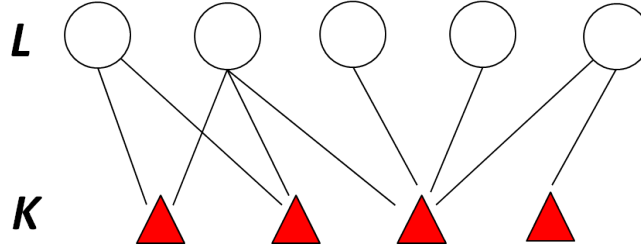


Figure 4.4: The relationship between mmWave links ( $U$ ) and relays ( $S$ ).

The relationship between mmWave links and relays is modeled as an undirected bi-partite graph  $G(U, S, E)$  in Fig. 4.4, where  $U$  is the set of mmWave links, and  $S$  is the set of relays. An edge  $e = (u, s)$  exists between link  $u \in U$  and relay  $s \in S$  if  $s$  is located in the overlapped visibility region of  $s_u$  and  $d_u$ . The set of feasible mmWave links that can utilize relay  $k$  as the relay is defined as:

$$L_k = \{i \mid k \in V(s_i) \cap V(d_i), \forall i \in \Omega\}, \forall k. \quad (4.3)$$

If a relay device is selected as a relay by more than one mmWave link, a time division medium access (TDMA) scheme is applied for scheduling the transmissions of these links. We assume any mmWave device cannot relay traffic for other devices. At most 2-hop paths (via a relay) are considered due to stringent time requirements in delay sensitive applications. We assume the interference among concurrent transmis-

sions is negligible as a result of high directionality of the transmitters and receivers. This assumption is also supported by the measurement studies [63]. We also envision that relays are installed with the electronically steerable phased array antennas, which can steer the radiation pattern rapidly. It is believed in [89, 90] that, the switching time is within 250 us. Thus, we assume that relays can tune the beam direction to the transmitters and receivers one at a time without costing any additional switching overhead.

On the other hand, relays can be placed at a set of candidate locations to relay traffic for feasible mmWave links, either to provide connectivity when direct communication between the devices is infeasible, or to facilitate backup paths when the primary paths are blocked. For each feasible link, two vertex-disjoint paths are provisioned, one as a primary path, and the other as a secondary path.

We define two problems of relay placement in 60GHz mmWave WPANs:

Definition 4.2. (Robust Minimum Relay Placement problem (RMRP)) Given a mmWave network with a set of feasible mmWave links with fixed flow utility, the objective of the RMRP is to find the minimum number of relays and their locations out of the  $K$  candidate locations that satisfy the connectivity, bandwidth requirements as well as robustness constraints.

Definition 4.3. (Robust Maximum Utility Relay Placement Problem (RMURP)) Given a mmWave network with a set of feasible mmWave links and a limited number of relays, the objective of RMURP is to determine the maximum overall network utility by placing the relays into the  $K$  candidate locations that satisfy the connectivity, bandwidth requirements as well as robustness constraints.

The key notations used in this chapter are summarized in Table. 4.1.

Table 4.1: Key notations

$l$	a logical mmWave link $l$ , where $s_l, d_l$ are sender and receiver
$i$	a physical mmWave link $i$
$k$	a relay device $k$
$f_l$	the traffic demand of logical link $l$
$r_i$	the flow rate of physical link $i$
$\Omega$	the set of all feasible logical links in the network
$\Omega_k$	the set of feasible logical links can use $k$ as relay
$Q$	the radiation pattern of transmit antenna
$D$	the transmission radii of mmWave devices
$\theta$	the beamwidth of transmit antenna
$\phi$	the transmit antenna direction
$K$	the number of candidate relays
$O$	the number of obstacles
$N$	the number of mmWave devices
$M$	the number of moving human objects
$c_{uv}$	a binary indicator for spatial contention of $u$ and $v$
$x_{lk}$	a binary variable of logical link $l$ selecting relay $k$ in its primary path
$y_{lk}$	a binary variable of logical link $l$ selecting relay $k$ in its secondary path
$z_k$	a binary variable of relay $k$ being selected
$\eta_l$	a binary indicator for NLOS of logical link $l$
$\tau_{lk}$	the unit data relay time of $l$ via $k$
$\alpha$	the scaling factor for traffic demand
$U$	total network utility
$d_0$	the grid spacing for relay placement
$m$	the maximum number of relays to be used
$\rho$	the robustness index

#### 4.5.2 Robust Minimum Relay Placement

In this section, we formulate the RMRP problem in an interference-free 60GHz mmWave WPANs which accounts for network dynamics due to uncertain blockages of primary paths.

Before providing the formulation, we first introduce some notations:

- Primary indicator:  $x_{ik} = 1$  if relay  $k$  is selected by link  $i$  as its primary relay, otherwise  $x_{ik} = 0$ ;
- Secondary indicator:  $y_{ik} = 1$  if relay  $k$  is selected by link  $i$  as its secondary

relay, otherwise  $y_{ik} = 0$ ;

- Selection indicator:  $z_k = 1$  if relay  $k$  is selected by at least one link, otherwise  $z_k = 0$ ;
- NLOS indicator:  $\eta_i = 1$  if link  $i$  does not have a LOS path.

If a link  $i$  has a LOS path, no relay is needed for the primary path, otherwise one relay should be selected for the primary path, which should satisfy the following condition,

$$\sum_{k=1}^K x_{ik} = \eta_i, \forall i \in \Omega. \quad (4.4)$$

On the other hand, at least one relay is needed to facilitate the secondary path, that is,

$$\sum_{k=1}^K y_{ik} = 1, \forall i \in \Omega. \quad (4.5)$$

In addition, a relay cannot be used for the primary path and secondary path simultaneously. Therefore, we have

$$x_{ik} + y_{ik} \leq 1, \forall i \in L_k, \forall k. \quad (4.6)$$

The transmission time of unit data over link  $i$  via relay  $k$  is computed as

$$\tau_{ik} = \frac{1}{R_{s_i,k}} + \frac{1}{R_{k,d_i}}, \quad (4.7)$$

where  $R_{s_i,k}$ ,  $R_{k,d_i}$  are the transmission rates of the link between the transmitter and the relay, and between the relay and the receiver respectively. For the AWGN channel, they can be bounded by

$$R_{s_i,k} = W \log \left[ 1 + \frac{P_t G_t G_r}{P_n D(s_i, k)^\alpha} \right], \quad (4.8)$$

and

$$R_{k,d_i} = W \log \left[ 1 + \frac{P_t G_t G_r}{P_n D(k, d_i)^\alpha} \right], \quad (4.9)$$

respectively, where  $W$  is the channel bandwidth in Hz,  $P_t$  is the transmit power,  $P_n$  is the noise floor level,  $G_t, G_r$  are transmit and receive antenna gain,  $\alpha$  is the propagation factor and  $D(a, b)$  denotes the distance from  $a$  to  $b$ .

For a relay  $k$ , the TDMA scheduling for the associated links should satisfy

$$\sum_{i \in L_k} \eta_i x_{ik} r_i \tau_{ik} + g_k(\mathbf{y}_k, \mathbf{r}) \leq z_k, \forall k, \quad (4.10)$$

where  $r_i$  is the flow rate of link  $i$ ,  $\tau_{ik}$  is the transmission time of unit data of link  $i$  via relay  $k$ ,  $\eta_i$  is an indicator used to exclude the links with direct path. The first term on left represents the percentage of relay capability occupied by all the links utilizing this relay as their primary relay. The second term represents the protection function for the set of links selecting  $k$  as the secondary path, which is used to account for the case when some links have the uncertain blockage of the primary paths and selects their secondary paths.

To this end, the RMRP problem can be formally stated as

$$\begin{aligned} & \underset{\mathbf{x}, \mathbf{y}, \mathbf{z}}{\text{minimize}} && \sum_k z_k \\ & \text{subject to} && \text{Constraints (4.4)(4.5)(4.6)(4.7)(4.8)(4.9)(4.10)} \\ & \text{variables} && x_{ik}, y_{ik}, z_k \in \{0, 1\}, \forall i \in \Omega, k = 1, \dots, K. \end{aligned} \quad (4.11)$$

The protection function in (4.10) guarantees the robustness of the solution, which will be discussed next.

#### 4.5.2.1 Reformulation under $D$ -norm Uncertainty Model

The uncertainty models can be characterized with different protection functions. For example, if  $g_k(\cdot)$  is chosen to include the bandwidth demand of all the secondary

paths using relay  $k$ , the RMRP problem is equivalent to finding the minimum number of relays possible and their respective locations, such that there exist two vertex-disjoint paths with no more than 2-hops for every feasible mmWave link. However, such requirement is too stringent and may not be feasible. To this end, several uncertainty models have been proposed in literature to tradeoff between robustness and performance, including General Polyhedron,  $D$ -norm, Ellipsoid [91]. In this chapter, we adopt the  $D$ -norm uncertainty model to account for the case that at most a subset of primary paths may be blocked simultaneously in the worst case.

In the  $D$ -norm uncertainty model, the protection function is given by

$$g_k(\mathbf{y}_k, \mathbf{r}) = \max_{S_k: S_k \subseteq L_k, |S_k| = \Gamma_k} \sum_{i \in S_k} y_{ik} r_i \tau_{ik}. \quad (4.12)$$

In essence, among the set of mmWave links  $L_k$  that use relay  $k$  as their secondary paths, we consider a subset of size  $\Gamma_k$  that have the largest fraction of channel occupation time. Clearly, if  $\Gamma_k = |L_k|$ ,  $g_k(\mathbf{y}_k, \mathbf{r}) = \sum_{i \in L_k} y_{ik} r_i \tau_{ik}$ . Every link in  $L_k$  suffers from the blockage on their primary paths and have to select their secondary paths. If  $\Gamma_k = 0$ , then none of the links are under blockage.

Thus, (4.10) can be rewritten as

$$\sum_{i \in L_k} \eta_i x_{ik} r_i \tau_{ik} + \max_{S_k: S_k \subseteq L_k, |S_k| = \Gamma_k} \sum_{i \in S_k} y_{ik} r_i \tau_{ik} \leq z_k, \forall k. \quad (4.13)$$

The RMRP problem under the  $D$ -norm model is to maintain scheduling feasibility under the condition that at most  $\Gamma_k$  links in  $L_k$  fail in their primary paths. Thus,  $\Gamma_k$  is a parameter to tradeoff between robustness and efficiency.

A direct solution for (4.13) is not tractable since it involves a inner-optimization in the protection function. To this end, we reformulate the protection function as

follows [91],

$$\begin{aligned}
& \max_{\{0 \leq s_{ik} \leq 1\} \forall i \in L_k} \sum_{i \in L_k} y_{ik} r_i \tau_{ik} s_{ik}, \\
& \text{s.t.} \quad \sum_{i \in L_k} s_{ik} \leq \Gamma_k.
\end{aligned} \tag{4.14}$$

Due to the special structure of problem, the relaxed LP problem has exactly same optimal solution with the original one. Taking the dual of (4.14), we have

$$\begin{aligned}
& \min_{\{p_{ik} \geq 0\} \forall i \in L_k, q_k \geq 0} q_k \Gamma_k + \sum_{i \in L_k} p_{ik}, \\
& \text{s.t.} \quad q_k + p_{ik} \geq y_{ik} r_i \tau_{ik}.
\end{aligned} \tag{4.15}$$

Substituting (4.15) into (4.11), we can obtain the equivalent formulation of the RMRP problem as a mixed integer linear programming (MILP) problem as follows:

$$\begin{aligned}
& \min_{\mathbf{x}, \mathbf{y}, \mathbf{z}, \mathbf{p}, \mathbf{q}} \sum_k z_k \\
& \text{s.t.} \quad \sum_{i \in L_k} \eta_i x_{ik} r_i \tau_{ik} + q_k \Gamma_k + \sum_{i \in L_k} p_{ik} \leq z_k, \quad \forall k
\end{aligned} \tag{4.16}$$

$$q_k + p_{ik} \geq y_{ik} r_i \tau_{ik}, \quad \forall i \in L_k, \forall k$$

Constraints (4.4)(4.5)(4.6)(4.7)(4.8)(4.9)

variables  $x_{ik}, y_{ik}, z_k \in \{0, 1\}, p_{ik} \geq 0, q_k \geq 0$ .

#### 4.5.2.2 RMRP NP-hardness

In the following section, we aim to examine the NP-hardness of the RMRP problem.

Lemma 4.4. Consider a special case of RMRP as MRP when there is no uncertainty set, MRP is a NP-hard problem.

Proof. Since there is no uncertainty set in MRP, the protection function is null. We only consider the primary path scheduling on relay  $k$ 's in (4.10). In MRP,  $r_i\tau_{ik}$  represents the percentage of relay  $k$ 's capability occupied by link  $i$  that utilizes this relay as its primary relay. If we consider a bin as the relay capacity, the volume of item as the percentage of relay  $k$ 's capability occupied by link  $i$ , the Bin-Packing problem can be reduced as MRP problem in a polynomial time. Since Bin-Packing is NP-hard [92], we prove that the MRP problem is also a NP-hard problem.  $\square$

In the RMRP problem where the protection function is modeled by D-norm uncertainty model in (4.13), it would take more extra work for solving the inner optimization of protection function, which aims to search the maximum portion of relay  $k$ 's capacity occupied by secondary paths over all the uncertainty link sets with the set size  $\Gamma_k$ . Therefore, we confirm the RMRP problem is much harder than MRP. Since MRP is proved to be NP-hard in Lemma 4.9, we conclude that, RMRP (4.16) is also a NP-hard problem.

The MILP problem can be solved by any MILP solver. In our implementation, we utilize the MILP solver of IBM optimization tool – CPLEX.

### 4.5.3 Robust Maximum Utility Relay Placement

Distinguished from the RMRP problem, the RMURP problem is to achieve the maximum overall utility of the mmWave WPANs with the limited number of available relays, while satisfying the constraints of link connectivity, scheduling capability and robustness.

We consider  $r_i$  be the base flow rate for every mmWave link  $i$ . However, due to network dynamics, not all the links can maintain the transmissions with  $r_i$ . We expect to higher the flow rate for better channel environments, and lower it otherwise. Therefore, a scalar notation  $\alpha$  is introduced to adapt the best flow rate for every

feasible mmWave link in the network with fairness.

The overall utility of network is computed as

$$U_T = \sum_i U_i(r_i) = \sum_i \alpha r_i. \quad (4.17)$$

Therefore, the scheduling constraint for the associated links using relay  $k$  becomes

$$\sum_{i \in L_k} \eta_i x_{ik} \alpha r_i \tau_{ik} + g_k(\mathbf{y}_k, \alpha \mathbf{r}) \leq z_k, \forall k. \quad (4.18)$$

Furthermore, the number of available relays should be constrained as

$$\sum_k z_k \leq K. \quad (4.19)$$

Therefore, the robust maximum utility relay placement (RMURP) problem can be formally presented as:

$$\begin{aligned} & \underset{\mathbf{x}, \mathbf{y}, \mathbf{z}, \alpha}{\text{maximize}} && \sum_i \alpha r_i \\ & \text{subject to} && \text{Constraints (4.4)(4.5)(4.6)(4.7)(4.8)(4.9)(4.18)(4.19)} \\ & \text{variables} && x_{ik}, y_{ik}, z_k \in \{0, 1\}, \alpha \geq 0, \forall i \in \Omega, k = 1, \dots, K. \end{aligned} \quad (4.20)$$

#### 4.5.3.1 Reformulation under $D$ -norm Uncertainty Model

Similarly using robust optimization techniques, the  $D$ -norm uncertainty model can be applied to account for the uncertainty on link blockage in mmWave WPANs. Therefore, we can obtain the equivalent formulation of the RMURP problem as a

mixed integer non-linear programming problem (MINLP) as follows:

$$\begin{aligned}
& \underset{\mathbf{x}, \mathbf{y}, \mathbf{z}, \mathbf{p}, \mathbf{q}, \alpha}{\text{Maximize}} && \sum_i \alpha r_i \\
& \text{subject to} && \sum_{i \in L_k} \eta_i x_{ik} \alpha r_i \tau_{ik} + q_k \Gamma_k + \sum_{i \in L_k} p_{ik} \leq z_k, \forall k \\
& && q_k + p_{ik} \geq y_{ik} \alpha r_i \tau_{ik}, \forall i \in L_k, \forall k \\
& && \text{Constraints (4.4)(4.5)(4.6)(4.7)(4.8)(4.9)(4.19)} \\
& \text{variables} && x_{ik}, y_{ik}, z_k \in \{0, 1\}, p_{ik} \geq 0, q_k \geq 0, \alpha \geq 0.
\end{aligned} \tag{4.21}$$

#### 4.5.3.2 RMURP NP-hardness

In the following section, we show that the RMURP problem is a NP-hard problem.

Lemma 4.5. Consider a special case of RMURP as MURP when there is no uncertainty set and only one relay in the network, MURP is NP-hard.

Proof. Since there is no uncertainty set in MURP, the protection function term is null. Also, consider only one relay in the network, we can rewrite the scheduling constraint of MURP in (4.18) as:  $\sum_i \eta_i x_{ik} \alpha r_i \tau_{ik} \leq z$ . Therefore,  $\alpha r_i$  represents the value of item  $i$ , while  $\eta_i \alpha r_i \tau_{ik}$  denotes the weight of item  $i$ . Then, the 0-1 knapsack problem can be reduced as MURP problem in a polynomial time. Since the Knapsack problem is NP-hard [92], then the MURP problem is proved to be NP-hard.  $\square$

Similarly, RMURP problem would take more extra work for solving the inner optimization of protection function. Therefore, we can confirm that, the RMURP problem is much harder than MURP. Since MURP is NP-hard as shown in 4.5, we conclude that, RMURP (4.21) is also a NP-hard problem.

In the formulation in (4.21), the scalar variable  $\alpha$  is coupled with other binary variables, which makes it even harder to solve directly. To solve the problem, we have proposed two different algorithms as follows:

- A heuristic algorithm using Bisection Search method is proposed to solve it fast;
- The MINLP problem has a special property that if the discrete variables are fixed in constraints, it is actually convex with respect to the continuous variables. The Generalized Benders' Decomposition (GBD) has been used in [93–95] for MINLP problem with this convex property. It has been proved that GBD can achieve the optimal solution.

#### 4.5.3.3 Bisection Search Algorithm

The Bisection Search method is a straightforward method to find the root which repeatedly bisects an interval and then selects a subinterval in which a root must lie for further processing. Therefore, it is guaranteed to converge to a root of  $f()$  if and only if:  $f$  is a continuous function on the interval  $[A, B]$ , and  $f(A)$  and  $f(B)$  have opposite signs. From observation, our problem (4.21) has the similar characteristic with the given  $\alpha$  where the feasibility of the problem partially depends on the selected variable  $\alpha$ . If a given  $\alpha$  is 0, the remaining problem should be feasible. On the other hand, if a given  $\alpha$  is too large, then the problem may become infeasible.

Therefore, we can employ the Bisection Search method to decouple  $\alpha$  from other binary variables, which makes (4.21) into a solvable MILP problem. After that, the IBM CPLEX solver can be applied to verify the feasibility of the problem, feasible and infeasible as two opposite signs. The Bisection Search procedure for best  $\alpha$  is shown in Algorithm 4. Although it runs fast, Bisection Search does not guarantee the optimal solution.

---

Algorithm 4: Bisection Search for RMURP in an Interference-free Model

---

Input : Traffic demands of every feasible mmWave links  $r_i, \forall i$ , Tolerance  $TOL$  and proper range of  $\alpha$ :  $[A, B]$

Output: Maximum network utility  $U_T$  and relay selection variables for every feasible mmWave links  $\mathbf{x}, \mathbf{y}, \mathbf{z}$

```
begin
  Set  $n = 1$ ;
  while  $n \leq \max N$  do
     $C \leftarrow \frac{(A+B)}{2}$ ;
    Solve the MILP problem  $RMURP(C)$ .
    if  $RMURP(C)$  is feasible then
       $A \leftarrow C$ ;
      Obtain the solutions of  $RMURP(C)$ :  $\mathbf{x}^{(n)}, \mathbf{y}^{(n)}, \mathbf{z}^{(n)}$ .
    else
       $B \leftarrow C$ ;
    end
     $n \leftarrow n + 1$ ;
    if  $\frac{(B-A)}{2} \leq TOL$  then
      The optimal  $\alpha$  found,  $\alpha_{opt} \leftarrow A$ ;
      Return  $U_T, \mathbf{x}^{(n)}, \mathbf{y}^{(n)}, \mathbf{z}^{(n)}$ .
    end
  end
end
```

---

#### 4.5.3.4 Generalized Benders' Decomposition Algorithm

The principle of the GBD algorithm is to decompose the original MINLP problem into a primal problem and a master problem and then solve them iteratively. The primal problem corresponds to the original problem with fixed binary variables. Solving the primal problem provides the information about the lower bound and the Lagrange multipliers corresponding to the constraints. The master problem is derived through nonlinear duality theory using the Lagrange multipliers obtained from the primal problem. The solution of the master problem presents the information about the upper bound as well as the binary variables that can be used for primal problem in next iteration.

**Primal Problem** Let  $\Lambda := (x, y, z)$  represents the set of binary variables,  $\hat{\Lambda} := (\hat{x}, \hat{y}, \hat{z})$  indicates the binary variables with specific values in  $\{0, 1\}$ . The primal problem  $\mathcal{P}(\hat{\Lambda})$  of our RMURP problem (4.21) is obtained by fixing all the binary variables to  $\hat{\Lambda}$  as follows:

$$\mathcal{P}(\hat{\Lambda}) \left\{ \begin{array}{l} f(\hat{\Lambda}) = \underset{\mathbf{p}, \mathbf{q}, \alpha}{\text{maximize}} \quad \sum_i \alpha r_i \\ \text{subject to} \quad \sum_{i \in L_k} \eta_i \hat{x}_{ik} \alpha r_i \tau_{ik} + q_k \Gamma_k + \sum_{i \in L_k} p_{ik} \leq \hat{z}_k, \quad \forall k \\ q_k + p_{ik} \geq \hat{y}_{ik} \alpha r_i \tau_{ik}, \quad \forall i \in L_k, \forall k \\ \text{variables} \quad \mathbf{p} \succeq 0, \mathbf{q} \succeq 0, \alpha \geq 0. \end{array} \right. \quad (4.22)$$

This is a linear program problem, that can be solved by any LP solver. Since the optimal solution of  $\mathcal{P}(\hat{\Lambda})$  is also a feasible solution to (4.21). Therefore, the optimal value  $f(\hat{\Lambda})$  provides a lower bound to our RMURP problem. It is also clear that, not all the choices of given binary variables can lead to a feasible primal problem. We need to treat it differently depending on whether the primal problem is feasible or not:

- Feasible Primal:

If the primal problem is feasible, let

$$T_k(\hat{\Lambda}, \mathbf{p}, \mathbf{q}, \alpha) = \hat{z}_k - \left( \sum_{i \in L_k} \eta_i \hat{x}_{ik} \alpha r_i \tau_{ik} + q_k \Gamma_k + \sum_{i \in L_k} p_{ik} \right), \forall k, \quad (4.23)$$

$$g_{ik}(\hat{\Lambda}, \mathbf{p}, \mathbf{q}, \alpha) = q_k + p_{ik} - \hat{y}_{ik} \alpha r_i \tau_{ik}, \forall i \in L_k, \forall k.$$

Then, we can compute the partial Lagrangian function for the primal problem as follows,

$$L(\hat{\Lambda}, \mathbf{p}, \mathbf{q}, \alpha, \lambda, \nu) = \sum_i \alpha r_i + \sum_k \lambda_k T_k + \sum_k \sum_i \nu_{ik} g_{ik}, \quad (4.24)$$

where  $\lambda_k, \nu_{ik} \geq 0, \forall i \in L_k, \forall k$  are the Lagrange multipliers.

Thus, the Lagrange dual problem of  $\mathcal{P}(\hat{\Lambda})$  can be stated as

$$\min_{\lambda, \nu} \max_{p, q, \alpha} L(\hat{\Lambda}, \mathbf{p}, \mathbf{q}, \alpha, \lambda, \nu). \quad (4.25)$$

Since the problem is convex and satisfies linearity constraint qualification, the duality gap is 0. Thus, solving the Lagrange dual problem would give the optimal solution of  $\mathcal{P}(\hat{\Lambda})$ .

• Infeasible Primal:

If the primal problem is infeasible, we first define a set  $\Delta$  as

$$\Delta = \{\hat{\Lambda} | T_k \geq 0, g_{ik} \geq 0, \forall i \in L_k, \forall k, \text{ for some } \mathbf{p}, \mathbf{q}, \alpha\}, \quad (4.26)$$

and consider the following feasibility-checking problem:

$$\mathcal{F}(\hat{\Lambda}) \begin{cases} \text{minimize} & \delta \\ \text{subject to} & \sum_{i \in L_k} \eta_i \hat{x}_{ik} \alpha r_i \tau_{ik} + q_k \Gamma_k + \sum_{i \in L_k} p_{ik} - \hat{z}_k \leq \delta, \forall k \\ & \hat{y}_{ik} \alpha r_i \tau_{ik} - q_k - p_{ik} \leq \delta, \forall i \in L_k, \forall k \\ \text{variables} & \mathbf{p} \succeq 0, \mathbf{q} \succeq 0, \alpha \geq 0, \delta \geq 0 \end{cases}, \quad (4.27)$$

It is straightforward to see that, for any given  $\hat{\Lambda}$ ,  $\mathcal{P}(\hat{\Lambda})$  is infeasible if and only if  $\mathcal{F}(\hat{\Lambda})$  has a positive optimal value  $\delta^* > 0$ .

The Lagrangian function for  $\mathcal{F}(\hat{\Lambda})$  can be presented as

$$G(\hat{\Lambda}, \mathbf{p}, \mathbf{q}, \alpha, \mu, \sigma) = \sum_k \mu_k \left( \sum_{i \in L_k} \eta_i \hat{x}_{ik} \alpha r_i \tau_{ik} + q_k \Gamma_k + \sum_{i \in L_k} p_{ik} - \hat{z}_k \right) + \sum_k \sum_{i \in L_k} \sigma_{ik} (\hat{y}_{ik} \alpha r_i \tau_{ik} - q_k - p_{ik}), \forall (\mu, \sigma) \in \Omega, \quad (4.28)$$

where  $\mu_k, \sigma_{ik}$  are Lagrange multipliers and  $\Omega = \{(\mu, \sigma) | \mu_k, \sigma_{ik} \geq 0, \sum_k (\mu_k + \sum_{i \in L_k} \sigma_{ik}) = 1, \forall i \in L_k, \forall k\}$ .

The Lagrangian dual of  $\mathcal{F}(\hat{\Lambda})$  becomes

$$\max_{\mu, \sigma} \min_{\mathbf{p}, \mathbf{q}, \alpha} G(\hat{\Lambda}, \mathbf{p}, \mathbf{q}, \alpha, \mu, \sigma). \quad (4.29)$$

Therefore, for any  $\hat{\Lambda} \in \Delta$  can be characterized by the inequality constraint,

$$0 \geq \min_{p, q} G(\hat{\Lambda}, \mathbf{p}, \mathbf{q}, \alpha, \mu, \sigma). \quad (4.30)$$

Master Problem The original problem in (4.21) can be written as:

$$\begin{aligned} \max_{\Lambda} \sum_i \alpha r_i &= \max_{\Lambda \in \Delta} f(\Lambda) \\ &= \max_{\Lambda \in \Delta} \left[ \min_{\lambda, \nu} \max_{\mathbf{p}, \mathbf{q}, \alpha} L(\Lambda, \mathbf{p}, \mathbf{q}, \alpha, \lambda, \nu) \right] \\ &= \max \beta \end{aligned} \quad (4.31)$$

$$\text{s.t. } \beta \leq \max_{\mathbf{p}, \mathbf{q}, \alpha} L(\Lambda, \mathbf{p}, \mathbf{q}, \alpha, \lambda, \nu), \forall \lambda, \nu \succeq 0$$

$$\Lambda \in \{0, 1\} \cap \Delta,$$

where the second equality comes from (4.25) because of no duality gap. Incorporating (4.30) into (4.31), we finally obtain the master problem  $\mathcal{M}(\mathbf{p}, \mathbf{q}, \alpha, \lambda, \nu, \mu, \sigma)$  as:

$$\mathcal{M}(\cdot) \begin{cases} \max_{\Lambda} & \beta \\ \text{s.t.} & \beta \leq \max_{\mathbf{p}, \mathbf{q}, \alpha} L(\Lambda, \mathbf{p}, \mathbf{q}, \alpha, \lambda, \nu), \forall \lambda, \nu \succeq 0 \\ & 0 \geq \min_{\mathbf{p}, \mathbf{q}, \alpha} G(\Lambda, \mathbf{p}, \mathbf{q}, \alpha, \mu, \sigma), \forall (\mu, \sigma) \in \Omega \\ & \text{Constraints of (4.4)(4.5)(4.6)(4.7)(4.8)(4.9)(4.19)} \\ & \Lambda \in \{0, 1\}, \beta \geq 0. \end{cases} \quad (4.32)$$

Note that, the master problem has two inner optimization problems as its constraints, which need to be considered for all  $\lambda, \nu$  and  $\mu, \sigma$ . This implies that the master problem has a very large number of constraints. In order to obtain a solvable mixed-integer linear programming problem, we employ the following relaxation for the master problem at iteration  $n$  as described in [93],

$$\begin{aligned} \beta &\leq L(\Lambda^n, \mathbf{p}^n, \mathbf{q}^n, \alpha^n, \lambda^n, \nu^n) + \nabla_{\Lambda} L(\cdot)(\Lambda - \Lambda^n), \forall n \in \mathcal{P}^k, \\ 0 &\geq G(\Lambda^n, \mathbf{p}^n, \mathbf{q}^n, \alpha^n, \mu^n, \sigma^n) + \nabla_{\Lambda} G(\cdot)(\Lambda - \Lambda^n), \forall n \in \mathcal{F}^k, \end{aligned} \quad (4.33)$$

where  $\mathcal{P}^k$  and  $\mathcal{F}^k$  are the sets of feasible and infeasible primal problems solved up to iteration  $k$ , respectively.

The relaxed problem provides the upper bound of the original master problem and can be used to generate the primal problem in the next iteration. The detail of GBD algorithm is shown in algorithm 5.

#### 4.5.4 Simulation Results

Consider a a 10mX10m region as a typical mmWave based home network environment,  $N$  mmWave devices and  $M$  obstacles are uniformly placed. The relays are located in grid points in this area with a separation  $d_0$  between neighboring relays. For decoding threshold, the transmission radii of both mmWave devices and relays

---

Algorithm 5: Generalized Benders' Decomposition

---

Input : Traffic demands of every feasible mmWave link  $r_i, \forall i$   
Output: Maximum network utility boost factor  $\alpha$  and relay selection variables for every feasible mmWave link  $\Lambda = (\mathbf{x}, \mathbf{y}, \mathbf{z})$  and  $\mathbf{p}, \mathbf{q}$

begin

  set  $n = 1$  and choose  $\Lambda \in \{0, 1\}$ ,  
   $LB^0 \leftarrow -\infty, UB^0 \leftarrow \infty, \mathcal{P}^0 \leftarrow \emptyset, \mathcal{F}^0 \leftarrow \emptyset$ .  
  while  $LB^{n-1} \leq UB^{n-1}$  do

    if the primal problem is feasible then

      Solve the primal problem  $\mathcal{P}(\Lambda^n)$  to obtain optimal solution  $\mathbf{p}^n, \mathbf{q}^n, \alpha^n$   
      and Lagrangian multipliers  $\lambda^n, \nu^n$ ;  
       $\mathcal{P}^n \leftarrow \mathcal{P}^{n-1} \cup \{n\}, \mathcal{F}^n \leftarrow \mathcal{F}^{n-1}$ ;  
       $LB^n \leftarrow \max(LB^{n-1}, f(\Lambda^n))$ ;  
      if  $LB^n == f(\Lambda^n)$  then

$(\Lambda^*, \tilde{\mathbf{p}}^*, \tilde{\mathbf{q}}^*, \tilde{\alpha}^*) \leftarrow (\Lambda^n, \tilde{\mathbf{p}}^n, \tilde{\mathbf{q}}^n, \tilde{\alpha}^n)$ ;  
        end

    else if the primal problem is infeasible then

      Solve the feasibility-check problem  $\mathcal{F}(\hat{\Lambda})$  to obtain the optimal solution  $\mathbf{p}^n, \mathbf{q}^n, \alpha^n$  and Lagrangian multipliers  $\mu^n, \sigma^n$ ;  
       $\mathcal{P}^n \leftarrow \mathcal{P}^n, \mathcal{F}^n \leftarrow \mathcal{F}^{n-1} \cup \{n\}$ ;

    end

    Solve the master problem  $\mathcal{M}(\mathbf{p}^n, \mathbf{q}^n, \alpha^n, \lambda^n, \nu^n, \mu^n, \sigma^n)$   
    and obtain the optimal solution  $\Lambda^{n+1}$  and  $\beta^n$ ;  
     $UB^n \leftarrow \beta^n, n \leftarrow n + 1$ ;

  end

  return  $\Lambda^*, \mathbf{p}^*, \mathbf{q}^*, \alpha^*$ .

end

---

are 6m. The traffic demand of each link  $r_i$  is given as the average 1/10 of channel capacity. The PHY parameters in simulation are listed in Table. 4.2.

Table 4.2: Simulation setup

PHY parameters	Values
Channel	AWGN channel with gain 1
Path Loss	free space with factor 2
Transmit power	20mW (13dBm)
Noise floor	-100dBm

#### 4.5.4.1 RMRP Performance

In this section, we examine the performance of RMRP under different configurations by varying the number of mmWave logical links ( $N$ ), the number of moving subjects ( $M$ ) and the robustness index ( $\rho$ ).

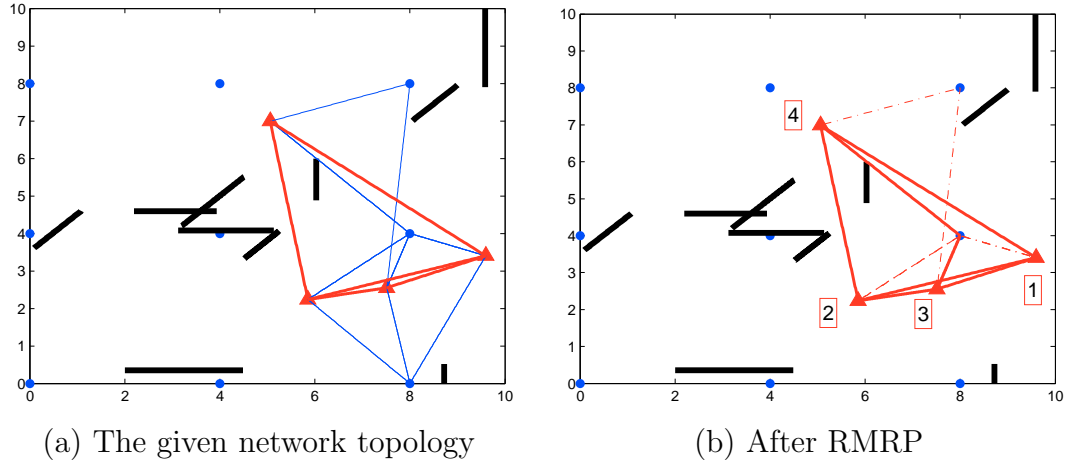
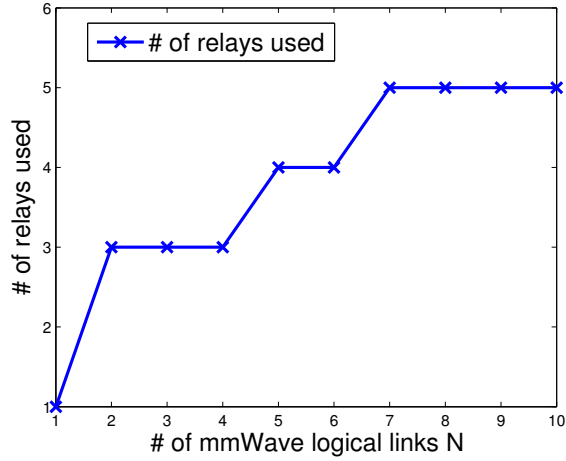
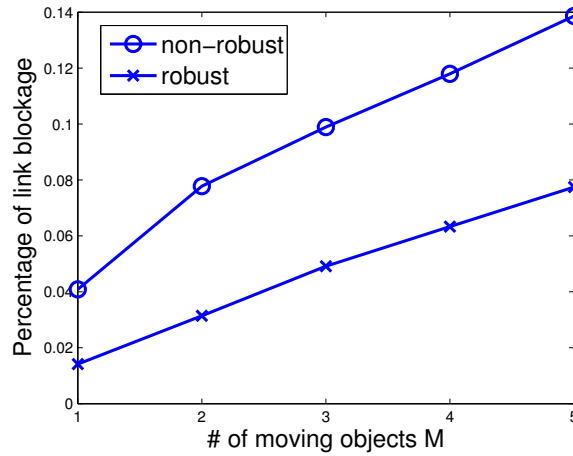


Figure 4.5: An illustration of RMRP in an example network with  $N=4$ ,  $d_0=4$ ,  $M=10$  and  $\Gamma_k/|L_k|=1$ . In (a), the solid blue lines denote indirect paths, the solid red lines denote direct paths; In (b) the solid red lines are primary paths, the dash red lines are secondary paths.

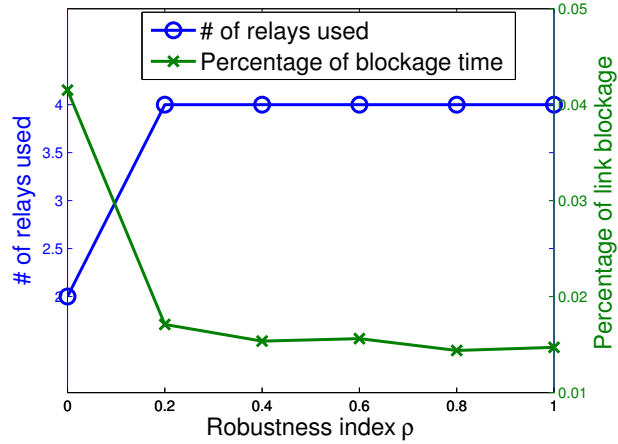
First, we would like to illustrate how RMRP perform the relay placement in a simple example network under the same simulation setup. Fig. 4.5 (a) gives an example network topology with 4 mmWave devices (denoted by red triangles) and 10 obstacles (denoted by black bars)), where the solid red and blue lines indicate the



(a) Effect of the number of logical links with  $\rho = 1$



(b) Effect of the number of moving subjects with  $\rho = 1, N = 5$



(c) Effect of the robustness index with  $M = 1, N = 5$

Figure 4.6: Performance of RMRP in an mmWave home network deployed in a  $10\text{m} \times 10\text{m}$  room.

direct paths and 2-hop paths among the devices. The relays (denoted by blue dots) are placed in grid with a separation 4 meters. Fig. 4.5 (b) shows the result of RMRP, where solid red lines are the primary paths, and dashed lines are the secondary paths. We can see that, only two relay is selected in this case, which is the minimum relay number needed to support robust connectivity of all feasible mmWave links.

Fig. 4.6(a) shows the number of relays when relay candidate locations and obstacles are fixed, while the number of mmWave logical links varies. In this set of experiments, all logical links are feasible. More relays are needed as the number of logical links increases. However, the relationship is not always linear due to the absence of LOS paths between TX/RX pairs and the multiplexing of relays.

Fig. 4.6(b) show the percentage of link blockage per link when human subjects move randomly in the room. The mobility setup is similar to that in Section 4.4. Clearly, As the number of human subjects increases, the percentage of link blockage increases as well. However, the robust scheme leads to 50% less blockage.

Next, we evaluate the impact of robustness index  $\rho$ . In this setup, 1 human subject moves randomly and there are 5 logical links. Figure 4.6(c) shows the number of relays used and the percentage of link blockage. As expected, as  $\rho$  increases, more relays are used and the link blockage reduces.

#### 4.5.4.2 RMURP Performance

We now evaluate the performance of the Bisection Search and GBD algorithm on RMURP. The error tolerance of Bisection Search is set to  $TOL = 1.0$ .

First, we want to illustrate how RMURP perform the relay placement differently from RMRP. Given a example network in Fig. 4.5 (a), Fig. 4.7 (a) (b) demonstrate the RMURP results for Bisection Search algorithm and GBD algorithm, respectively. As demonstrated, both algorithms approach a similar solution in this example network

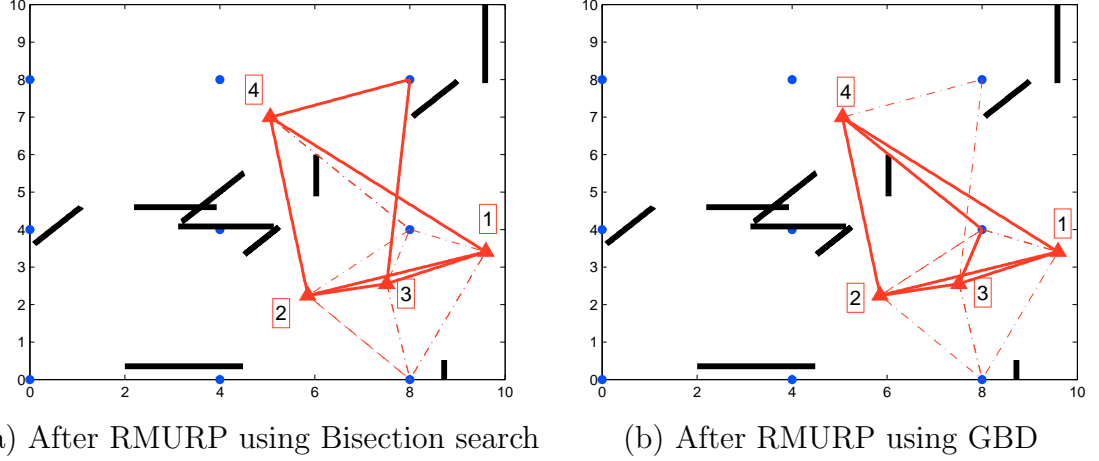


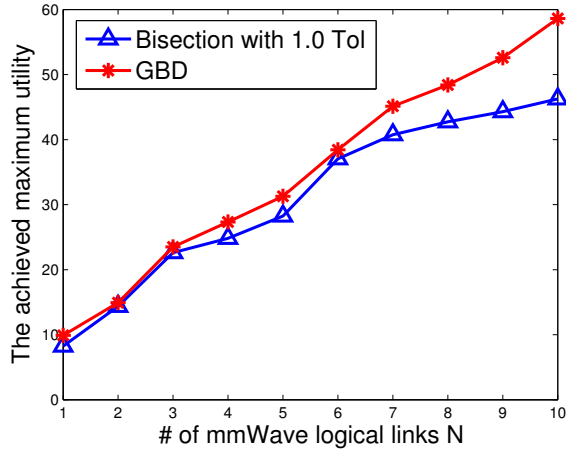
Figure 4.7: An illustration of RMURP in an example network with  $N=4$ ,  $d_0=4$ ,  $M=10$  and  $\Gamma_k/|L_k|=1$ . The solid red lines are primary paths, the dash red lines are secondary paths.

with 3 relays required. Furthermore, the GBD solution can always achieve the optimal solution that has larger network utility than Bisection Search.

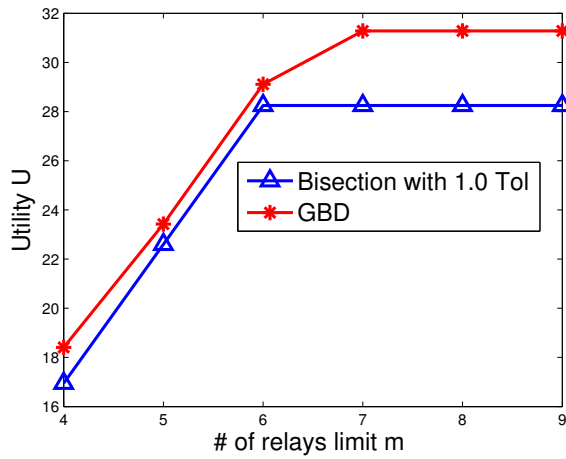
Fig. 4.8 shows the utility achieved using both methods by varying the number of logical links (Fig. 4.8(a)), the total number of relays (Fig. 4.8(b)) and the robustness index (Fig. 4.8(c)). In all cases, GBD achieves higher utility compared to Bisection Search. Reducing the threshold  $TOL$  improves the performance of Bisection Search but comes at a higher computation cost.

Fig. 4.9(a) demonstrates the convergence of the GBD algorithm. As shown in Fig. 4.9(a), over time, the upper bound (solutions to the master problem) is non-increasing; and the lower bound (solutions to the primary problem) is non-decreasing. The algorithm converges to the optimal solution after 50 iterations when the upper bound equals to the lower bound.

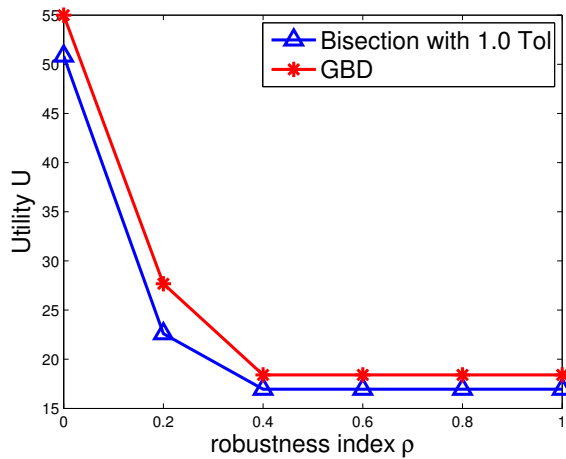
Fig. 4.9(b)(c) shows the percentage of link blockage per link under RMURP when human subjects move randomly in the room by varying the number of moving subjects and the robustness index, respectively. In both cases, GBD achieves lower percentage of blockage. This implies that the relay selection in GBD has more spatial



(a) Effect of the number of logical links with  $m = 7$  and  $\rho = 1$

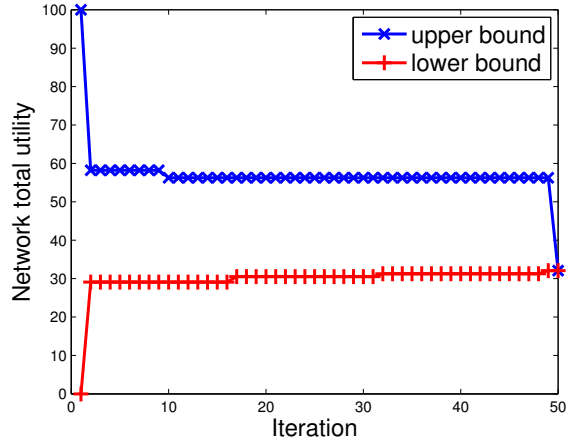


(b) Effect of the maximum number of relays with  $N = 5$  and  $\rho = 1$

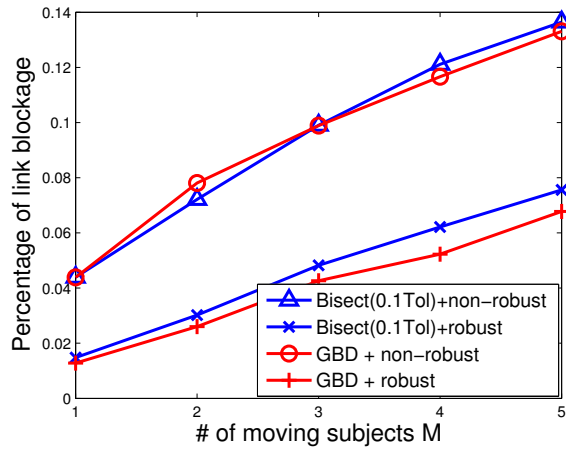


(c) Effect of the robustness index with  $m = 7$  and  $N = 5$

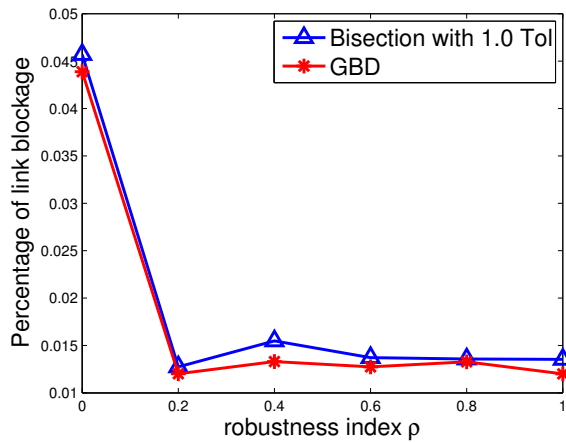
Figure 4.8: Performance of RMURP on utility in an mmWave home network deployed in a  $10\text{m} \times 10\text{m}$  room, Bisection Search algorithm with 1.0 tolerance and GBD algorithm.



(a) GBD convergence with  $N = 5$ ,  $m = 7$  and  $\rho = 1$



(b) Effect of the number of moving subjects with  $N = 5$ ,  $m = 7$ , and  $\rho = 1$



(c) Effect of the robustness index with  $N = 5$ ,  $m = 7$ , and  $M = 1$

Figure 4.9: Performance of RMURP on link blockage in an mmWave home network deployed in a  $10\text{m} \times 10\text{m}$  room, Bisection Search algorithm with 1.0 tolerance and GBD algorithm.

diversity.

## 4.6 Robust Relay Placement and Route Selection in 60GHz WPANs with Directional Antenna

### 4.6.1 Problem Statement

In this section, we consider a more complex interference model, instead of assuming a perfect interference-free model. A classic directional antenna model [64, 79] is adopted to explore the spatial contention for every pair of mmWave physical links.

Consider an mmWave network consisting of a set of  $L$  logical mmWave links (simplified as logical links), each logical link  $l \in L$  is associated with a source device (transmitter)  $s_l$ , a destination device (receiver)  $d_l$ , and a traffic demand  $f_l$  bps. mmWave relay devices (simplified as relays) equipped with steerable antennas can relay data between the transmitters and receivers. The relays can be placed at a set of  $K$  candidate locations. We further consider a set of  $O$  obstacles in the environment with known locations.

Relay placement concerns with the selection of relays among a finite set of candidate locations to optimize for certain network utilities. We consider two variants of the problem.

**Definition 4.6.** (Robust Minimum Relay Placement (RMRP)) Given an mmWave WPAN employing directional antenna, and a set of feasible logical links with fixed traffic demands, find the minimum number of relays and their locations among candidate location set  $\mathcal{K}$  that satisfy connectivity, bandwidth, and robustness constraints.

**Definition 4.7.** (Robust Maximum Utility Relay Placement (RMURP)) Given an mmWave WPAN employing directional antenna, and a set of feasible logical links

with fixed traffic demands, find the placement of at most  $m$  relays among candidate location set  $\mathcal{K}$  such that the ratio of the achievable rates over the base rate is maximized subject to robustness constraints.

We restrict forwarding of data to relays only. In the robust formulation, for each feasible logical link, two vertex-disjoint (except for the endpoints) communication paths are provisioned, one as the primary path, and the other as the secondary path. Both the primary and secondary paths between mmWave transmitters and receivers cannot be more than 2-hops. If a relay serves more than one logical links, time division medium access (TDMA) scheduling is adopted. Similarly, an mmWave node also adopts TDMA scheduling when serving TX or RX for more than one logical links. The interference among concurrent transmissions is determined based on the directional antenna radiation pattern in Section 4.6.2. Therefore, the main sources of contention arise from the half-duplex constraint, multiplexing at the mmWave and relay nodes, as well as spatial contention among the concurrent transmissions.

#### 4.6.2 Link-Link Spatial Contention

In this work, we consider a classic directional antenna model [64, 79], in which the radiation pattern can be modeled as  $Q(D, \theta, \phi)$ , where  $D$ ,  $\theta$ ,  $\phi$  denote the radius, beamwidth and antenna direction, respectively. Therefore, consider two physical links  $u(s_u, d_u)$  and  $v(s_v, d_v)$ , their TX covered regions are represented as  $Q_u(D, \theta, \phi_u)$  and  $Q_v(D, \theta, \phi_v)$ . Note for simplicity, we assume the same radius and beamwidth across all transmitters. However, the methodologies can be readily extended to the case with heterogeneous transmission radius and beamwidth. The (binary) spatial contention between the physical link  $u$  and  $v$  is denoted by  $c_{uv}$ , defined as

$$c_{uv} = \begin{cases} 0, & \text{if } d_v \notin Q_u \cap \text{Min}(\|d_v - d_u\|, \|d_v - s_u\|) > 0.635, \\ 1, & \text{otherwise.} \end{cases} \quad (4.34)$$

In other words, link  $u$  does not contend with  $v$  iff i) the receiver of  $v$  (denoted as  $d_v$ ) is outside  $u$ 's TX covered region, and ii)  $d_v$  is at least 0.635 meter (interference-free distance [55]) from both  $u$ 's TX and RX. Clearly, the spatial contention relationship is not symmetrical, namely,  $c_{uv} \neq c_{vu}$ , due to directionality.

### 4.6.3 Robust Minimum Relay Placement

In this section, we present the analytical form of the RMRP problem. The following notations are used:

- Primary indicator:  $x_{lk} = 1$  if relay  $k$  is selected by logical link  $l$  as its primary path relay; otherwise,  $x_{lk} = 0$ ;
- Secondary indicator:  $y_{lk} = 1$  if relay  $k$  is selected by logical link  $l$  as its secondary path relay; otherwise,  $y_{lk} = 0$ ;
- Selection indicator:  $z_k = 1$  if relay  $k$  is selected by at least one logical link; otherwise,  $z_k = 0$ ;
- NLOS indicator:  $\eta_l = 1$  if logical link  $l$  does not have a LOS path; otherwise,  $\eta_l = 0$ .

If a logical link  $l$  has a LOS path, no relay is needed for the primary path; otherwise, one relay should be selected for the primary path, which should satisfy the following condition:

$$\sum_{k=1}^K x_{lk} = \eta_l, \forall l \in \Omega, \quad (4.35)$$

where  $\Omega$  is the set of all feasible logical links in the network.

On the other hand, at least one relay is needed to facilitate the secondary path, that is,

$$\sum_{k=1}^K y_{lk} = 1, \forall l \in \Omega. \quad (4.36)$$

In addition, a relay cannot be used for the primary path and the secondary path simultaneously. Therefore, we have

$$x_{lk} + y_{lk} \leq 1, \forall l \in \Omega_k, \forall k, \quad (4.37)$$

where  $\Omega_k$  is the set of feasible logical links that can  $k$  as the relay.

As mentioned before, for simplicity, we assume each relay has only one half-duplex transceiver. Therefore, the transmission time  $\tau_{lk}$  of relaying a unit data of logical link  $l$  via relay  $k$  is

$$\tau_{lk} = \frac{1}{R_{s_l, k}} + \frac{1}{R_{k, d_l}}, \quad (4.38)$$

where  $R_{s_l, k}$ ,  $R_{k, d_l}$  are the mmWave data bandwidth between the source and the relay, and between the relay and the destination, respectively. In the AWGN channel, they can be modeled as

$$R_{s_l, k} = \begin{cases} W \log \left[ 1 + \frac{P_t G_t G_r}{P_n D(s_l, k)^\gamma} \right] & (\text{when } D(s_l, k) \leq \Theta) \\ 0 & (\text{when } D(s_l, k) > \Theta), \end{cases} \quad (4.39)$$

and

$$R_{k, d_l} = \begin{cases} W \log \left[ 1 + \frac{P_t G_t G_r}{P_n D(k, d_l)^\gamma} \right] & (\text{when } D(k, d_l) \leq \Theta) \\ 0 & (\text{when } D(k, d_l) > \Theta), \end{cases}, \quad (4.40)$$

respectively, where  $W$  is the channel bandwidth in Hz,  $P_t$  is the transmission power,  $P_n$  is the noise floor level,  $G_t$ ,  $G_r$  are transmitter and receiver antenna gains,  $\gamma$  is the large-scale path loss index,  $D(a, b)$  is the distance from  $a$  to  $b$ , and  $\Theta$  is a constant threshold on communication radius, determined by receiver sensitivity threshold.

For a relay  $k$ , the TDMA scheduling for the associated logical links should satisfy

$$\sum_{l \in \Omega_k} \eta_l f_l \tau_{lk} x_{lk} + g_k(\mathbf{y}_k, \mathbf{f}) \leq z_k, \forall k, \quad (4.41)$$

where  $f_l$  is the traffic demand of logical link  $l$ ,  $\tau_{lk}$  is the unit data relay time of  $l$  via relay  $k$ . The first term on the left side represents the percentage of relay capacity occupied by all the logical links using this relay on their primary path. The second term represents the protection function for the set of logical links using this relay as their secondary path relay. A protection function  $g_k(\cdot)$  measures the robustness of an mmWave WPAN. Its meaning will be further explained in Section 4.6.3.1.

In addition to multiplexing contention at relay nodes, we are also interested in the contention of concurrent transmissions among physical links. Given a physical link  $i(s_i, d_i)$  where  $s_i$  is the transmitter and  $d_i$  is the receiver,  $i$  may belong to one and only one of the following three categories, as illustrated in Fig. 4.10:

- LOS logical link:  $\delta_1^i = 1$  if physical link  $i$  corresponds to a LOS logical link (otherwise,  $\delta_1^i = 0$ ). In this case, both  $s_i$  and  $d_i$  are mmWave nodes.
- 1st hop of an NLOS logical link:  $\delta_2^i = 1$  if physical link  $i$  is the 1st hop of an NLOS logical link (otherwise,  $\delta_2^i = 0$ ). In this case,  $s_i$  is an mmWave node while  $d_i$  is a relay.
- 2nd hop of an NLOS logical link:  $\delta_3^i = 1$  if physical link  $i$  is the 2nd hop of an NLOS logical link (otherwise,  $\delta_3^i = 0$ ). In this case,  $s_i$  is a relay while  $d_i$  is an mmWave node.

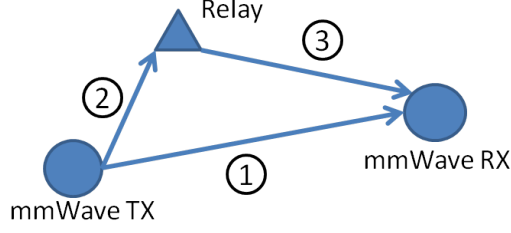


Figure 4.10: Three types of physical links.

The flow rate of a physical link is the sum of traffic demands of all logical links passing through it. Thus, the flow rate of physical link  $i$  ( $s_i, d_i$ ) can be computed as

$$\begin{aligned}
 r_i = & \delta_1^i f_i + \delta_2^i \left[ \sum_{l \in L_{src}(s_i)} \eta_l f_l x_{ld_i} + g_i(\mathbf{y}_{d_i}, \mathbf{f}) \right] \\
 & + \delta_3^i \left[ \sum_{l \in L_{des}(d_i)} \eta_l f_l x_{ls_i} + g_i(\mathbf{y}_{s_i}, \mathbf{f}) \right], \tag{4.42}
 \end{aligned}$$

where  $f_l$  is the given traffic demand of logical link  $l$ ,  $f_i$  is the flow rate of  $i$  when  $\delta_1^i = 1$ .  $L_{src}(s_i)$  and  $L_{des}(d_i)$  denote the logical link set sharing same  $s_i$  and  $d_i$ , respectively.  $g_i(\cdot)$  represents the protection function for the set of logical links through their secondary path relay.

Therefore, for a physical link  $i$  ( $s_i, d_i$ ), the TDMA schedule for the associated physical links should satisfy

$$\begin{aligned}
 \frac{r_i}{R_{s_i, d_i}} + \sum_{j \in U_{src}(s_i)} \frac{r_j}{R_{s_j, d_j}} + \sum_{j \in U_{des}(d_i)} \frac{r_j}{R_{s_j, d_j}} \\
 + \sum_{j \notin (U_{src}(s_i) \cup U_{des}(d_i))} c_{ji} \frac{r_j}{R_{s_j, d_j}} \leq 1, \forall i, \tag{4.43}
 \end{aligned}$$

where  $U_{src}(s_i)$  and  $U_{des}(d_i)$  denote the physical link set sharing the same  $s_i$  and  $d_i$ , respectively;  $c_{ji}$  is the binary spatial contention indicator to denote if  $j$  contends with  $i$ , defined in Section 4.6.2. The first term on the left hand side represents the percentage of physical link  $i$ 's capacity for its own transmission. The second

term represents the percentage of  $i$ 's capacity occupied by all other physical links contending at  $s_i$ . Similarly, the third term denotes the percentage occupied by all other physical links contending at  $d_i$ . The last term on the left hand side corresponds to the percentage occupied by the physical links contending with  $i$  spatially.

To this end, the RMRP problem in the directional antenna model can be formally stated as:

$$\begin{aligned}
& \underset{\mathbf{x}, \mathbf{y}, \mathbf{z}}{\text{minimize}} && \sum_k z_k \\
& \text{subject to} && \text{Constraints (4.35) – (4.43)} \\
& \text{variables} && x_{lk}, y_{lk}, z_k \in \{0, 1\}, \forall l \in \Omega, k = 1, \dots, K.
\end{aligned} \tag{4.44}$$

#### 4.6.3.1 Reformulation under the $D$ -norm uncertainty model

Several uncertainty models have been proposed in literature, including General Polyhedron,  $D$ -norm, Ellipsoid, etc [91]. In this chapter, we adopt the  $D$ -norm uncertainty model the protection function  $g_k(\mathbf{y}_k, \mathbf{f})$  from (4.41),

$$g_k(\mathbf{y}_k, \mathbf{f}) = \max_{S_k: S_k \subseteq \Omega_k, |S_k| = \Gamma_k} \sum_{l \in S_k} f_l \tau_{lk} y_{lk}. \tag{4.45}$$

Under the  $D$ -norm uncertainty model, among the set of logical links  $\Omega_k$  that can use relay  $k$ , at most  $\Gamma_k$  links will be blocked simultaneously on the primary path and consequently transmit on their secondary path via relay  $k$ . The maximization gives the worst case traffic loads induced on the relay.

Two special cases are of particular interest. If  $\Gamma_k = |\Omega_k|$ , then  $g_k(\mathbf{y}_k, \mathbf{r}) = \sum_{l \in \Omega_k} f_l \tau_{lk} y_{lk}$ . This means all logical links in  $\Omega_k$  fail simultaneously, which requires the maximum robustness. In this case, more relays may be needed. At the other extreme, if  $\Gamma_k = 0$ , no logical link is blocked. Fewer relays are in use. However,

there is little fault tolerance in the resulting relay placement. Denote  $\rho \equiv \Gamma_k/|\Omega_k|$  the robustness index, is a parameter to tradeoff between robustness and resource usage.

Under the above  $D$ -norm uncertainty model, (4.41) can be rewritten as

$$\sum_{l \in \Omega_k} \eta_l f_l \tau_{lk} x_{lk} + \max_{S_k: S_k \subseteq \Omega_k, |S_k| = \Gamma_k} \sum_{l \in S_k} f_l \tau_{lk} y_{lk} \leq z_k, \forall k. \quad (4.46)$$

Equation (4.46) is not directly tractable since it involves an inner-optimization in the protection function. The protection function can be reformulated as an integer linear programming problem as follows [91]:

$$\begin{aligned} & \max_{\{\beta_{lk} \in \{0, 1\}\}_{\forall l \in \Omega_k}} \sum_{l \in \Omega_k} f_l \tau_{lk} y_{lk} \beta_{lk}, \\ & \text{s.t.} \quad \sum_{l \in \Omega_k} \beta_{lk} \leq \Gamma_k, \\ & \beta_{lk} \in \{0, 1\}, \forall l \in \Omega_k. \end{aligned} \quad (4.47)$$

Consider a linear relaxation of the above problem where  $\beta_{lk} \in [0, 1]$ . Due to the linearity of the constraints, the optimal solution occurs at the vertices of the feasibility region. Hence the optimal solution  $\beta_{lk}^*$  must be either 0 or 1, as there is no gap between the integer linear programming and the linear programming solutions.

Taking the dual of the linear programming problem (4.47), we have:

$$\begin{aligned} & \min_{\{\mu_{lk} \geq 0\}_{\forall l \in \Omega_k}, \nu_k \geq 0} \nu_k \Gamma_k + \sum_{l \in \Omega_k} \mu_{lk}, \\ & \text{s.t.} \quad \nu_k + \mu_{lk} \geq f_l \tau_{lk} y_{lk}, \end{aligned} \quad (4.48)$$

where  $\mu_{lk}$  and  $\nu_k$  are lagrangian multipliers.

Similarly, we can apply  $D$ -norm uncertainty model to (4.42), which can be rewritten as:

$$\begin{aligned}
r_i = & \delta_1^i f_i + \delta_2^i \left[ \sum_{l \in L_{src}(s_i)} \eta_l f_l x_{ld_i} + \max_{H_i: H_i \subseteq L_{src}(s_i), |H_i| = \Gamma_i} \sum_{l \in H_i} f_l y_{ld_i} \right] \\
& + \delta_3^i \left[ \sum_{l \in L_{des}(d_i)} \eta_l f_l x_{ls_i} + \max_{H_i: H_i \subseteq L_{des}(d_i), |H_i| = \Gamma_i} \sum_{l \in H_i} f_l y_{ls_i} \right].
\end{aligned} \tag{4.49}$$

Using same methodology of (4.47) and (4.48), we can have the equivalent terms for the protection function  $g_i(\mathbf{y}_{d_i}, \mathbf{f})$  and  $g_i(\mathbf{y}_{s_i}, \mathbf{f})$ , respectively:

$$\begin{aligned}
& \min_{\{p_{ld_i} \geq 0\} \forall l \in L_{src}(s_i), q_{d_i} \geq 0} q_{d_i} \Gamma_i + \sum_{l \in L_{src}(s_i)} p_{ld_i}, \\
& \text{s.t. } q_{d_i} + p_{ld_i} \geq f_l y_{ld_i},
\end{aligned} \tag{4.50}$$

and

$$\begin{aligned}
& \min_{\{p_{ls_i} \geq 0\} \forall l \in L_{des}(d_i), q_{s_i} \geq 0} q_{s_i} \Gamma_i + \sum_{l \in L_{des}(d_i)} p_{ls_i}, \\
& \text{s.t. } q_{s_i} + p_{ls_i} \geq f_l y_{ls_i}.
\end{aligned} \tag{4.51}$$

Substituting (4.48)(4.49)(4.50)(4.51) into (4.44), we can obtain the equivalent formulation of the RMRP problem as a mixed integer linear programming (MILP)

problem as follows:

$$\begin{aligned}
& \min_{\mathbf{x}, \mathbf{y}, \mathbf{z}, \boldsymbol{\mu}, \boldsymbol{\nu}, \mathbf{p}, \mathbf{q}} \sum_k z_k, \\
& \text{s.t.} \quad \sum_{l \in \Omega_k} \eta_l x_{lk} f_l \tau_{lk} + \nu_k \Gamma_k + \sum_{l \in \Omega_k} \mu_{lk} \leq z_k, \quad \forall k, \\
& \quad \nu_k + \mu_{lk} \geq f_l \tau_{lk} y_{lk}, \quad \forall l \in \Omega_k, \forall k, \\
& \quad \frac{r_i}{R_{s_i, d_i}} + \sum_{j \in U_{src}(s_i)} \frac{r_j}{R_{s_j, d_j}} + \sum_{j \in U_{des}(d_i)} \frac{r_j}{R_{s_j, d_j}} \\
& \quad \quad + \sum_{j \notin (U_{src}(s_i) \cup U_{des}(d_i))} c_{ji} \frac{r_j}{R_{s_j, d_j}} \leq 1, \quad \forall i, \\
& \quad r_i = \delta_1^i f_i + \delta_2^i \left[ \sum_{l \in L_{src}(s_i)} (\eta_l f_l x_{ld_i} + p_{ld_i}) + q_{d_i} \Gamma_i \right] \\
& \quad \quad + \delta_3^i \left[ \sum_{l \in L_{des}(d_i)} (\eta_l f_l x_{ls_i} + p_{ls_i}) + q_{s_i} \Gamma_i \right], \\
& \quad q_{d_i} + p_{ld_i} \geq f_l y_{ld_i}, \quad \forall l \in L_{src}(s_i), \forall i, \\
& \quad q_{s_i} + p_{ls_i} \geq f_l y_{ls_i}, \quad \forall l \in L_{des}(d_i), \forall i, \\
& \quad \text{Constraints (4.35) – (4.40),} \\
& \quad \text{variables } x_{lk}, y_{lk}, z_k \in \{0, 1\}, \\
& \quad \mu_{lk} \geq 0, \nu_k \geq 0, p_{lk} \geq 0, q_k \geq 0.
\end{aligned} \tag{4.52}$$

#### 4.6.3.2 Hardness of RMRP

We prove in the following that RMRP is NP-hard.

**Definition 4.8.** We call the special case of RMRP problem, where the robustness index  $\rho = 0$ , the MRP problem.

**Lemma 4.9.** MRP is NP-hard.

Proof. Since  $\rho = 0 \Rightarrow \Gamma_k \equiv 0$  in MRP, the protection function of (4.46) is null, which means only primary paths are considered in (4.41). In MRP,  $f_l \tau_{lk}$  represents the percentage of relay  $k$ 's capacity occupied by logical link  $l$ 's primary path, if  $l$  chooses to route its primary path via  $k$ . If we treat a bin as a relay's capacity, and treat the volume of an item as the percentage of relay capacity occupied by an logical link, the Bin-Packing problem can be reduced to MRP in a polynomial time. Since Bin-Packing is NP-hard [92], MRP is also a NP-hard problem.  $\square$

As MRP is just a special case of RMRP, RMRP is henceforth harder than MRP, so RMRP is also NP-Hard.

The MILP problem in (4.52) can be solved by any MILP solver. In our implementation, we adopt the MILP solver of the IBM optimization tool – CPLEX [96].

#### 4.6.4 Robust Maximum Utility Relay Placement

In contrast to RMRP, which tries to minimize the number of relays, RMURP aims to maximize the total utility of an mmWave WPAN given a fixed number of relays.

Let  $f_l$  be the base traffic demand on logical link  $l$ . We allow  $f_l$  to be scaled up/down according to resource constraints. That is, the actual data rate supported is  $\alpha f_l$ , where  $\alpha$  is a scaling parameter. This formulation is particularly relevant for transferring multimedia content that allows adaptive encoding. The objective of RMURP is henceforth to maximize the total utility  $U$  of the network, given by  $U = \sum_l \alpha f_l$ .

The constraints of RMURP are similar to those of RMRP, except that the TDMA schedulability constraint (4.41) now becomes

$$\sum_{l \in \Omega_k} \eta_l \alpha f_l \tau_{lk} x_{lk} + g_k(\mathbf{y}_k, \alpha \mathbf{f}) \leq z_k, \forall k. \quad (4.53)$$

The TDMA schedulability constraint for a physical link  $i(s_i, d_i)$  remains same as (4.43), while the flow rate  $r_i$  now becomes

$$r_i = \delta_1^i \alpha f_i + \delta_2^i \left[ \sum_{l \in L_{src}(s_i)} \alpha \eta_l f_l x_{ld_i} + g_i(\mathbf{y}_{\mathbf{d}_i}, \alpha \mathbf{f}) \right] + \delta_3^i \left[ \sum_{l \in L_{des}(d_i)} \alpha \eta_l f_l x_{ls_i} + g_i(\mathbf{y}_{\mathbf{s}_i}, \alpha \mathbf{f}) \right]. \quad (4.54)$$

The additional cardinality constraints need to be included,

$$\sum_k z_k \leq m, \quad (4.55)$$

where  $m$  is the maximum number of relays to be used.

To this end, the RMURP in the directional antenna model can be formalized as:

$$\begin{aligned} & \underset{\mathbf{x}, \mathbf{y}, \mathbf{z}, \alpha}{\text{maximize}} && \sum_l \alpha f_l \\ & \text{subject to} && \text{Constraints (4.35) – (4.40)(4.43)(4.53)(4.54)(4.55)} \\ & \text{variables} && x_{lk}, y_{lk}, z_k \in \{0, 1\}, \alpha \geq 0, \forall l, k. \end{aligned} \quad (4.56)$$

#### 4.6.4.1 Reformulation under $D$ -norm Uncertainty Model

Again we can apply the  $D$ -norm uncertainty model (see Section 4.6.3.1) to the RMURP problem of (4.56). This will transform (4.56) into a mixed integer non-linear

programming problem (MINLP) as follows:

$$\begin{aligned}
& \text{Maximize}_{\mathbf{x}, \mathbf{y}, \mathbf{z}, \mu, \nu, \mathbf{p}, \mathbf{q}, \alpha} && \sum_l \alpha f_l \\
& \text{s.t.} && \sum_{l \in \Omega_k} \eta_l \alpha f_l \tau_{lk} x_{lk} + \nu_k \Gamma_k + \sum_{l \in \Omega_k} \mu_{lk} \leq z_k, \forall k, \\
& && \nu_k + \mu_{lk} \geq \alpha f_l \tau_{lk} y_{lk}, \forall l \in \Omega_k, \forall k, \\
& && \frac{r_i}{R_{s_i, d_i}} + \sum_{j \in U_{src}(s_i)} \frac{r_j}{R_{s_j, d_j}} + \sum_{j \in U_{des}(d_i)} \frac{r_j}{R_{s_j, d_j}} \\
& && \quad + \sum_{j \notin (U_{src}(s_i) \cup U_{des}(d_i))} c_{ji} \frac{r_j}{R_{s_j, d_j}} \leq 1, \forall i, \\
& && r_i = \delta_1^i \alpha f_i + \delta_2^i \left[ \sum_{l \in L_{src}(s_i)} (\eta_l \alpha f_l x_{ld_i} + p_{ld_i}) + q_{d_i} \Gamma_i \right] \\
& && \quad + \delta_3^i \left[ \sum_{l \in L_{des}(d_i)} (\eta_l \alpha f_l x_{ls_i} + p_{ls_i}) + q_{s_i} \Gamma_i \right], \\
& && q_{d_i} + p_{ld_i} \geq \alpha f_l y_{ld_i}, \forall l \in L_{src}(s_i), \forall i, \\
& && q_{s_i} + p_{ls_i} \geq \alpha f_l y_{ls_i}, \forall l \in L_{des}(d_i), \forall i, \\
& && \text{Constraints (4.35) – (4.40),} \\
& \text{variables} && x_{lk}, y_{lk}, z_k \in \{0, 1\}, \\
& && \mu_{lk} \geq 0, \nu_k \geq 0, p_{lk} \geq 0, q_k \geq 0, \alpha \geq 0.
\end{aligned} \tag{4.57}$$

#### 4.6.4.2 Hardness of RMURP

We prove in the following that RMURP is NP-hard. The inclusion of variable  $\alpha$  renders RMURP an MINLP. Specialized algorithms need to be designed.

**Definition 4.10.** We call the special case of RMURP problem, where the mmWave network adopts robustness index of  $\rho = 0$  and only has one candidate relay location, as MURP problem.

Lemma 4.11. MURP is NP-hard.

Proof. Since  $\rho = 0 \Rightarrow \Gamma_k \equiv 0$  in MURP, the protection function term is null. Also, consider only one candidate relay location  $k$  in the network, the scheduling constraint of MURP in (4.53) can be rewritten as:  $\sum_{l \in \Omega_k} \eta_l \alpha f_l \tau_{lk} x_{lk} \leq z_k$ . Let  $\alpha f_l$  represent the value of item  $l$ ,  $\eta_l \alpha r_l \tau_{lk}$  represent the weight of item  $l$ , the 0-1 knapsack problem can be reduced to MURP in a polynomial time. Since the Knapsack problem is NP-hard [92], MURP is NP-hard.  $\square$

As MURP is a special case of RMURP, RMURP is henceforth harder than MURP. This proves the lemma.

Next, we propose an efficient greedy algorithm to solve the RMURP. The algorithm is based on Bisection Search, which is shown to be fast and has near-optimal performance.

#### 4.6.4.3 Bisection Search

Bisection Search is a heuristic method for finding the roots of an equation. It iteratively bisects an interval and then selects the subinterval where a root must reside for the next iteration, until some termination condition is met. It is guaranteed to converge to a root of  $F(\cdot)$  if and only if:  $F$  is a continuous function on the interval  $[A, B]$ , and  $F(A)$  and  $F(B)$  have opposite signs.

In (4.57), if  $\alpha$  is given, RMURP becomes a MILP, which can be solved by CPLEX. The key is thus to determine the value of  $\alpha$ . When  $\alpha$  is large, RMURP is infeasible. When  $\alpha = 0$ , RMURP is always feasible. Treating feasibility and infeasibility as opposite signs, we apply the Bisection Search principle to decide the range of  $\alpha$  iteratively until it is smaller than a threshold  $2 \times TOL$ . Starting from an initial interval  $[A, B]$ , where  $\alpha = A$  renders RMURP feasible and  $\alpha = B$  renders

RMURP infeasible, we substitute  $A$  or  $B$  with  $\frac{A+B}{2}$  depending on the feasibility of RMURP under  $\alpha = \frac{A+B}{2}$ . The “monotonicity” in the feasibility of RMURP with respect to  $\alpha$  makes the Bisection Search converge fast but the optimality of the final results depends on the choice of  $TOL$ .

The Bisection Search based algorithm is summarized in Algorithm 6.

---

Algorithm 6: Bisection Search for RMURP in a Directional Antenna Model

---

Input : Base logical data rate  $f_l$  for each feasible logical link  $l$ ; error tolerance  $TOL$  (which serves as the iteration termination condition); and the up-to-date known range for  $\alpha$ :  $[A, B]$

Output: Maximum network utility  $U$  and relay selection variables for every feasible links  $\mathbf{x}, \mathbf{y}, \mathbf{z}$

```

begin
  Set  $n = 1$ ;
  while  $n \leq \max N$  do
     $C \leftarrow \frac{(A+B)}{2}$ ;
    Solve the MILP problem  $RMURP(C)$ .
    if  $RMURP(C)$  is feasible then
       $A \leftarrow C$ ;
      Obtain the solutions of  $RMURP(C)$ :  $\mathbf{x}^{(n)}, \mathbf{y}^{(n)}, \mathbf{z}^{(n)}$ .
    else
       $B \leftarrow C$ .
    end
     $n \leftarrow n + 1$ ;
    if  $\frac{(B-A)}{2} \leq TOL$  then
      The best  $\alpha$  found,  $\alpha_{best} \leftarrow A$ ;
      Return  $U, \mathbf{x}^{(n)}, \mathbf{y}^{(n)}, \mathbf{z}^{(n)}$ .
    end
  end
end
end

```

---

#### 4.6.5 Simulation Results

In this section, we evaluate the performance of the relay placement solutions using numerical simulations. In the simulations, an mmWave home network is deployed in a  $10\text{m} \times 10\text{m}$  room, where  $N$  mmWave devices and  $O$  obstacles are uniformly placed. The relays can be placed at any grid point in a grid separated by distance  $d_0$ .

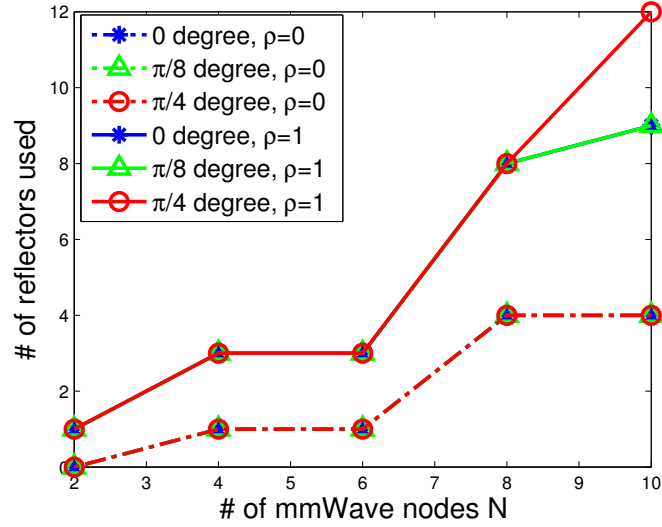
The transmission radii of all mmWave end devices and relays are set to 6 meters. The (base) traffic demand  $f_l$  of each logical link  $l$  is chosen as  $\frac{1}{7}$  of the AWGN Shannon channel capacity of the slowest LOS path to ensure feasibility. The PHY parameters are given in Table 4.2. In all experiments,  $d_0 = 2m$ ,  $O = 10$ .

#### 4.6.5.1 RMRP Performance

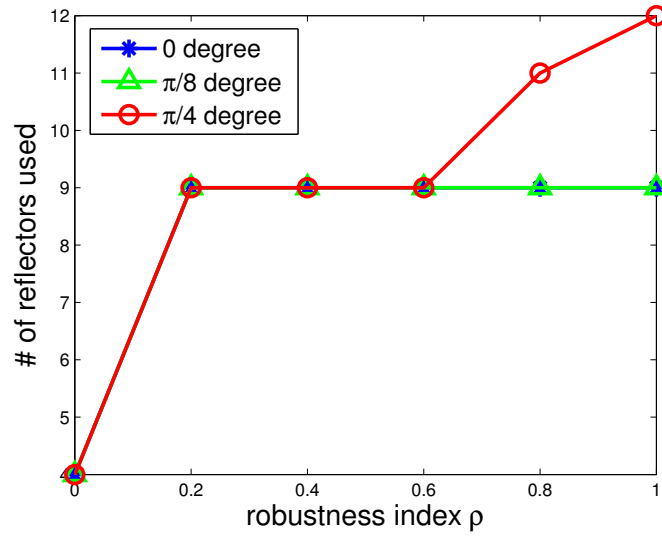
In this section, we examine the performance of RMRP under different configurations by varying the number of mmWave nodes ( $N$ ), the robustness index ( $\rho$ ) as well as the beamwidth of directional antenna and the number of moving objects ( $M$ ).

Fig. 4.11(a) shows the number of relays needed when relay candidate locations and obstacles are fixed, while the number of mmWave nodes varies. We also vary the beamwidth from 0 degree to  $\pi/4$  degree under the robustness index  $\rho = 0$  and  $\rho = 1$  respectively. Clearly, more relays are needed as the number of mmWave nodes increases. However, the relationship is not always linear due to the absence of LOS paths between TX/RX pairs and the multiplexing of relays. In addition, larger beamwidth of directional antenna in each mmWave node would result in more spatial contention, which leads to a larger number of relays needed to support all the feasible logical links. We also observe that, when  $\rho = 1$  (denoted as "100%-robust"), more relays are needed compared to  $\rho = 0$ , as more bandwidth is allocated for the secondary paths of every feasible logical link. This observation is also supported by Figure 4.11(b).

Fig. 4.12(a)(b) shows the percentage of link blockage time when varying the robustness index and the number of human subjects moving randomly in a  $10m \times 10m$  room. The mobility setup is similar to that in Section III-C, where there are 10 mmWave nodes and 10 obstacles uniformly deployed. Clearly, a larger robustness



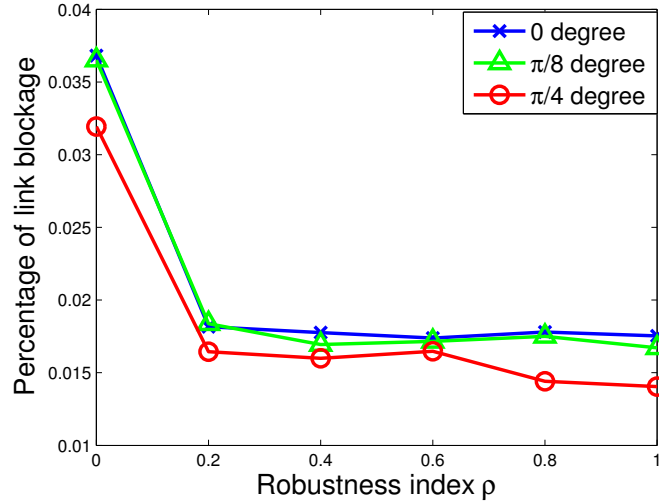
(a) Effect of the number of mmWave nodes  $N$



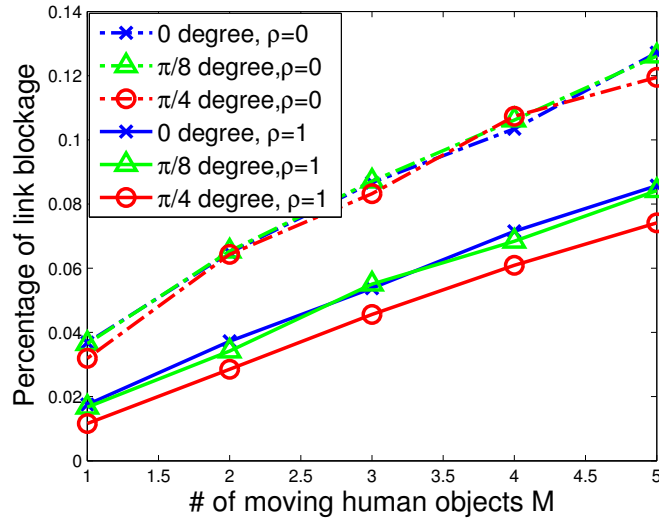
(b) Effect of the robustness index  $\rho$  with  $N = 10$

Figure 4.11: Performance of RMRP in an mmWave home network deployed in a  $10\text{m} \times 10\text{m}$  room.

index results in a smaller percentage of link blockage, due to more backup paths provided. As the number of human subjects increases, the percentage of link blockage increases as well. However, the 100%-robust ( $\rho = 1$ ) scheme leads to around 50% less blockage.



(a) Effect of the robustness index  $\rho$  with  $N = 10$  and  $M = 1$



(b) Effect of the number of moving objects  $M$  with  $N = 10$

Figure 4.12: Mobility performance of RMRP in an mmWave home network deployed in a  $10\text{m} \times 10\text{m}$  room.

#### 4.6.5.2 RMURP Performance

We now evaluate the performance of RMURP using the Bisection Search algorithm. The error tolerance  $TOL$  of Bisection Search is set to 0.01.

Fig. 4.13(a) shows the maximum utility achieved by varying the number of mmWave nodes under the robustness index  $\rho = 0$  and  $\rho = 1$ , respectively. Generally, the utility increases as the number of mmWave nodes increases. However, in some

scenario such as  $N = 4$ , multiple mmWave logical links have to share a relay, which may lead to a drop on network utility. Another observation is, larger beamwidth of directional antenna employed on each mmWave node would introduce more spatial contention, therefore reduce the utility. Similar observations can be made in Fig. 4.13(b).

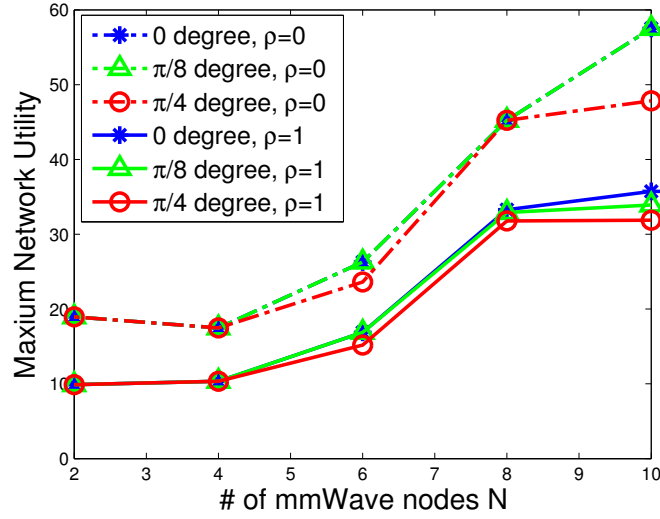
Next, we evaluate the impact of robustness index  $\rho$ , the number of candidate relays as well as the antenna beamwidth, respectively. In Fig. 4.13(b), as  $\rho$  increases, a smaller utility can be achieved as expected.

Fig. 4.14(a) shows the maximum utility achieved by varying the number of candidate relays. Clearly, as more relays become available, a larger utility can be achieved.

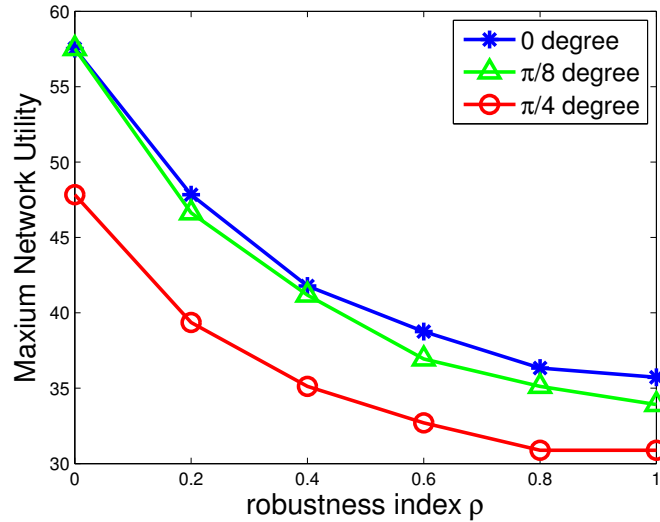
Fig. 4.14(b) demonstrates the performance of RMURP when varying the antenna beamwidth under two setups,  $N = 6$  and  $N = 10$ , respectively. As expected, a larger antenna beamwidth results in less utility.

In Fig. 4.15(a)(b), we evaluate the mobility performance of RMURP in terms of the percentage of link blockage time when varying the robustness index and the number of moving human subjects as well as the antenna beamwidth, respectively. We use a similar mobility setup as shown in Section 4.4, where there are 10 mmWave nodes and 10 obstacles uniformly deployed, and total 20 candidate relays. Clearly, as the robustness index increases, more relays are used, which results in a less link blockage. In addition, larger beamwidth of directional antenna would incur a lower link blockage, due to a more scattered relay placement.

In Fig. 4.15(b), as the number of human subjects increases, the percentage of link blockage increases accordingly. In contrast to the non-robust case ( $\rho = 0$ ), the 100%-robust ( $\rho = 1$ ) scheme can achieve much less link blockage.



(a) Effect of the number of mmWave nodes  $N$  with  $m = 20$

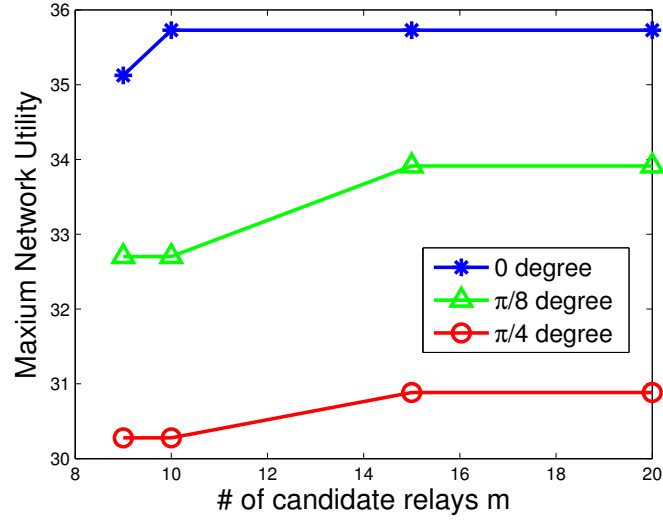


(b) Effect of the robustness index  $\rho$  with  $m = 20$  and  $N = 10$

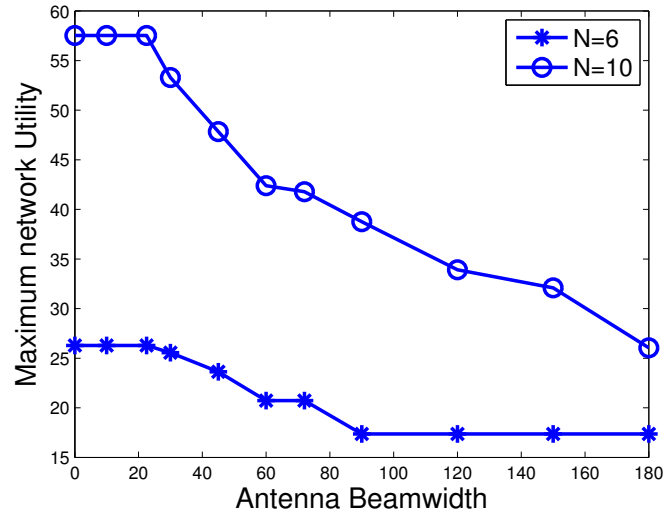
Figure 4.13: Performance of RMURP using Bisection Search algorithm with 0.01  $TOL$ , in an mmWave home network deployed in a  $10m \times 10m$  room.

#### 4.6.6 Summary

In this chapter, we formulated two robust relay placement problems in mmWave WPANs, namely, the robust minimum relay placement problem (RMRP) and robust maximum utility relay placement (RMURP), for better connectivity and robustness against link blockage. Two network models are explored respectively, an interference-free network model and a classic directional antenna model. Under the D-norm uncer-



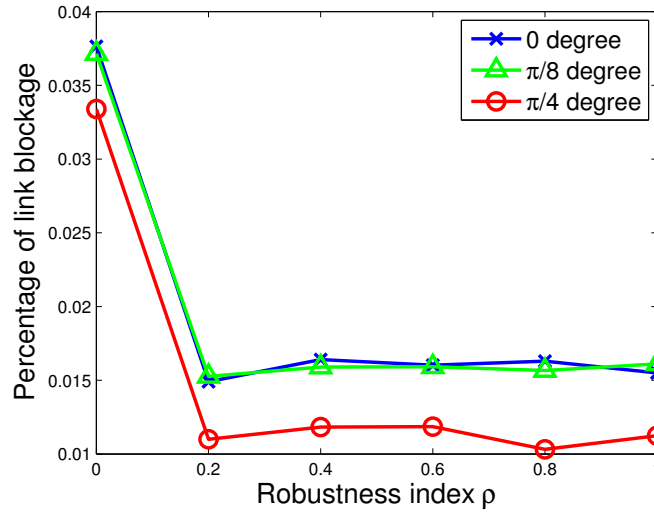
(a) Effect of the number of candidate relays  $m$  with  $N = 10$  and  $\rho = 1$



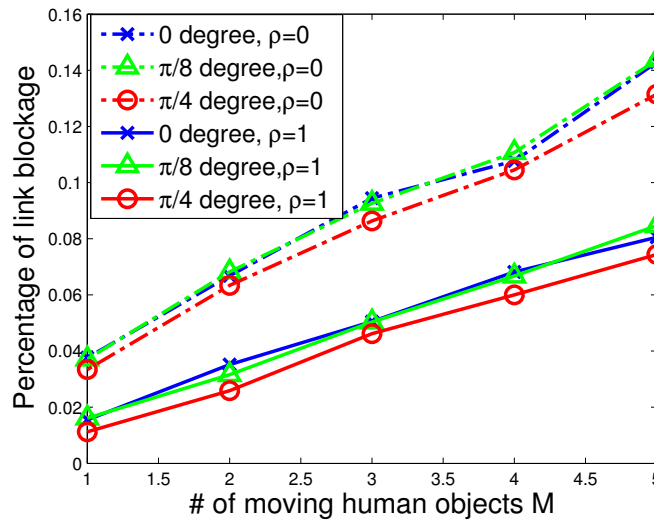
(b) Effect of the antenna beamwidth with  $m = 20$  and  $\rho = 0$

Figure 4.14: Performance of RMURP using Bisection Search algorithm with 0.01  $TOL$ , in an mmWave home network deployed in a  $10\text{m} \times 10\text{m}$  room.

tainty model, RMRP and RMURP were casted as MILP and MINLP problems. The efficient heuristic algorithms were devised and evaluated using extensive simulations.



(a) Effect of the robustness index  $\rho$  with  $M = 1$  with  $N = 10$ ,  $m = 20$ .



(b) Effect of the number of moving subjects  $M$  with  $N = 10$ ,  $m = 20$ .

Figure 4.15: Mobility performance of RMURP using Bisection Search algorithm with 0.01  $TOL$ , in an mmWave home network deployed in a  $10\text{m} \times 10\text{m}$  room.

## Chapter 5

### Conclusions and Future Work

#### 5.1 Summary of Contributions

In this dissertation, we presented our work toward designing reliable and robust WPANs to satisfy the better QoS and resource provisioning. Our work explored different applications of WPANs and researched the new analytical methodologies and robust solutions. The key contributions that we made can be divided as follows:

- **Link Quality Prediction** : We revisit the issue of link quality prediction in IEEE 802.15.4 low rate wireless personal area networks (LR-WPAN) and examine the available readings available at commodity Zigbee radios. To the best of our knowledge, our work is the first that provides experimental evidence that validates *LQI* readings truly reflects the *SNR* at receiver. In addition, we proposed an inference model which can predict the instantaneous link quality for Zigbee radios by using instantaneous *LQI* readings as input given the knowledge of channel models. The proposed model is validated through extensive simulation and experiment study. We believe it will lead to more informed resource management decisions in WPANs.
- **Neighbor and Link Contention Relationships Inference** : We investigate neighbor discovery and contention graph inference solutions in ad-hoc WPANs which can provide more accurate knowledge of the network environment using as few measurement as possible. An active inference algorithm is proposed, called the ternary inference algorithm, that utilizes decentralized randomized schedules to infer the neighboring and contention relationships through mixed signal at the receiver nodes. Simulation studies show that the proposed approach outper-

forms an Aloha-like approach in neighbor discovery time, and can achieve high accuracy in determining the relationships.

- Robust Relay Placement and Route Selection : We focus on the resource provisioning issue in 60 GHz mmWave WPANs and proposed the robust solutions for joint relay placement and route selection subject to the constraints of link connectivity, bandwidth and robustness. Two network models are explored respectively, an interference-free network model and a classic directional antenna model. In essence, we proposed the robust formulations for two relay placement problems, namely, the robust minimum relay placement problem (RMRP) and robust maximum utility relay placement (RMURP), to combat the uncertainty in link failure. Under the D-norm uncertainty model in robust optimization theory, RMRP and RMURP were casted as MILP and MINLP problems. The efficient heuristic algorithm and optimal algorithm were devised and evaluated using extensive simulations.

## 5.2 Future Work

In this section, we summarize some further research directions that extend our current work:

- Channel profiling : Our prediction model in its current form is based on the prior knowledge of a channel model. Channel profiling is needed to not just classify the channel models but also obtain key parameters of the fading channel. Kurtosis and Kewness are defined as the degree of peakedness of a distribution, and the degree of departure from symmetry of a distribution, respectively. They are the proven stochastic properties that can be applied to classify the distributions of different data. It is therefore interesting to see if we can apply these

properties to identify different channel models and build a complete prediction model.

- Linear inference algorithm for jointly inference of neighbor and contention relationships : Instead of using ternary inference approach, we are interested in a linear inference approach which explores the received signal strength (RSS) to solve the pair-wise channel gains by formulating a sparse linear least square optimization problem. Then, the neighbor and contention relationships can be inferred from the estimated pairwise RSS. The linear inference model is believed to achieve the better inference while incurring the higher computation complexity. As a future work, it would be interesting to evaluate the performance of the linear inference approach compared to the ternary inference approach for jointly inference of neighboring and contention relationships.
- The Mass-Spring Model for jointly inference of neighbor and contention relationships : Another possible approach is to use the Mass-Spring model for distributed localization of all the target nodes in the network. In the Mass-Spring model, the total force on every target node can be formulated, and the energy incurred by the discrepancy of current locations and true locations is obtained at each state. The Mass-Spring algorithm would update the locations of nodes by following the direction of the forces for each nodes, in order to reduce the total energy. The algorithm iterates through all the tests until no further improvement can be made on the total energy. It is believed that the Mass-Spring model can achieve very good approximation on the pair-wise locations of any two target nodes. This knowledge can be used to infer neighbor and contention relationships. Therefore, it would be very interesting to evaluate the performance of Mass-Spring model in the neighbor and contention relationships inference work.

- Placement of passive relays : Current robust resource provisioning solutions utilize active relays, which can amplify and forward the mmWave signal from TX to any intended directions, at the cost of high complexity and extra processing overhead. An alternative approach is to utilize passive relays, which can be as simple as a flat metal plate [30-32] with fast response and does not require any power source. Placing Passive relays in a network introduce additional challenges on controlling the unwanted interference due to reflections. The dimensions of passive relay would also be an important factor.

## Bibliography

- [1] “IEEE 802.15 working group for WPAN,” <http://ieee802.org/15/index.html>, Sep. 2009.
- [2] IEEE 802.15.1: Wireless Medium Access Control and Physical Layer Specifications for Wireless Personal Area Networks (WPANs), Jun. 2002.
- [3] “Bluetooth specifications 4.0,” <https://www.bluetooth.org>, Aug 2011.
- [4] “IEEE 802 WPAN task group 3 (tg3),” <http://www.ieee802.org/15/pub/TG3.html>, Aug. 2011.
- [5] IEEE 802.15.4: Wireless Medium Access Control and Physical Layer Specifications for Low-Rate Wireless Personal Area Networks, Sep. 2006.
- [6] “Zigbee specifications,” <http://www.zigbee.org/>, Aug. 2009.
- [7] N. Golmie, D. Cypher, and O. Rebala, “Performance analysis of low rate wireless technologies for medical applications,” *Computer Communications*, vol. 28, no. 10, pp. 1266–1275, Jun. 2005.
- [8] D. G. Yoon, S. Y. Shin, W. H. Kwon, and H. S. Park, “Packet error rate analysis of IEEE 802.11b under IEEE 802.15.4 interference,” *IEEE Vehicular Technology Conference*, pp. 1186–1190, 2006.
- [9] A. Soomro and D. Cavalcanti, “Opportunities and challenges in using wpan and wlan technologies in medical environments,” *IEEE Commun. Mag.*, vol. 45, no. 2, pp. 114–122, Feb. 2007.
- [10] R. de Francisco, L. Huang, and G. Dolmans, “Coexistence of wban and wlan in medical environments,” in *IEEE Vehicular Technology Conference Fall (VTC)*, Anchorage, Alaska, USA, Sep. 2009.

- [11] Y. Wang, Q. Wang, G. Zheng, Z. Zeng, and R. Zheng, “WiCop: Engineering WiFi temporal white-spaces for safe operations of wireless body area networks in medical applications,” in IEEE 32nd Real-time Systems Symposium, 2011.
- [12] J. Lansford, A. Stephens, and R. Nevo, “Wi-fi (802.11b) and bluetooth: enabling coexistence,” IEEE Network, vol. 15, no. 5, pp. 20–27, Sep. 2001.
- [13] R. C. Shah and L. Nachman, “Interference detection and mitigation in iee 802.15.4 networks,” in International Conference on Information Processing in Sensor Networks (IPSN), St. Louis, MO, Apr. 2008.
- [14] K. Ghanem and P. S. Hall, “Interference cancellation using cdma multi-user detectors for on-body channels,” in IEEE International Symposium on Personal, Indoor and Mobile Radio Communications (PIMRC), Tokyo, Japan, Sep. 2009.
- [15] I. Khan, Y. I. Nechayev, K. Ghanem, and P. S. Hall, “Ban-ban interference rejection with multiple antennas at the receiver,” IEEE Transactions on Antennas and Propagation, vol. 58, no. 3, pp. 927–934, Mar. 2010.
- [16] M. Filo, A. Hossain, A. R. Biswas, and R. Piesiewicz, “Cognitive pilot channel: enabler for radio system coexistence,” in International Workshop on Cognitive Radio and Advanced Spectrum Management (CogART), Aalborg, Denmark, May 2009.
- [17] J. D. P. Pavon and S. Choi, “Link adaptation strategy for iee 802.11 wlan via received signal strength measurement,” in Proc.of IEEE International Conference on Communications (ICC), Alaska, US, May 2003.
- [18] G. Holland, N. Vaidya, and P. Bahl, “A rate-adaptive mac protocol for multi-hop wireless networks,” in Proc.of ACM Mobicom, Rome, Italy, Jul. 2001.

- [19] K. Benkic, M. Malajner, P. Planinsic, and Z. Cucej, "Using rssi value for distance estimation in wireless sensor networks based on zigbee," in Proc.of 15th International Conference on Systems, Signals and Image Processing (IWSSIP), Bratislava, Slovak Republic, Jun. 2008.
- [20] A. T. Parameswaran, M. I. Husain, and S. Upadhyaya, "Is rssi a reliable parameter in sensor localization algorithms - an experimental study," in Proc.of 28th IEEE Symposium on Reliable Distributed Systems (SRDS), Niagara Falls, US, Sep. 2009.
- [21] D. Kelly, S. McLoone, B.Logan, and T.Dishongh, "Single access point localization for wearable wireless networks," in Proc.of 30th International Conference of IEEE Engineering in Medicine and Biology Society (EMBC), Vancouver, CA, Aug. 2008.
- [22] A. Woo, T. Tong, and D. Culler, "Taming the underlying challenges of reliable multihop routing in sensor networks," in Proc.of SenSys, Los Angeles, CA, Nov. 2003.
- [23] S. J. Halder, T.-Y. Choi, J.-H. Park, S.-H. Kang, S. W. Park, and J. G. Park, "Enhanced ranging using adaptive filter of zigbee rssi and lqi measurement," in Proc.of International Organization for Information Integration and Web-based Applications and Services (iiWAS), Liniz, Austria, Nov. 2008.
- [24] J. Polastre, R. Szewczyk, and D. Culler, "Telos: Enabling ultra-low power wireless research," in Proc.of 4th International Symposium on Information Processing in Sensor Networks (IPSN), Los Angeles, CA, Apr. 2005.
- [25] K. Srinivasan and P. Levis, "Rssi is under appreciated," in Proc.of 3rd Workshop on Embedded Networked Sensors(EmNets), Cambridge, MA, May 2006.

- [26] “Cc2420 radio datasheet, texas instruments,” <http://focus.ti.com/docs/prod/folders/print/cc2420.html>, Sep. 2009.
- [27] N. T. Nguyen, G. Zheng, Z. Han, and R. Zheng, “Device fingerprinting to enhance wireless security using nonparametric bayesian method,” in INFOCOM, 2011 Proceedings IEEE, 2011, pp. 1404–1412.
- [28] “Universal software radio peripheral,” [http://www.ettus.com/downloads/ettus\\_ds\\_usrp2\\_v5.pdf](http://www.ettus.com/downloads/ettus_ds_usrp2_v5.pdf), Sep. 2009.
- [29] Y. Chen and A. Terzis, “On the mechanisms and effects of calibrating rssi measurements for 802.15.4 radios,” in Proc. of 7th European Conference on Wireless Sensor Networks (EWSN 2010), Coimbra, Portugal, Feb. 2010.
- [30] D. Tse and P. Viswanath, *Fundamentals of Wireless Communication*. Cambridge University Press, 2005.
- [31] J. Sun and I. S. Reed, “Performance of mdpsk, mpsk, and noncoherent mfsk in wireless rician fading channels,” *IEEE Transaction on Communications*, vol. 47, no. 6, pp. 813–816, Jun. 1999.
- [32] J. Luo and D. Guo, “Neighbor discovery in wireless ad hoc networks based on group testing,” in *Communication, Control, and Computing, 2008 46th Annual Allerton Conference on*, 2008, pp. 791–797.
- [33] L. Zhang, J. Luo, and D. Guo, “Neighbor discovery for wireless networks via compressive sensing,” *CoRR*, vol. arXiv:1012.1007, 2012.
- [34] K. Jang, “Passive online inband interference inference in centralized w lans,” Technical Report 916, USC, 2010.

- [35] V. Shrivastava, S. Rayanchu, S. Banerjee, and K. Pagaginnaki, “Pie in the sky: Online passive interference estimation for enterprise wlans,” in 8th USENIX Symposium on Networked Systems Design and Implementation, 2011.
- [36] J. Yang, S. Draper, and R. Nowak. (2012, Dec.) Learning the interference graph of a wireless network. [Online]. Available: <http://arxiv.org/abs/1208.0562>.
- [37] N. Ahmed and S. K. Smarta, “A self-managing architecture for thin access points,” in ACM CoNEXT, 2006.
- [38] A. Keshavarzian, E. Uysal-Biyikoglu, F. Herrmann, and A. Manjeshwar, “Energy-efficient link assessment in wireless sensor networks,” in INFOCOM 2004. Twenty-third Annual Joint Conference of the IEEE Computer and Communications Societies, vol. 3, 2004, pp. 1751–1761 vol.3.
- [39] D. Niculescu, “Interference map for 802.11 networks,” in 7th ACM SIGCOMM conference on Internet measurement, 2007.
- [40] P. Dutta and D. Culler, “Practical asynchronous neighbor discovery and rendezvous for mobile sensing applications,” in Proceedings of the 6th ACM conference on Embedded network sensor systems, ser. SenSys '08, 2008.
- [41] M. Kohvakka, J. Suhonen, M. Kuorilehto, V. Kaseva, M. Hännikäinen, and T. D. Hämäläinen, “Energy-efficient neighbor discovery protocol for mobile wireless sensor networks,” *Ad Hoc Netw.*, vol. 7, no. 1, pp. 24–41, Jan. 2009.
- [42] W. Zeng, S. Vasudevan, X. Chen, B. Wang, A. Russell, and W. Wei, “Neighbor discovery in wireless networks with multipacket reception,” in Proceedings of the Twelfth ACM International Symposium on Mobile Ad Hoc Networking and Computing, ser. MobiHoc '11, 2011.

- [43] L. You, X. Zhu, and G. Chen, “Neighbor discovery in peer-to-peer wireless networks with multi-channel mpr capability,” in Communications (ICC), 2012 IEEE International Conference on, 2012, pp. 4975–4979.
- [44] D. Angelosante, E. Biglieri, and M. Lops, “A simple algorithm for neighbor discovery in wireless networks,” in Acoustics, Speech and Signal Processing, 2007. ICASSP 2007. IEEE International Conference on, vol. 3, 2007, pp. 169–172.
- [45] “Neighbor discovery in wireless networks: A multiuser-detection approach,” *Physical Communication*, vol. 3, no. 1, pp. 28 – 36, 2010.
- [46] J. Luo and D. Guo, “Compressed neighbor discovery for wireless ad hoc networks: the rayleigh fading case,” in Proceedings of the 47th annual Allerton conference on Communication, control, and computing, ser. Allerton’09, 2009, pp. 308–313.
- [47] J. Padhye, S. Agarwal, V. N. Padmanabhan, L. Qiu, A. Rao, and B. Zill, “Estimation of link interference in static multi-hop wireless networks,” in Proceedings of the 5th ACM SIGCOMM conference on Internet Measurement, ser. IMC ’05, 2005, pp. 28–28.
- [48] Z. Haas, J. Winters, and D. Johnson, “Simulation study of the capacity bounds in cellular systems,” in Personal, Indoor and Mobile Radio Communications, 1994. Wireless Networks - Catching the Mobile Future., 5th IEEE International Symposium on, vol. 4, 1994, pp. 1114–1120 vol.4.
- [49] L. Yang, L. Cao, and H. Zheng, “Physical interference driven dynamic spectrum management,” in New Frontiers in Dynamic Spectrum Access Networks, 2008. DySPAN 2008. 3rd IEEE Symposium on, 2008, pp. 1–12.
- [50] X. Zhou, Z. Zhang, G. Wang, X. Yu, B. Y. Zhao, and H. Zheng, “Practical conflict graphs for dynamic spectrum distribution,” in Proceedings of the ACM

- SIGMETRICS/international conference on Measurement and modeling of computer systems, ser. SIGMETRICS '13, 2013, pp. 5–16.
- [51] C. Anderson and T. Rappaport, “In-building wideband partition loss measurements at 2.5 and 60GHz,” *IEEE Transactions on Wireless Communication*, vol. 3, no. 3, pp. 922–928, May 2004.
- [52] F. Giannetti, M. Luise, and R. Reggiannini, “Mobile and personal communications in the 60GHz band: A survey,” *Wireless Personal Communication*, vol. 10, no. 2, pp. 207–243, Jul. 1999.
- [53] R. C. Daniels, J. N. Murdock, T. S. Rappaport, and R. W. Heath, “60GHz wireless: Up close and personal,” *IEEE Microwave Magazine*, vol. 11, no. 7, pp. 44–50, Dec. 2010.
- [54] C. Cordeiro, D. Akhmetov, and M. Park, “IEEE 802.11ad: Introduction and performance evaluation of the first multi-Gbps WiFi technology,” in *ACM international workshop on mmWave communications*, Sep. 2010.
- [55] D. Halperin, S. Kandula, J. Padhye, P. Bahl, and D. Wetherall, “Augmenting data center networks with multi-gigabit wireless links,” in *ACM SIGCOMM*, Aug. 2011.
- [56] “IEEE 802.11 working group, very high throughput in 60ghz,” <http://www.ieee802.org/11/>, Sep. 2011.
- [57] X. Zhu, A. Doufexi, and T. Kocak, “On the performance of IEEE 802.15.3c Millimeter-Wave WPANs: PHY and MAC,” in *IEEE Wireless Advanced*, Jun. 2010.

- [58] IEEE 802.15.3c: Wireless Medium Access Control and Physical Layer Specifications for High Rate Wireless Personal Area Networks (WPANs): Amendment2: Millimeter-wave based Alternative Physical Layer Extension, Sep. 2009.
- [59] “Wireless gigabit alliance,” <http://wirelessgigabitalliance.org/>, Sep. 2011.
- [60] “Wirelesshd,” <http://www.wirelesshd.org/>, Sep. 2011.
- [61] C. Yiu and S. Singh, “Empirical capacity of mmWave WLANs,” *IEEE Journal Selected Area in Communications*, vol. 27, no. 8, pp. 1479–1487, Oct. 2009.
- [62] S. Singh, R. Mudumbai, and U. Madhow, “Medium access control for 60GHz outdoor mesh networks with highly directional links,” in *IEEE INFOCOM*, Apr. 2009.
- [63] S. Singh and U. Madhow, “Distributed coordination with deaf neighbors: efficient medium access for 60GHz mesh networks,” in *IEEE INFOCOM*, May 2010.
- [64] S. Singh, R. Mudumbai, and U. Madhow, “Interference analysis for highly directional 60GHz mesh networks: The case for rethinking medium access control,” *IEEE/ACM Transactions on Networking*, vol. 19, no. 5, pp. 1513 – 1527, Oct. 2011.
- [65] S. Singh, F. Ziliotto, U. Madhow, E. M. Belding-Royer, and M. J. W. Rodwell, “Millimeter wave WPAN: Cross-layer modeling and multi-hop architecture,” in *IEEE INFOCOM*, May 2007.
- [66] C. Yiu and S. Singh, “Link selection for point-to-point 60GHz networks,” in *IEEE ICC*, May 2010.

- [67] J. Qiao, L. X. Cai, X. Shen, and J. W. Mark, "Enabling multi-hop concurrent transmissions in 60 ghz wireless personal area networks," *IEEE Transactions on Wireless Communications*, vol. 10, no. 11, pp. 3824–3833, Nov. 2011.
- [68] A. Valdes-Garcia, "Millimeter-wave communications using a reflector," Patent, Aug., 2012. [Online]. Available: <http://www.google.com/patents/US20120206299>.
- [69] K. W. Brown, "Directed energy beam virtual fence," Patent, Oct., 2009. [Online]. Available: <http://www.google.com/patents/US20090256706>.
- [70] X. Zhou, Z. Zhang, Y. Zhu, Y. Li, S. Kumar, A. Vahdat, B. Y. Zhao, and H. Zheng, "Mirror mirror on the ceiling: Flexible wireless links for data centers," in *ACM SIGCOMM*, Aug. 2012.
- [71] C.-S. Sum, Z. Lan, and etc, "A multi-gbps Millimeter-wave WPAN system based on STDMA with heuristic scheduling," in *IEEE Globecom*, Nov. 2009.
- [72] L. X. Cai, L. Cai, X. Shen, and J. W. Mark, "Efficient resource management for mmWave WPANs," in *IEEE WCNC*, Mar. 2007.
- [73] L. X. Cai, X. Shen, and J. W. Mark, "Spatial multiplexing capacity analysis of mmWave WPANs with directional antennae," in *IEEE GLOBECOM*, Nov. 2007.
- [74] L. X. Cai, L. Cai, X. Shen, and J. W. Mark, "Rex: A randomized exclusive region based scheduling scheme for mmWave WPANs with directional antenna," *IEEE Transactions on Wireless Communications*, vol. 9, no. 1, pp. 113–121, Jan. 2010.
- [75] S. Singh, F. Ziliotto, U. Madhow, E. M. Belding, and M. Rodwell, "Blockage and directivity in 60 GHz wireless personal area networks: From cross-layer model

- to multihop mac design,” *IEEE Journal Selected in Communications*, vol. 19, no. 5, pp. 1513–1527, Oct. 2009.
- [76] M. X. Gong, R. Stacey, D. Akhmetov, and S. Mao, “A directional CSMA/CA protocol for mmWave wireless PANs,” in *IEEE WCNC*, Apr. 2010.
- [77] M. X. Gong, D. Akhmetov, and S. Mao, “Directional CSMA/CA protocol with spatial reuse for mmWave wireless networks,” in *IEEE GLOBECOM*, Dec. 2010.
- [78] M. X. Gong, D. Akhmetov, R. Want, and S. Mao, “Multi-user operation in mmWave wireless networks,” in *IEEE ICC*, Jun. 2011.
- [79] Z. Lan, J. Wang, and etc, “Directional relay with spatial time slot scheduling for mmWave WPAN systems,” in *IEEE VTC Spring*, May 2010.
- [80] J. Wang, Z. Lan, and etc, “A pro-active beamforming protocol for multi-Gbps Millimeter-Wave WPAN systems,” in *IEEE WCNC*, Apr. 2010.
- [81] Z. Lan, C. sean Sum, J. Wang, T. Baykas, J. Gao, H. Nakase, H. Harada, and S. Kato, “Deflect routing for throughput improvement in muti-hop millimeter-wave wpan system,” in *IEEE WCNC*, Apr. 2009.
- [82] P. Dutta, V. Mhatre, D. Panigrahi, and R. Rastogi, “Joint routing and scheduling in multi-hop wireless networks with directional antennas,” in *IEEE Infocom*, Mar. 2010.
- [83] D. Li, C. Yin, and C. Chen, “A selection region based routing protocol for random mobile ad hoc networks with directional antennas,” in *IEEE Globecom*, Dec. 2010.
- [84] G. Zheng, C. Hua, K. Vu, R. Zheng, and Q. Wang, “Robust reflector placement in 60GHz mmWave wireless personal area networks,” in *IEEE RTAS, Work-in-Progress*, Apr. 2012.

- [85] G. Zheng, C. Hua, R. Zheng, and Q. Wang, “A robust relay placement framework for 60GHz mmWave wireless personal area networks,” to appear in IEEE Globecom, 2013.
- [86] G. Zheng, C. Hua, Q. Wang, and R. Zheng, “A robust relay placement framework for 60GHz mmwave wireless personal area networks,” arXiv:1207.6509, 2012.
- [87] F. Bai and A. Helm, A Survey of Mobility Modeling and Analysis in Wireless Adhoc Networks. Springer, Oct. 2006.
- [88] S. Chawla. (2007, Feb.) Lecture notes on random walk model. [Online]. Available: <http://pages.cs.wisc.edu/~shuchi/courses/880-S07/scribe-notes/lecture05.pdf>.
- [89] X. Liu, A. Sheth, M. Kaminsky, K. Papagiannak, S. Seshan, and P. Steenkiste, “DIRC: increasing indoor wireless capacity using directional antennas,” in ACM SIGCOMM, Aug. 2009.
- [90] V. Navda, A. P. Subramanian, K. Dhanasekaran, A. Timm-Giel, and S. R. Das, “MobiSteer: using steerable beam directional antenna for vehicular network access,” in ACM MobiSys, Jun. 2007.
- [91] K. Yang, J. Huang, Y. Wu, X. Wang, and M. Chiang, “Distributed robust optimization part I: Framework and example,” in Technical Report, Princeton University, Jan. 2009.
- [92] T. H. Cormen, Introduction to Algorithms. The MIT Press, Jul. 2009.
- [93] D. Li and X. Sun, Nonlinear Integer Programming. Springer, 2006.
- [94] A.M.Gepffropm, “Generalized benders decomposition,” Journal of Optimization Theory and Applications, 1972, 10(4):237-260.

- [95] C. Hua and R. Zheng, "Robust topology engineering in multiradio multichannel wireless networks," *IEEE Transactions on Mobile Computing*, vol. 11, no. 3, pp. 492–503, Mar. 2012.
- [96] "IBM ILOG CPLEX optimization studio for academics," [http://www-01.ibm.com/software/websphere/products/optimization /academic-initiative/.](http://www-01.ibm.com/software/websphere/products/optimization/academic-initiative/), Feb. 2012.